

**Design of Dry-Stacked Blocks with High Thermal Resistance for Exterior
Walls**

By

Marzieh Mohammadi

A thesis submitted in partial fulfillment of the requirements for the degree of

Master of Science

in

Civil (Cross-disciplinary)

Department of Civil and Environmental Engineering

University of Alberta

© Marzieh Mohammadi, 2024

Abstract

The escalating energy consumption of buildings highlights the significance of adopting energy-efficient building design and construction practices. The growing demand for higher thermal resistance within building envelopes also necessitates innovative solutions for energy-efficient building components. Dry-stacked masonry blocks have gained considerable attention as a viable construction material for masonry walls, primarily due to their rapid assembly, absence of mortar, and diminished reliance on skilled labor. However, there has been a notable absence of a comprehensive review of these blocks' thermal performance. Furthermore, there is a distinct lack of evaluation pertaining to the thermal performance of dry-stacked blocks within cold climate zones.

This study fills the gap in existing literature by conducting a thorough review of the thermal performance of dry-stacked masonry blocks. The review includes considerations tailored for cold climate zones and insights into both market-available and research-based dry-stacked blocks. Additionally, to address the thermal performance of dry-stacked blocks, this study develops two novel dry-stacked blocks: a simple block and a composite block. The composite block incorporates an integral insulation within its components, while the simple block does not include any insulation. These blocks have been meticulously designed for optimal performance within cold climate zones. Using the finite element method, the thermal resistance of these blocks is carefully assessed. Detailed comparative analyses are conducted on both simple and composite block walls, alongside a conventional masonry wall. Additionally, the performance of the composite block is examined in relation to existing market counterparts.

Based on the review, the employment of novel materials such as cement and palm oil clinker powder mixture, rubberized concrete, and concrete including recycled masonry aggregates and

expanded polystyrene (EPS) show promise in enhancing both thermal resistance and compressive strength. However, these materials are still relatively novel and costly. Furthermore, the review underscores the significance of incorporating insulation into the block structure. Filling block cavities with foam proves to be more effective in enhancing thermal performance than the removal of exterior side webs.

The review highlights that in cold climate zones, the integral insulation and cavity walls play crucial roles in achieving thermal efficiency. In such cases, the thermal performance of masonry assemblies with integral insulation is primarily governed by the insulation component. Hence, the utilization of composite blocks with integral insulation offers significant advantages for buildings located in cold climate zones.

The simulation results show a significant impact of thermal bridging on the thermal resistance of the simple block, resulting in an 11% decrease in the effective thermal resistance (R-value) of a simple block wall assembly when compared to the composite block wall assembly. Furthermore, in comparison to a conventional masonry wall with hollow grouted units and the same insulation thickness, the composite block wall exhibits a 24% higher R-value by eliminating thermal bridging through insulation, while the simple block wall demonstrates an 11% higher R-value due to different ties' shape and grouted masonry cores. When comparatively assessing the composite block against existing market options, it emerges as the superior choice in terms of thermal resistance. Consequently, the composite block is ideal for fast construction, limited labor, and lightweight requirements. Conversely, the simple block is the preferred choice in situations where complicated manufacturing tools are unavailable.

Acknowledgment

I wish to convey my profound appreciation to those who have lent their unwavering support during the culmination of this academic pursuit. My heartfelt gratitude extends to my supervisor, Dr. Yuxiang Chen, whose consistent guidance and invaluable insights have played an indispensable role in shaping the trajectory of this research. I also express sincere thanks to my esteemed committee members, Dr. Farook Hamzeh and Dr. Carlos Cruz-Neguez, whose constructive critiques and valuable comments significantly contributed to the refinement of this thesis.

Special recognition is owed to my brother, Maziar, whose discerning criticism at various junctures of this study has been pivotal in elevating the caliber of my work. Appreciation is also extended to my colleagues and friends, Maysoun Ismaiel, Xiao Han, and Marjan Darabi, whose meaningful discussions, insightful suggestions, and unwavering moral support have profoundly enhanced the quality of this thesis. Their collaborative input has been instrumental in the enrichment of the scholarly discourse.

Furthermore, I am deeply thankful to my family, whose unwavering encouragement has been a wellspring of strength throughout this academic odyssey. Their steadfast support has been a cornerstone of my perseverance.

Finally, I extend gratitude to the authors, researchers, and institutions whose seminal works have been referenced in this thesis. Their scholarly contributions form the bedrock upon which this study stands. This thesis stands as a testament to the collective efforts of all these individuals and entities, without whom this endeavor would not have been conceivable. To each one of you, I offer my heartfelt thanks for being integral to this academic journey.

Table of Contents

1	Introduction.....	1
1.1	Background	1
1.2	Thesis Objectives and Research Methodology	4
1.3	Research Scope	6
1.4	Thesis layout	6
2	Literature Review on Influencing Parameters of Blocks and Wall Configurations	8
2.1	Block materials.....	9
2.1.1	Concrete	9
2.1.2	Earth	11
2.1.3	Wood.....	12
2.1.4	Polymer	12
2.1.5	Hempcrete	13
2.1.6	Other materials and section summary.....	13
2.2	Block spatial configurations.....	15
2.2.1	Simple Blocks	16
2.2.2	Composite Blocks	19
2.3	Veneer Ties	23
2.4	Insulation.....	24
2.5	Cavity Space.....	27
2.6	Blocks for Cold Climate Zones.....	28
2.7	Existing Dry-Stacked Blocks	30
2.8	Conclusion.....	39
3	Design Development of New Dry-Stacked Blocks	41
3.1	Block A	42

3.2	Block B.....	47
4	Numerical Modeling.....	53
4.1	Models Description.....	54
4.2	Material Properties.....	56
4.3	Boundary Conditions.....	57
4.4	Contact Resistances.....	59
4.5	Mesh Convergence.....	59
4.6	Validation.....	60
5	Results and Discussion.....	62
5.1	Analysis of Thermal Performance of Walls A and B.....	62
5.2	Comparative Analysis of Walls A, B, and C.....	65
5.3	Comparative Analysis of Block A Against Existing Dry-Stacked Blocks.....	68
6	Conclusion and Future Research Recommendations.....	73
	References.....	75

List of Tables

Table 1. Thermal conductivity and compressive strength of materials that are used in dry-stacked blocks arranged from low to high thermal conductivity.....	14
Table 2. Shape change effects on R-value of masonry blocks arranged from the highest positive effect to the highest negative effect.	22
Table 3. Changes in R-value of the wall assembly based on the material of ties.....	24
Table 4. characteristics of conventional insulation materials.....	26
Table 5. Existing simple dry-stacked blocks.....	31
Table 6. Existing composite dry-stacked blocks.....	32
Table 7. Characteristics of existing dry-stacked blocks.....	36
In Table 8, the permissible climate zones attributed to the blocks which are derived from NECB (2020) are presented. Blocks with R-values lower than $3.45 \text{ m}^2\cdot\text{K}/\text{W}$, such as Polycare (2021), Lok-N-Blok (2021), and CEB stabilized with fly ash (Leitão et al., 2017), are considered not applicable (N/A) in cold climate zones and require additional insulation to meet the standards.	
Table 8. Permissible climate zones for existing dry-stacked blocks.....	36
Table 9. Stabilization and compressive strength of existing dry-stacked blocks.....	37
Table 10. Material properties of the components in walls A, B, and C.....	56
Table 11. Contact resistances.....	59
Table 12. Percentage difference of simulated and reported values for validating the numerical modeling.....	60
Table 13. Minimum insulation thicknesses of walls A and B for climate zones in Canada.....	65
Table 14. Comparison among three investigated wall assemblies.....	66
Table 15. Comparison of Block A against existing market blocks.....	68

List of Figures:

Figure 1. Pioneers of interlocking dry-stacked blocks: 1) Haener, 2) Azar, 3) Sparlock, and 4) Hydraform.....	2
Figure 2. Different components in masonry blocks.....	16
Figure 3. Effect of shape changes on R-value of simple blocks: 1) rectangular to elliptical cavity cells, 2) increasing the cavity rows to five, 3) staggered cavity rows, 4) increasing the cavity rows from one to two, and 5) increasing the cavity rows from two to three.....	18
Figure 4. Walls made of 1) IITM SILBLOCK, 2) IITM HILBLOCK, 3) Sparlock, and 4) Armo System.....	19
Figure 5. Effects of inclined folded sheets within the cavities of blocks on their heat flux values.....	20
Figure 6. Effect of different shapes, insulations, and densities on R-value (Martínez et al., 2018).....	21
Figure 7. Examples of 1) prescriptive tie, 2) Proprietary tie (CSA-A370:14, 2018).....	23
Figure 8. Different locations of insulation in a wall assembly: 1) exterior insulation, 2) integral insulation, and 3) interior insulation.....	25
Figure 9. Weep holes in a ventilated cavity wall.....	27
Figure 10. Liatop50 insulated block (Liapor, 2022).....	29
Figure 11: Investigated blocks by Al-Jabri et al. (2005).....	29
Figure 12. One Step cavity block.....	30
Figure 13. Initial design options for Block A.....	43
Figure 14. Design process of Block A.....	44
Figure 15. Perforated layer: 1) location in the block, 2) Back and front walls of the cavity space.....	45
Figure 16. Configuration of Block A, corner and half blocks of type A, and wall A.....	46
Figure 17. Wall A section.....	47
Figure 18. Design process of block B.....	48
Figure 19. Configuration of Block B, corner and half blocks of type B, and wall B.....	49
Figure 20. Wall B with insulation, tie and veneer.....	50
Figure 21. Construction process of Block B courses.....	50

Figure 22. Wall B section	51
Figure 23. Dimensions of models: 1) A, and 2) B	55
Figure 24. Model dimensions and components of wall C	56
Figure 25. Boundary conditions of the ANSYS model	58
Figure 26. Results of mesh tests	60
Figure 27. Temperature distribution in wall A	63
Figure 28. Heat flux density distribution of Block A	63
Figure 29. Temperature distribution of wall assembly B	64
Figure 30. Temperature distribution of wall C	66
Figure 31. Temperature distribution and shapes of 1) Block A, 2) Faswall, 3) Almanaratain, 4) Isotex, 5) Comfort Block, and 6) Gablok	71

Abbreviations

AAC: Autoclaved aerated concrete

CEB: Compressed earth block

CMU: Concrete masonry unit

CO₂: Carbon dioxide

EPS: Expanded polystyrene

FEM: Finite element method

GFRP: Glass fiber reinforced polymer

H: Height (cm)

ICF: Insulated concrete formwork

k: Thermal conductivity (W/m·K)

L: Length (cm)

OSB: Oriented strand board

POCP: Palm oil clinker powder

q: The heat flux in watts per area of the addressed wall in square meters (W/m²)

R: Thermal Resistance (m²·K/W)

R-value: Effective thermal resistance of a wall assembly (m²·K/W)

t: Thickness (cm)

ΔT: The temperature difference between two interfaces (K)

ρ: Density (kg/m³)

σ: Compressive strength (MPa)

XPS: Extruded polystyrene

1 Introduction

1.1 Background

The building sector is responsible for a significant portion of global energy consumption, specifically around 30-40% (IEA, 2022). Due to the accelerating urbanization trends, energy usage in the building sector is projected to double by 2050 (Svetozarevic et al., 2019). Given the substantial energy consumption in buildings, the paramount focus has been on increasing the energy efficiency. This entails utilizing less energy while concurrently ensuring optimal comfort for the occupants. The building envelope serves as the interface between the interior and exterior spaces. It is responsible for more than 40% of heat loss of buildings in cold climates and overheating in warm climates (Barozzi et al., 2016; Yan et al., 2020). As a result, building envelope plays a crucial role in heat transfer and is thus a vital component to consider in reducing energy consumption (Ascione et al., 2019; Han et al., 2020). Recognizing the importance of energy efficiency, recent regulations including the national energy codes of Canada for buildings (NECB, 2017, 2020) have stipulated higher effective thermal resistances (R-values) for building envelope components. An R-value is the actual thermal resistance of a wall assembly, taking into account the thermal bridging effects of any wall components if there are any. NECB (2020) has defined R-value requirements for building envelope components that are, on average, 12% higher than the previous version (NECB, 2017). Moreover, the R-values specified in NECB (2017) were, on average, 6% higher than those in NECB (2015). These advancements highlight the increasing need for buildings with enhanced thermal performance. By incorporating energy-efficient technologies and components in the building envelope, energy usage can be reduced without compromising the occupants' comfort.

Masonry system, as a type of building system, finds extensive global application due to its modularity, durability, and exceptional thermal performance (Sathiparan et al., 2022). Masonry blocks can fulfill multiple functions such as load-bearing, space enclosure, fireproofing, and providing thermal and acoustic insulation simultaneously (Nambiar et al., 2004). However, the rising costs of materials and the shortage of skilled laborers have resulted in construction delays for masonry buildings (Ramli et al., 2014). Additionally, the use of cement and temporary supports in the traditional bricklaying process makes it time-consuming, labour-intensive, and expensive

(Saari et al., 2021). Consequently, researchers and practitioners have actively pursued innovative block designs to enhance the performance of masonry blocks. These endeavors have involved transforming traditional masonry into a wide array of construction techniques, shapes and applications (Beall, 2000; A. W. Hendry, 1998; Ramamurthy & Nambiar, 2004).

Dry-stacked masonry has emerged as an alternative solution that eliminates the need for mortar. In conventional masonry, mortar joints are prone to leakage. Mortar's porous nature makes it susceptible to moisture penetration, leading to functional problems such as freeze-thaw damage, mold growth, and degradation of adjacent materials (Hines & Mehta, 1991). Moreover, when considering mortars with a higher density than the blocks themselves, the inclusion of mortar can have an adverse impact on the R-value of masonry wall assemblies. According to Urban et al. (2011), the inclusion of mortar layers in lightweight concrete masonry walls led to a reduction in the R-value by 12%. Al-Sanea and Zedan (2012) investigated the impact of mortar thickness on R-value, finding that an increase in mortar thickness from zero to 2 cm decreases the R-value from 2.8 to 1.3 $\text{m}^2\cdot\text{K}/\text{W}$. As a result, the utilization of dry-stacked blocks as an alternative to conventionally mortared blocks has emerged as a viable solution that effectively addresses the limitations associated with the latter.

Interlocking blocks, as a sub-category of dry-stacked blocks, have garnered considerable attention since the mid-1980s (Bosro et al., 2018; Uzoegbo et al., 2007). These blocks enable secure fitting without the need for mortar. By incorporating various indentations, interlocking blocks can be seamlessly interconnected, resulting in a stable structure. Notable pioneers in the interlocking dry-stacked block industry include the Haener system (Haenerblock, 2021) in the US, Azar (Cécire, 2002) and Sparlock systems (R. G. Drysdale & Guo, 1995) in Canada, and Hydraform (2021) in South Africa (Figure 1).

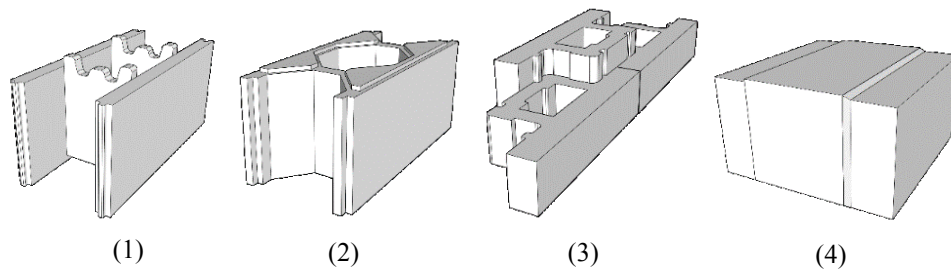


Figure 1. Pioneers of interlocking dry-stacked blocks: 1) Haener, 2) Azar, 3) Sparlock, and 4) Hydraform

Several types of interlocking blocks, varying in shape, size, ingredient composition, materials, and interlocking mechanisms have been introduced in recent years. These blocks are designed and constructed to ensure the alignment of units, facilitating construction with or without skilled labor and mortar, thereby enhancing time and cost efficiency (Safiee et al., 2011). Additionally, the interlocking feature contributes to the stability of the structure during the construction process (Uzoegbo, 2001). However, the absence of mortar necessitates stringent dimensional tolerances to ensure uniform load transfer among the components (Anand & Ramamurthy, 2000). It is important to note that the production cost of interlocking blocks tends to be higher compared to traditional blocks due to the complex geometries (such as tongue and groove) involved and the utilization of specialized mechanized manufacturing methods. Despite the increased complexity and expenses associated with the interlocking mechanism, these costs are typically offset by the reduction in labor, materials, and construction time.

Owing to their promising construction method, dry-stacked masonry blocks have been designed and studied recently. The information about the characteristics of existing dry-stacked blocks (e.g., component arrangements and materials) and the findings from research studies is beneficial to designers and block producers to improve their products by incorporating successful features including. However, only a limited number of papers have reviewed specific characteristics of dry-stacked blocks. Ramamurthy and Nambiar (2004) categorized dry-stacked masonry blocks, with an emphasis on their structural performance. The authors further addressed techniques that can improve the structural performance of the assessed dry-stacked blocks. Several studies have reviewed the structural behavior of interlocking dry-stacked masonry blocks. Bosro et al. (2018), Al-Fakih et al. (2018) and Aswad et al. (2022) examined the effects of different material ingredients on the structural performance of interlocking dry-stacked blocks in separate studies. Their investigations shed light on the significance of material properties in determining the structural behavior of these blocks. In the context of sustainability in masonry construction, Subasic (2022) explored innovative strategies such as integrating nonconventional low-embodied-energy materials and dry-stacked blocks as a response to the demand for producing building components using less energy. The study demonstrated how these advancements contribute to more sustainable building construction practices. However, to the author's best knowledge, there is no review on the thermal performance of dry-stacked masonry blocks. Moreover, there exists a noticeable absence of assessments concerning the thermal performance of dry-stacked blocks in

cold climate zones. The following section focuses on elucidating the objectives of this study and outlining the methodology employed to achieve them.

1.2 Thesis Objectives and Research Methodology

For thermally efficient design of dry-stacked block walls, it becomes imperative to evaluate the parameters impacting their thermal performance, material and shape of the blocks, ties, insulations and cavity spaces. A comprehensive understanding of the influence of these parameters on the thermal performance of dry-stacked masonry blocks can be obtained through an investigation of prior studies. However, there is a gap in the literature regarding a comprehensive review of the influential parameters on the thermal performance of dry-stacked masonry blocks. Therefore, this study aims to address this gap by conducting an extensive review, encompassing both the market and research literature, to investigate the influence of material and shape on the thermal performance of dry-stacked blocks. Special considerations will also be given for the application of dry-stacked masonry blocks in cold climate zones. By exploring and analyzing the existing literature on this topic, this study seeks to provide valuable insights and knowledge for developing thermally efficient dry-stacked masonry blocks.

Data gathered from the literature review for thermally efficient design of dry-stacked blocks is used to suggest two different designs for dry-stacked blocks for cold climate zones. The two new designs have specific characteristics: the first one is a composite block incorporating an integral insulation within its components, while the second is a simple block without any insulation. Two distinct wall assemblies constructed using these blocks are compared to a conventional masonry cavity wall with hollow grouted concrete masonry units (CMUs) and the same insulation thickness. This comparison aims to assess the new block walls in relation to a well-established benchmark, thereby facilitating a comprehensive understanding of their performance.

To determine the final design of these blocks, an iterative process involving design, simulation and evaluation was undertaken, aiming to achieve the required R-value for exterior wall assemblies in Edmonton (zone 7A), which is $4.65 \text{ m}^2 \cdot \text{K}/\text{W}$ as specified in NECB (2020). The finite element method (FEM) is employed as a practical means of simulating the thermal performance of the new blocks. FEM modeling has emerged as a valuable practical tool for addressing building physics problems including heat transfer analysis (Bathe, 2006; Brenner et al., 2008). FEM modeling

allows for the simulation of complex building components through a numerical approach. Moreover, FEM modeling offers notable advantages in terms of cost and time efficiency when compared to experimental tests. Research studies that utilized experimental methods to validate their simulation results verified the reliability of the simulation approach in conducting thermal analysis (Gu & Hunt, 2007; Martínez et al., 2018; Nayak et al., 2010; Ratanathavorn et al., 2015; Wakili & Tanner, 2003; Zukowski & Haese, 2010). Hence, this study utilizes ANSYS (2022), a FEM software, to evaluate the thermal resistance of the innovated block designs.

In summary, the objectives of this thesis can be outlined as follows:

- Investigate the impact of different materials and shape configurations on thermal performance of dry-stacked blocks
- Explore the specific considerations for thermally efficient dry-stacked blocks suitable for cold climate zones.
- Assess the current state of dry-stacked masonry blocks in terms of their thermal performance.
- Suggest two simple and composite dry-stacked block designs for cold climate zones.

In addition, the methodology of this thesis can be summarized as follows:

- Explore the impact of different materials on thermal performance of dry-stacked blocks by examining materials used in prior research and market-available dry-stacked blocks.
- Evaluate the influence of block shape on thermal performance, including parameters like hole size, quantity, internal barriers, web shape, and insulation arrangement, to determine their effect on block R-values.
- Apply the collected data from the literature review to design two novel dry-stacked blocks.
- Compare the performance of these new blocks in distinct wall assemblies against a conventional masonry wall.
- Conduct a comparative analysis between the new composite block and existing market-available blocks.

By achieving these objectives, this study aims to contribute to the understanding of the thermal performance of dry-stacked masonry blocks.

1.3 Research Scope

To ensure a focused investigation into the thermal performance of dry-stacked masonry blocks, several strategies are employed to narrow down the research area. The strategies implemented are summarized as follows:

- The new blocks are compared specifically to dry-stacked blocks available in the market and research studies, excluding mortared ones.
- Dry-stacked blocks with insufficient information regarding their thermal properties are excluded from the study.
- The materials used in the numerical modeling are assumed to be isotropic, meaning they exhibit same thermal properties in all directions.
- The thermal efficiency of masonry blocks in this thesis is primarily defined by their R-value. Other aspects of thermal performance, such as hygrothermal analysis, are beyond the scope of this research.
- Structural analysis of dry-stacked blocks involves complex and extensive investigations that require comprehensively addressing factors such as load-bearing capacity, material strengths, and resistance to forces. This endeavor goes beyond the scope of this research.

By employing these strategies, this study ensures a focused and systematic exploration of the thermal performance of dry-stacked masonry blocks.

1.4 Thesis layout

This thesis is presented in six chapters to provide a comprehensive analysis of thermal efficiency in dry-stacked masonry blocks. The first chapter is the introduction, outlining the importance of energy-efficient building envelopes and the need for the development of dry-stacked blocks. The second chapter is dedicated to the literature review, which examines the influence of shape and material of blocks, ties, insulation, and cavity spaces on the thermal performance of dry-stacked blocks. This chapter draws insights from a range of published studies and industry-specific blocks. Chapter three, “Design Development of New Dry-Stacked Blocks”, provides an overview of the design processes and specifications of the new dry-stacked blocks. The fourth chapter, titled “Numerical Modeling”, delves into the details of the numerical modeling approach used in this research to evaluate the thermal performance of the new blocks. This chapter provides a

comprehensive explanation of the modeling methodology employed and model validation. Chapter five, “Results and Discussion”, presents the findings and discussions derived from the simulations conducted in this study. The sixth chapter of the thesis is the conclusion. It offers a concise summary of the significant findings drawn from the study. Additionally, this chapter provides recommendations for future research directions and areas that merit further investigation.

2 Literature Review on Influencing Parameters of Blocks and Wall Configurations

In order to improve the thermal performance of dry-stacked block walls, it is crucial to thoroughly investigate parameters that impact their thermal performance. The influencing parameters from the design of the blocks can be grouped into spatial configuration and material. Other parameters impacting on the thermal performance of the masonry walls include veneer ties, thermal insulation and cavity spaces. Therefore, in this chapter, the effects of these parameters on the thermal performance of masonry block walls are elaborated. The first section focuses on the thermal properties of materials utilized in both research studies and market blocks. Various aspects are examined, including methods for reducing the thermal conductivity of blocks, the influence of density on thermal performance, the incorporation of recycled materials in the development of dry-stacked blocks, and the impact of ingredients on the thermal properties of concrete blocks. Furthermore, this section delves into topics such as the production of low CO₂ earth blocks, the use of earth stabilizers and their effect on thermal performance, the thermal properties of wood and polymers, and the utilization of hemp and industrial waste for improving thermal performance. In the second section, the effect of blocks' spatial configurations on its thermal performance is elucidated. This includes an exploration of thermal bridging in specific shape components and an analysis of the effects of changes in shape on heat transfer mechanisms within the block. The effects of size, number and arrangement of cavities, barriers in cavities, webs, and the insulation shape on thermal performance of the blocks are thoroughly investigated. The third section delves into the impact of veneer ties on the thermal performance of masonry walls, exploring various tie types and materials and their implications for the wall's thermal characteristics. The fourth section assesses the influence of insulation, providing insights into the effects of different insulation locations relative to the wall and commonly employed insulation materials. The fifth section elucidates the effect of cavity spaces on the thermal performance of masonry walls. The sixth section focuses on considerations specific to cold climate zones, including blocks with integral insulation and cavity walls. In the seventh section, a comprehensive compilation of existing dry-stacked blocks is presented in tabular format. This section offers a valuable resource for gaining insights into the current landscape of dry-stacked blocks. Finally, in the conclusion section, the findings from this chapter are presented.

2.1 Block materials

Dry-stacked blocks have been produced from different material compositions during the last few decades. Notable examples include coconut fiber reinforced concrete blocks (Ali et al., 2012), stabilized compressed earth blocks (Leitão et al., 2017; Sturm et al., 2015), sawdust interlocking blocks (Mohammed & Aswin, 2016), rubberized geopolymer interlocking blocks (Mohammed et al., 2018), and rubberized concrete interlocking blocks (Al-Fakih et al., 2022). Lightweight insulating materials have been developed to enhance blocks thermal performance. However, the challenge is to improve thermal performance while upholding structural integrity and moisture resistance. Introducing pores of different sizes into materials improves thermal performance (Sutcu et al., 2014). However, the effect of pores on structural performance and moisture resistance should be carefully investigated. The pores can be microporosities generated by pore-making additives or hollows in the shape. In these cases, the thermal efficiency of the blocks arises from their low density ($500\text{-}1000\text{ kg/m}^3$) in addition to pores and holes that are filled with air and act as barriers to heat transfer. This section of the study explores materials used in developing dry-stacked blocks, focusing on their thermal properties and how they impact the overall R-value of the blocks.

2.1.1 Concrete

Concrete is one of the most widely used materials in the production of dry-stacked masonry blocks (Almanaratain, 2022; ArmoSystem, 2021; ComfortBlock, 2022; EPIC-Block, 2022; Thanoon et al., 2004; Versaloc, 2021). However, due to its inherently low R-value, various techniques have been employed to enhance its thermal properties. One effective approach involves reducing the density of concrete blocks, as this can significantly improve their thermal performance. A 33% reduction in density can lead to a remarkable 60% decrease in thermal conductivity (Al-Jabri et al., 2005). According to ASTM-C90 (2022), normal weight CMUs have a density of over 2000 kg/m^3 . In addition, medium weight and lightweight CMUs demonstrate densities ranging from $1680\text{ to }2000\text{ kg/m}^3$ and less than 1680 kg/m^3 , respectively. Lightweight concrete provides high thermal insulation and fire resistance for the masonry units. The production of lightweight concrete can be accomplished through the use of lightweight aggregates or by employing an aeration process, both of which provide the concrete with a porous nature, ultimately enhancing its thermal performance.

The thermal performance of concrete blocks can be significantly enhanced through the utilization of lightweight aggregates. This improvement arises from the fact that the properties of concrete, including physical, thermal, structural, and longevity, depend on the properties of its constituent ingredients (Pavlu et al., 2019). Factors such as type (Marshall, 1972), thermal properties, density and porosity (Callejas et al., 2017) of the aggregates are the most influential factors on the thermal properties of the concrete. Recent studies have focused on incorporating waste materials as additives to produce lightweight concrete, thereby improving the thermal performance of masonry units. Rubberized concrete interlocking blocks demonstrated a 61% improvement in R-value compared to conventional masonry units (Al-Fakih et al., 2022). The relatively high thermal performance of the rubberized concrete with a thermal conductivity of $0.731 \text{ W/m}\cdot\text{K}$ is attributed to the increased air content within the concrete mixture and the low thermal conductivity of crumb rubber particles ($0.16 \text{ W/m}\cdot\text{K}$ for rubber compared to $1.5 \text{ W/m}\cdot\text{K}$ for the fine aggregate). Incorporating recycled masonry and recycled expanded polystyrene (EPS) aggregates into concrete for dry-stacked masonry units was investigated by Pavlu et al. (2019). Their findings indicated that a concrete mixture containing both recycled masonry aggregate and EPS could decrease the thermal conductivity to $0.784 \text{ W/m}\cdot\text{K}$. Consequently, the use of recycled materials in the manufacturing of dry-stacked masonry blocks improves the thermal performance, resulting in a reduction in the required thermal insulation thickness.

Autoclaved aerated concrete (AAC) is produced by ejecting air into the concrete mixture and curing it under high-pressure steam conditions (Chaipanich & Chindapasirt, 2015). This process provides lightweight blocks with exceptional insulating properties as well as resistance to rot and fire. AAC material exhibits a thermal performance that is at least 50% better than conventional concrete (Kyriakidis et al., 2016). AAC units have considerably lower thermal conductivity, typically around $0.11 \text{ W/m}\cdot\text{K}$ in contrast to $0.84 \text{ W/m}\cdot\text{K}$ for clay blocks (A. Hendry, 2001). Pierquet et al. (1998) obtained an R-value of $3.7 \text{ m}^2\cdot\text{K/W}$ by dry-stacking 46-cm-thick AAC blocks following design details provided by Schierhorn (1994) that allowed for mortar application in the first and last courses. As a result, AAC units offer a practical solution for achieving thermal-efficient dry-stacked blocks.

2.1.2 Earth

Earth has been used in building construction since ancient times (Houben & Guillaud, 1994) and continues to be prevalent in many developing countries. The popularity of earth as a building material is attributed to its low carbon dioxide (CO₂) emissions and low cost in comparison with modern construction techniques such as reinforced concrete and fired bricks (Silva et al., 2015). In addition to its inherent fire resistance and low cost, the ability of earth to naturally decompose and its notable acoustic properties make it an excellent candidate for sustainable building construction (Pacheco-Torgal & Jalali, 2012). However, using earth in construction comes with some challenges, including non-standard units, the lack of codes of practice, and the absence of quality control in both block manufacturing and the assembly process. Despite these hurdles, earth construction can still be a sustainable solution, especially in areas where it is already prevalent.

Compressed earth block (CEB) units represent a sustainable approach as they do not require burning in their manufacturing process. CEB units are composed of compressed unfired earth with less than 10% stabilizer content (Walker, 1999). The thermal conductivity of these units ranges from 0.81 to 1.04 W/m·K (Uzoegbo, 2020). In light of their eco-friendly manufacturing process and relatively low thermal conductivity, CEB units offer a sustainable alternative in construction.

The influence of stabilizers on the performance of CEB units is multifaceted, affecting various properties. The stabilizer, typically Portland cement or lime, is added to guarantee the strength of CEB units, as they are highly susceptible to water damage (Shakir et al., 2020). Stabilizers increase the soil's stability in contact with water and improve its compressive strength (Bahar et al., 2004). However, the use of such stabilizers reduces the soil's R-value (Sindanne et al., 2014), increases the environmental impact of the material (Leitão et al., 2017), and considerably raises the cost and embodied energy of CEB units (Reddy & Kumar, 2010). To mitigate these drawbacks, researchers attempted to use other stabilizers with lower CO₂ emissions in comparison with cement and lime additives. The incorporation of geopolymers (Sore et al., 2018) and fly ash (Leitão et al., 2017) as stabilizers are two examples of low-CO₂-emitting materials utilized.

Despite environmentally friendly CEB units made with sustainable stabilizers, certain limitations hinder the widespread adoption of earth construction. Leitão et al. (2017) developed eco-friendly dry-stacked CEB units with an R-value of 0.34 m²·K/W, which highlights the need for additional insulation, similar to CMUs, to ensure thermal comfort for occupants. In addition, the thermal

performance of the CEB units challenges the traditional belief of a high R-value associated with earth construction. In fact, earth exhibits thermal mass properties that prove beneficial in moderate climates (Leitão et al., 2017) as well as hot, dry climates (Uzoegbo, 2020). CEB units have a higher density than lightweight concrete blocks but a lower density than medium-weight concrete blocks (Uzoegbo, 2020). Their relatively high density is considered a drawback, especially when the blocks need to be transported from a distant manufacturer rather than being manufactured on-site. Hence, although earth construction with sustainable stabilizers offers an environmentally friendly alternative, several challenges impede its wider adoption.

2.1.3 Wood

Wood is widely used in the construction industry, particularly in colder regions, owing to its inherent thermal insulation properties and abundant availability of raw materials (Caniato et al., 2017). Wood provides a balance of strength and lightness, making it an efficient material choice for building applications (Perković et al., 2021). Notably, recent innovations in dry-stacked masonry units have incorporated wood as a key component in their manufacturing process. One such example is Gablok (2021), where oriented strand board (OSB) with a thermal conductivity of $0.13 \text{ W/m}\cdot\text{K}$ is used to create dry-stacked masonry units. The composition of OSB and EPS provides a relatively high R-value of $6.66 \text{ m}^2\cdot\text{K/W}$ for the blocks. Another product, known as cement-bonded wood fiber or woodcrete, combines the strength of concrete with the insulation properties and lightweight nature of wood (Wolfe & Gjinolli, 1996). Isotex (2021) is a type of woodcrete dry-stacked block that is composed of two main materials: recycled Spruce softwood and Portland cement. This block functions as an insulated concrete formwork (ICF) system and offers an R-value range of 2.94 to $6.66 \text{ m}^2\cdot\text{K/W}$ by varying the thickness of Neopor insulation. Incorporating wood in dry-stacked masonry units showcases promising innovations, offering efficient thermal properties, and thereby contributing to the advancement of sustainable construction solutions.

2.1.4 Polymer

The utilization of recycled polymers as insulating materials in building construction offers a promising solution to address polymer waste and provides notable thermal efficiency (Pěňčík & Matějka, 2011). Researchers and manufacturers have actively investigated the incorporation of polymers in the production of masonry blocks. Lok-N-Blok (2021) is an example of dry-stacked

masonry block that is manufactured from recycled polypropylene with a 30% recycled content, developing a thermal conductivity of 0.148 W/m·K. Another innovative approach involves mixing natural sand and unsaturated polyester resin to create geopolymer concrete with a thermal conductivity of 0.233 W/m·K. The unsaturated polyester resin is derived from recycled polyethylene terephthalate and acts as a binder in the mixture. The integration of a geopolymer concrete layer around an EPS block culminates in the creation of Polycare (2021) with an R-value of 2.7 m²·K/W. The exploration of recycled polymers as materials in building construction holds promise for addressing polymer waste and achieving thermal efficiency, as demonstrated by various innovative examples.

2.1.5 Hempcrete

The combination of hemp, lime, and water yields a material with a weight approximately one-eighth that of concrete while exhibiting high thermal properties (Shea et al., 2012). Hempcrete or hemp-concrete stands out as an environmentally friendly, durable, low-density, and low thermal conductivity material. Moreover, hemp is characterized by its rapid growth and low irrigation requirements, further enhancing its suitability for building construction applications (Shea et al., 2012). Developed non-loadbearing dry-stacked blocks made from hempcrete offer an R-value of 3.7 m²·K/W (HempcreteBlock, 2022). With a thermal conductivity ranging from 0.087 to 0.1 W/m·K and a density falling between 300 and 400 kg/m³ (Abdellatef et al., 2020), hempcrete emerges as an abundant and promising material for the production of non-loadbearing dry-stacked blocks with high thermal efficiency.

2.1.6 Other materials and section summary

Several alternative materials, including perlite and palm oil clinker powder (POCP), have been investigated for their viability in the production of dry-stacked blocks, each offering unique potential for enhancing thermal efficiency. Perlite, a natural volcanic glass, exhibits a lightweight and porous structure upon heating. This material, renowned for its excellent insulating properties with a thermal conductivity of 0.072 W/m·K, was combined with mineral binders to create a block known as System3E (2021). The resulting block yields an impressive R-value of 5.05 m²·K/W. Shakir et al. (2020) combined POCP, a byproduct of palm oil shell combustion, with 10% cement to create interlocking dry-stacked blocks. The resulting blocks achieved a thermal conductivity of 0.2 W/m·K, representing 26% of the thermal conductivity of conventional stabilized compressed

earth blocks. POCP, characterized by its lightweight nature and porous texture, serves as an effective, thermally efficient aggregate capable of enhancing the block's thermal performance without compromising its structural integrity (Omar & Mohamed, 2002). The presence of pores in the POCP significantly reduces the block's density and minimizes heat transfer. In conclusion, the exploration of alternative materials such as perlite and POCP has demonstrated their potential to enhance the thermal performance of dry-stacked blocks.

Table 1 summarizes the characteristics of materials used in the development of masonry dry-stacked blocks, arranged according to their thermal conductivity levels. A discernible correlation exists between thermal conductivity and compressive strength. Generally, an increase in thermal conductivity corresponds to an elevation in compressive strength. Nonetheless, certain anomalies defy this trend, such as woodcrete and glued wood strands, as well as compressed earth with fly ash stabilizer and cement stabilizer. These materials display reduced compressive strength when compared to materials with similar thermal conductivity values.

Among the materials investigated, perlite stands out for its remarkably low thermal conductivity, highlighting its exceptional thermal insulation properties. However, this advantage is offset by a compromise in compressive strength. Conversely, the combination of cement and POCP emerges as a promising candidate, boasting a thermal conductivity only one-seventh that of concrete and relatively high compressive strength. Rubberized concrete and concrete including recycled masonry aggregates and EPS exhibit thermal conductivities approximately half that of concrete while maintaining strong compressive strengths. These properties make them suitable for use in structural load-bearing walls and reduce the amount of thermal insulation compared to concrete blocks. Concrete, while ranking lower in thermal performance, excels in terms of compressive strength.

Table 1. Thermal conductivity and compressive strength of materials that are used in dry-stacked blocks arranged from low to high thermal conductivity.

Material	Thermal conductivity, k (W/m\cdotK)	Compressive strength, σ (MPa)
Perlite with mineral binders (System3E, 2021)	0.072	1.5
Hempcrete (HempcreteBlock, 2022)	0.087	-
AAC (A. Hendry, 2001)	0.11	7
Glued strands of wood (Gablok, 2021)	0.13	0.15

Woodcrete (Nardi et al., 2016)	0.13	2.8
Recycled polypropylene (Lok-N-Blok, 2021)	0.148	8.2
Cement and POCP (Shakir et al., 2020)	0.2	5-14.5
Geopolymer concrete (Polycare, 2021)	0.233	-
Compressed earth with fly ash stabilizer (Leitão et al., 2017)	0.41	3
Rubberized concrete (Al-Fakih et al., 2022)	0.731	18.4
Concrete mixture containing both recycled masonry aggregate and EPS (Pavlu et al., 2019)	0.784	20
Compressed earth with cement stabilizer (Uzoegbo, 2020)	0.81-1.04	3.2
Concrete (ASHRAE, 2021)	1.4	28

In recent research efforts, the optimization of materials has been a focal point in enhancing the thermal performance of dry-stacked blocks. The reduction of density emerges as a practical strategy for improving the thermal performance of concrete dry-stacked blocks. The utilization of recycled polymers in the development of dry-stacked blocks not only addresses environmental concerns but also offers high thermal performance. Additionally, perlite is combined with mineral binders to create a dry-stacked block with superior thermal performance. By exploring these various avenues, researchers aim to enhance the R-value of dry-stacked blocks, ultimately contributing to the development of more energy-efficient building envelopes.

2.2 Block spatial configurations

Masonry blocks exhibit a wide range of sizes and spatial configurations, resulting in variations in their thermal performance attributes. According to A. Hendry (2001), masonry blocks encompass a length range of 40-60 cm, a height spectrum of 15-30 cm, and a thickness range of 6-25 cm. An approach to improving the thermal performance of dry-stacked blocks involves the incorporation of insulation layers within the block's composition. Blocks devoid of insulation layers and constructed from a uniform material composition throughout are categorized as "simple blocks". Conversely, blocks featuring insulation layers and composed of at least two components with diverse materials are categorized as "composite blocks". In this section, the influence of changes in shape within each category on the R-value is examined in distinct subsections. Notably, modifications in the shape of simple blocks exhibit a similar impact; therefore, such changes are not addressed within the composite blocks' subsection.

2.2.1 Simple Blocks

The thermal performance of a block is influenced by several factors related to its spatial configuration. These factors include the geometry of block components and cavities, and the arrangement of components, including shells and webs, all of which collectively affect the airflow dynamics within the cells (Martínez et al., 2018). Certain components of masonry units, notably webs (Figure 2), give rise to thermal bridging (Ozel, 2011), which is recognized as a main contributor to thermal inefficiency within blocks. Therefore, careful evaluation of the thermal bridging components is crucial to improving the thermal performance of masonry blocks.

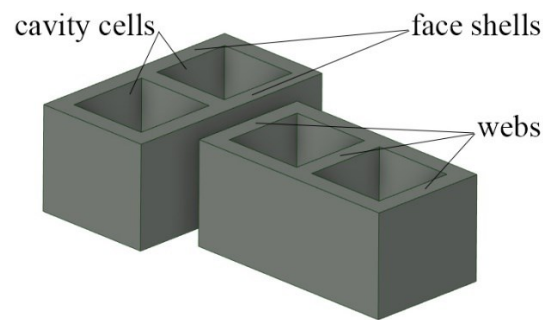


Figure 2. Different components in masonry blocks

Modifying the block's shape can increase thermal bridging and subsequently decrease the R-value. Reducing the cross-sectional area of thermal bridging components enhances the thermal properties of the blocks. One effective approach is to decrease the height of webs, which in turn reduces the overall cross-sectional area and consequently reduces the rate of heat transfer through conduction (Martínez et al., 2018). Studies have shown that decreasing the number of webs from three to two can increase the R-value of blocks by 30% (Bradfield & Szoke, 1992; Urban et al., 2011). Another strategy is the removal of side webs in two-core blocks and changing the shape to an "H" configuration, resulting in an 18% increase in R-value (Martínez et al., 2018). However, it is important to note that changes in webs can sometimes improve one heat transfer mechanism while worsening another. For instance, in hollow blocks, removing webs and widening the cavities decreases conduction but increases the temperature gradient between the two sides of the cavity, leading to enhanced convection and radiation. Therefore, it is crucial to carefully consider the interconnected relationships among various heat transfer mechanisms when making changes to webs or other components of the blocks.

Hollow blocks possess a high R-value due to the air cavities within them, which have significantly lower thermal conductivity than the block material itself (Alhazmy, 2010). In a hollow block, heat transfers through conduction across the solid parts and through convection within the air-filled cavities. Consequently, the thermal properties of hollow blocks are directly related to the number of cavities, their shape, and their arrangements (Bouchair, 2008; del Coz Díaz et al., 2008).

The R-value of hollow blocks can be improved by changing the shape and arrangement of cavities (Antar & Baig, 2009; Bouchair, 2008; del Coz Díaz et al., 2008; Li et al., 2008; Sassine et al., 2020). A study by Sassine et al. (2020) has shown that elliptical cavity shapes increase the air velocity at the edges of the cells compared to rectangular shapes, resulting in enhanced convection within the cell, as presented in Figure 3.1. Increasing the number of cavities inside the blocks has a positive effect on their thermal performance. Erdem et al. (2020) found that five rows of cavities arranged perpendicular to the heat flow improved the thermal performance of the block by 500% compared to a two-core CMU (Figure 3.2). Regarding cavity arrangement, staggered cavities offer a superior R-value compared to aligned ones, with an 89% increase reported (Pierzchlewicz, 1996) as illustrated in Figure 3.3. Antar and Baig (2009) investigated the effect of increasing the number of air cavity rows in blocks with a constant total width on the R-value of the blocks. They reported that increasing the number of rows from one to two (Figure 3.4) and from two to three (Figure 3.5) resulted in a 21% and 28% increase in R-value, respectively. As a result, increasing the cavity rows from one to five is the most influential change to improve the thermal performance of the hollow blocks.

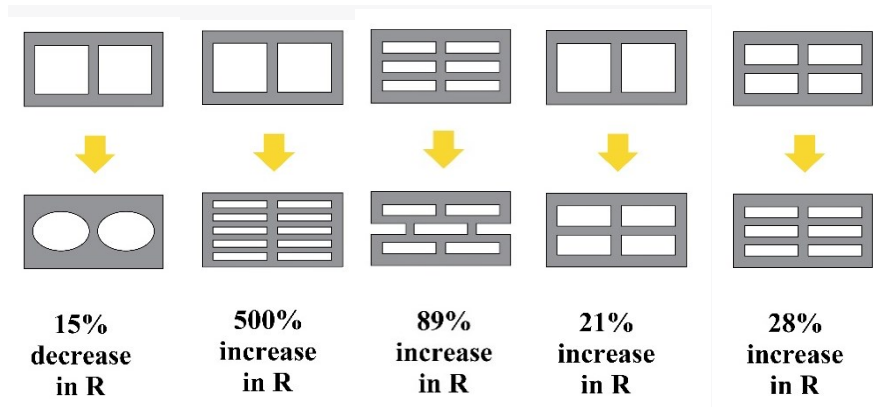


Figure 3. Effect of shape changes on R-value of simple blocks: 1) rectangular to elliptical cavity cells, 2) increasing the cavity rows to five, 3) staggered cavity rows, 4) increasing the cavity rows from one to two, and 5) increasing the cavity rows from two to three

The development of dry-stacked blocks includes a method wherein the hollow blocks are integrated within the wall thickness, consisting of two rows of complementary half-blocks that form a layer of blocks. Examples of such blocks are IITM SILBLOCK, IITM HILBLOCK (Nambiar et al., 2004; Ramamurthy & Nambiar, 2004), Sparlock (R. G. Drysdale & Guo, 1995), and ArmoSystem (2021), as presented in Figure 4. This design approach utilizes the air space between two horizontally adjacent layers as a thermal barrier, thereby slightly enhancing the thermal performance of the masonry system. Consequently, when comparing complementary half-blocks with solid blocks, these types of blocks exhibit higher R-value.

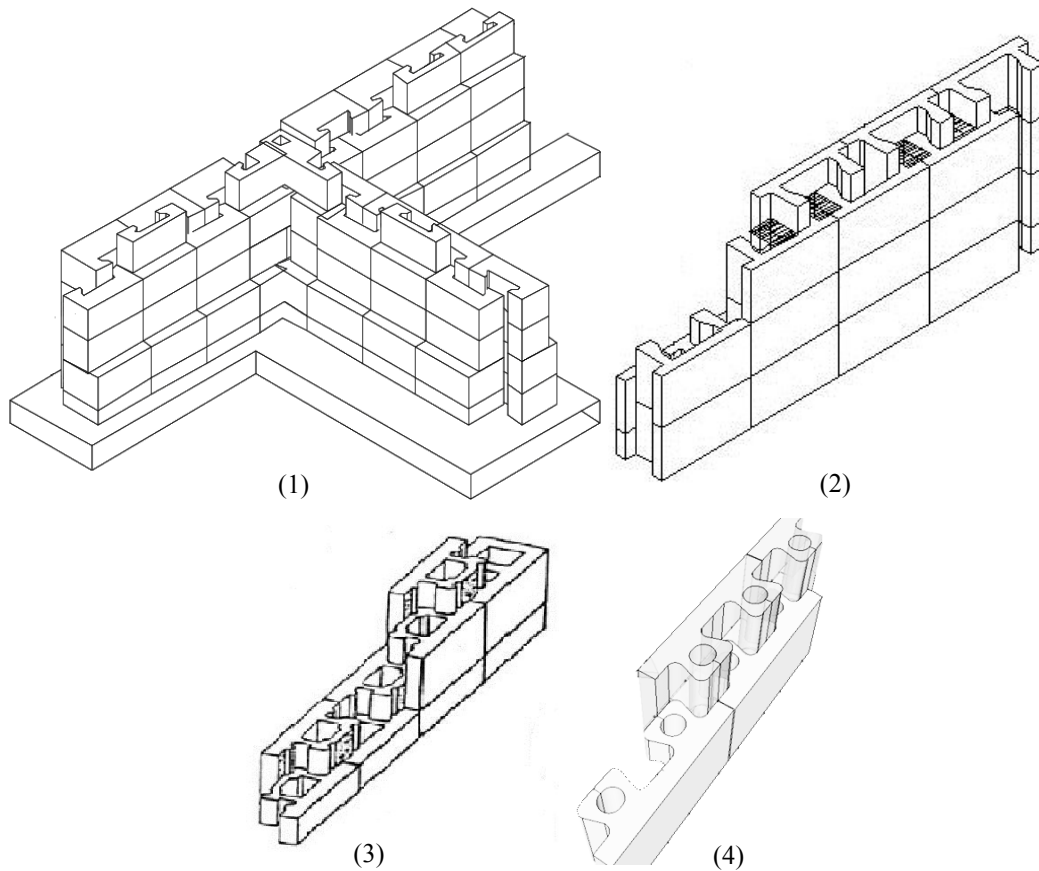


Figure 4. Walls made of 1) IITM SILBLOCK, 2) IITM HILBLOCK, 3) Sparlock, and 4) Armo System

2.2.2 Composite Blocks

Modifications to the shape of composite blocks can significantly affect their thermal performance. Specifically, filling the cavities with different materials (Al-Hazmy, 2006; Martínez et al., 2018; Mezrhab et al., 2006; Varol et al., 2009) and incorporating obstacles within the cavities (Alhazmy, 2010; Bilgen, 2002; Da Silva & Gosselin, 2005) have been shown to enhance the R-value of these blocks. This subsection focuses on examining the impact of such modifications on the R-value of composite blocks.

The presence of inclined folded sheets within the cavities of blocks influences thermal performance. Alhazmy (2010) presented that these sheets inside the cavities suppress convection currents by creating smaller cells (Figure 5). This method increased the R-value of the block by 37-42%, depending on the material, size, location and number of sheets. However, there exists an

upper limit to the number of sheets within the cavities; surpassing eight sheets increased heat transfer, indicating a shift towards conduction as the dominant heat transfer mechanism. In summary, the incorporation of inclined folded sheets within the cavities of hollow blocks improves the thermal performance; however, an upper limit of eight sheets must be maintained.

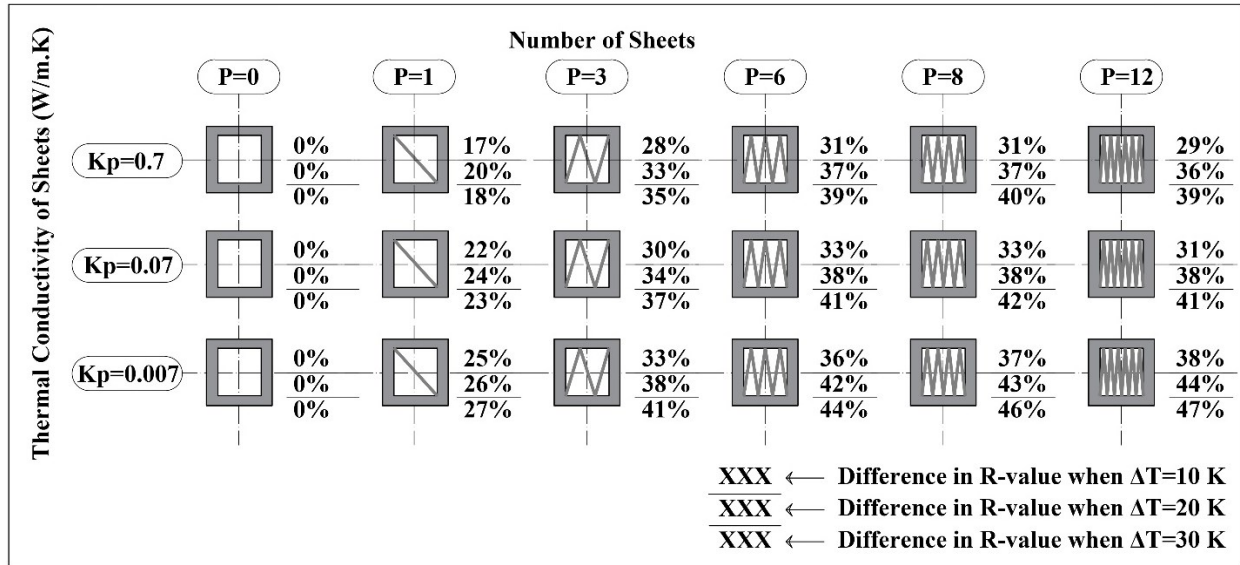


Figure 5. Effects of inclined folded sheets within the cavities of blocks on their heat flux values

Including polystyrene bars and porous materials in the cavities improves thermal performance. Filling cavities with polystyrene bars leads to a 36% decrease in heat transfer in hollow blocks (Al-Hazmy, 2006). This is because heat convection through the cavities can be significantly reduced by filling them with insulating materials. Filling the cavities with porous media, as studied by Varol et al. (2009), results in a 50-60% reduction in heat transfer. Hence, incorporating polystyrene bars and porous materials within cavities emerges as a practical strategy to enhance thermal efficiency.

Martínez et al. (2018) conducted comprehensive research on composite blocks, utilizing experiments and numerical simulations. Their investigation encompassed different hollow block geometries and insulation materials within cavities (Figure 6). This study considered six block configurations, four insulation types, and two block densities, resulting in 48 distinct models. Transitioning from unit type 1 to unit type 6 correlated with decreasing cross-sectional areas of thermal bridges, leading to an increase in the R-value. Reducing conduction enhanced the temperature gradient within the cavities, resulting in increased convection and radiation. The study

highlighted the efficacy of employing cardboard as an obstacle over rigid EPS. Moreover, including rigid EPS and foam in multicore blocks yielded marginal improvements. The most substantial thermal performance enhancement was observed in the H-shaped unit with injected foam and normal weight, demonstrating a remarkable 407% increase in R-value. Increasing the number of horizontal air cavities from one to three and incorporating cardboard sheets led to a 70% increase in R-value. Notably, filling the cavities with foam demonstrated an effect 21 times greater than mere removal of exterior side webs. This underscores the importance of including insulation, which transforms a simple block into a composite block rather than solely modifying the shape of a simple block.

It is noteworthy that strategies enhancing R-value via component shape and arrangement exert more than double the impact on medium-weight concrete compared to normal-weight concrete. Therefore, optimal thermal performance in masonry blocks mandates careful consideration of shape, material and their interrelationship.

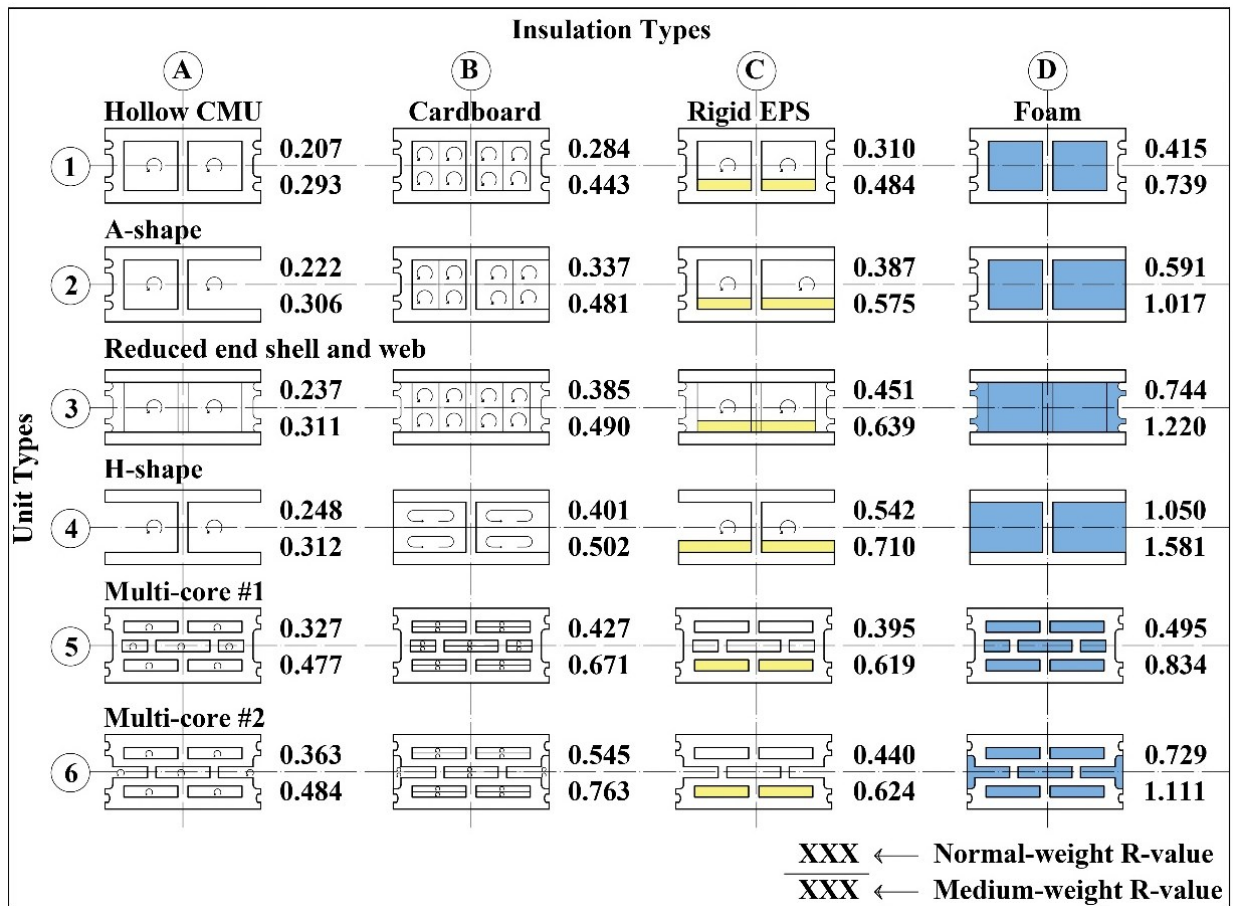


Figure 6. Effect of different shapes, insulations, and densities on R-value (Martínez et al., 2018)

The findings of Martínez et al. (2018), reveal that none of the R-values they obtained for composite blocks align with cold climate zones applications. The highest R-value recorded is 1.58 m²·K/W attributed to the foamed H-block, significantly falling short of the minimum R-value requirement for cold climate zones. Consequently, not all composite blocks are suitable for cold climate zones.

Table 2 provides a summary of the effects of shape changes on the R-value of masonry blocks, organized according to the level of their influence.

Table 2. Shape change effects on R-value of masonry blocks arranged from the highest positive effect to the highest negative effect.

Change	Effect on R-value of the block
Increase the number of cavity rows from one to five (Erdem et al., 2020)	500% increase
Change two-core to H-shape and inject foam inside (Martínez et al., 2018)	407% increase
Aligned cavities rather than solid block (Pierzchlewicz, 1996)	109% increase
Staggered cavities rather than aligned ones (Pierzchlewicz, 1996)	89% increase
Increase the number of parallel-to-length air cavities from one to three and place cardboard sheets in the cavities (Martínez et al., 2018)	70% increase
Fill the voids with a porous media (Varol et al., 2009)	50-60% increase
Place inclined folded sheets inside the cavities (Alhazmy, 2010)	37-42% increase depending on material, size, location and number of sheets
Place polystyrene bars in the cavities (Al-Hazmy, 2006)	36% increase
Change in holes arrangement from cavities by side to cavities parallel (Sassine et al., 2020)	35% increase
Decrease in webs number from three to two (Bradfield & Szoke, 1992; Urban et al., 2011)	30% increase
Increase the number of horizontal air cavities from two to three (Antar & Baig, 2009)	28% increase
Two-core block rather than solid block (Abdou & Murali, 1994)	25% increase
Increase the number of horizontal air cavities from one to two (Antar & Baig, 2009)	21% increase
Change a two-core to H-shape (Martínez et al., 2018)	18% increase
Increase the number of horizontal air cavities from five to six (Antar & Baig, 2009)	2.25% increase
Elliptical void shapes rather than rectangular ones (Sassine et al., 2020)	15% decrease
Increase the number of sheets to more than eight (Alhazmy, 2010)	40-50% decrease

Numerous research endeavors have focused on altering block shapes to enhance their thermal efficiency. The arrangement of voids within the blocks impacts airflow velocity and subsequently heat transfer rates. Circular voids, for instance, accelerate air currents within them, leading to

increased heat transfer. Filling these cavities with foam has demonstrated to be highly effective. As a result, the conversion of a simple block into a composite one, achieved by integrating insulation into the block structure, proves to be more effective than solely altering the shape of a simple block.

2.3 Veneer Ties

Veneer ties are essential components in cavity wall systems, commonly used in Canada. They serve to connect the veneer, which is the outer layer, to the inner or backup wall. These ties play a dual role: providing structural support and preventing any unintended movement of the veneer. In Canada, two primary types of veneer ties are employed: prescriptive ties and proprietary ties (CSA-A370:14, 2018; B. G. Drysdale & Hamid, 2005).

Prescriptive ties are nonadjustable and have certain limitations due to their fixed shape. They are not suitable when there are varying heights of mortar joints in the two layers of a cavity wall. In contrast, proprietary ties are adjustable and offer greater flexibility in their application. Examples of prescriptive and proprietary ties are depicted in Figure 7.

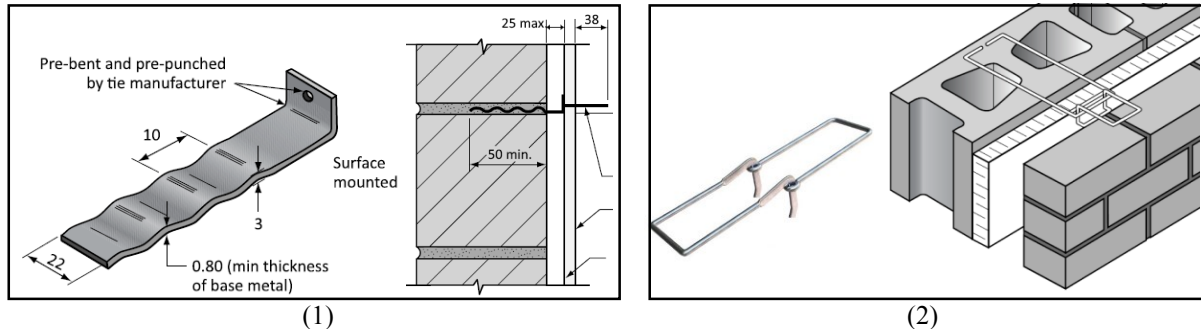


Figure 7. Examples of 1) prescriptive tie, 2) Proprietary tie (CSA-A370:14, 2018)

Steel veneer ties introduce multiple sources of thermal bridging in wall assemblies. The extent of this thermal bridging depends on factors such as the material, shape, and spacing of these ties (T. G. Theodosiou et al., 2015). Notably, the impact of thermal bridging becomes more pronounced when insulation is continuous (Huygen & Sanders, 2022).

Research findings by Love (2011) suggested that steel ties, with horizontal spacing of 40 cm and vertical spacing of 60 cm, could reduce the R-value of a wall by approximately 15%. Finch et al. (2013) conducted an extensive investigation into the influence of tie material and insulation levels

on the thermal performance of masonry wall assemblies (Table 3). They concluded that as the R-value of the insulation increases, the R-value of the wall decreases, signifying that the negative effect of ties on the thermal performance of the wall is more prominent when the insulation has a higher R-value.

Table 3. Changes in R-value of the wall assembly based on the material of ties

L-shape tie type	R-value of Exterior Insulation (m²·K/W)	Galvanized Steel	Stainless Steel	Basalt Fiber
With holes	3.5	-21%	-7%	-0.5%
Without holes	3.5	-26%	-11%	
With holes	1.75	-14%	-6%	-0.2%
Without holes	1.75	-19%	-9%	

In response to increasing demands for improved building envelope performance, changes have occurred in the materials and configurations of wall ties over recent decades. These changes aim to mitigate thermal bridging effects while maintaining structural integrity. Shao (2021) conducted an investigation into various ties parameters, including material and spacing, and their impact on the thermal performance of masonry walls. The study revealed a potential 12% improvement in the wall's R-value by doubling the ties' spacing in one direction. However, the primary determinant of the wall's R-value was identified as the tie material. Specifically, the utilization of ties constructed from composite materials, emerged as a viable solution to reduce the substantial thermal bridging associated with steel ties.

Research conducted by Asava and Rusu (2017) explored the impact of steel and fiberglass ties on the R-value of masonry wall assemblies. Their findings indicated that steel ties led to a notable 16% reduction in the R-value of the wall, while fiberglass ties had a much smaller effect, reducing the R-value by only 1%. Glass fiber reinforced polymer (GFRP) ties emerged as the optimal choice for enhancing the R-value of the wall, nearly eliminating the thermal bridging effect (Shao, 2021). However, it's essential to note that composite ties tend to be more expensive than steel ties, which has limited their application in cavity wall construction.

2.4 Insulation

Insulation predominantly determines the R-value of wall assemblies (Schumacher et al., 2013). The specifications of insulation in the building envelope, such as thickness and material, involve

achieving a balance among insulation cost, future conditioning energy costs, and maintenance expenses. Factors influencing insulation design include the thermal performance required for the wall assembly, climate conditions, and cost considerations.

Insulation can be applied in three positions relative to the wall: interior, integral, and exterior (NCMA, 2013). Interior insulation requires less maintenance but exposes the wall to external weather conditions, and the insulation does not contribute to the wall's durability. Integral insulation is positioned between two thermal mass layers, such as block holes or wythes of a cavity wall. In lightweight concrete blocks, integral insulation can enhance the R-value by up to 85% (McCall, 1985). While continuous integral insulation eliminates thermal bridging, it necessitates a special manufacturing process for block or wall. Finally, exterior insulation, covering the outer surface of the wall, addresses thermal bridging and provides weather protection. However, exterior insulation requires mesh and a protective finish for durability. Different insulation positions in a wall assembly are illustrated in Figure 8.

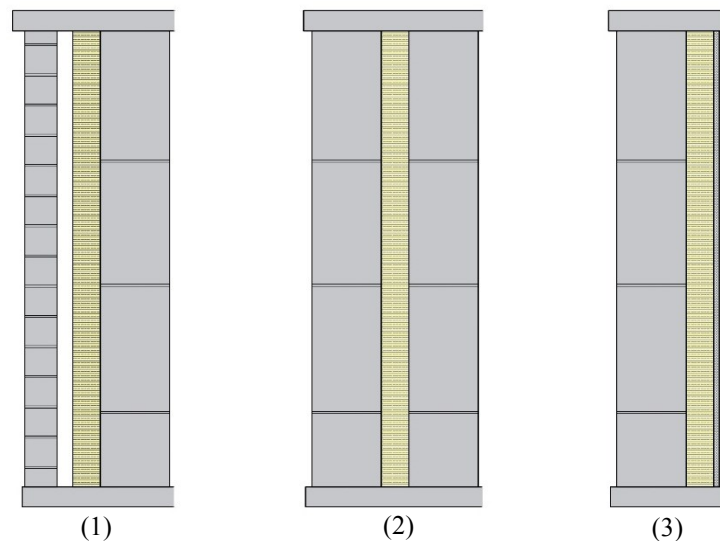


Figure 8. Different locations of insulation in a wall assembly: 1) exterior insulation, 2) integral insulation, and 3) interior insulation

Conventional insulation materials presently in use encompass stone wool, glass wool, expanded polystyrene, extruded polystyrene, polyurethane, cellulose, and expanded perlite. Table 4 provides an overview of the characteristics of these conventional insulation materials. The subsequent paragraphs provide detailed insights into each material:

Stone wool: Derived by melting rocks and spinning the resulting fibers into a bonded material (Fangueiro, 2011), stone wool has a thermal conductivity ranging from 0.033 to 0.04 W/m·K and a density of 40-200 kg/m³. Stone wool is cost-effective, easy to handle, and maintains insulation performance, making it a common choice for cavity walls (Schiavoni et al., 2016).

Glass wool: Produced by mixing glass and sand at high temperatures and transforming the mixture into fibers, glass wool exhibits thermal performance similar to stone wool (Fangueiro, 2011).

Expanded polystyrene (EPS): Manufactured by evaporating a mixture of pentane and polystyrene grains, EPS has a thermal conductivity of 0.031-0.037 W/m·K. However, its insulation properties can be reduced by moisture (Lakatos & Kalmár, 2013).

Extruded polystyrene (XPS): Produced by extruding melted polystyrene grains, XPS shares thermal properties with EPS but is less water absorbent and more expensive (Fangueiro, 2011).

Polyurethane: Created through a chemical reaction between polyisocyanate and polyol, polyurethane is applicable as panels or spray foams, with a thermal conductivity range of 0.022 to 0.040 W/m·K (Kuhn et al., 1992). Its thermal performance depends on particle sizes, with smaller particles contributing to higher performance (Wu et al., 1999).

Cellulose: Formed by mixing recycled papers, wood fibers, and chemical composites, cellulose is commonly blown into wall cavities (Hurtado et al., 2016). Its thermal conductivity ranges from 0.037 to 0.042 W/m·K, and the quality and texture of the paper impact its thermal performance (Kwon & Yarbrough, 2004).

Expanded Perlite: Produced by heating perlite at high temperatures (Singh & Garg, 1991), expanded perlite can be used as loose foam or panels. With a thermal conductivity between 0.040 and 0.052 W/m·K, it boasts the lowest thermal conductivity among mineral insulation materials (Topçu & Işıkdag, 2007; Zukowski & Haese, 2010).

Table 4. characteristics of conventional insulation materials

Insulation material	Density (kg/m³)	Thermal Conductivity (W/m·K)
Stone wool	40-200	0.033-0.040
Glass wool	15-75	0.031-0.037
Expanded Polystyrene	15-35	0.031-0.038
Extruded Polystyrene	32-40	0.032-0.037
Polyurethane	15-45	0.022-0.040

Cellulose	30-80	0.037-0.042
Expanded Perlite	80-150	0.040-0.052

In summary, the exploration into conventional insulation materials has revealed a spectrum of options with distinct characteristics catering to diverse thermal requirements. Stone wool emerges as a cost-effective and versatile choice, well-suited for cavity walls due to its ease of handling and reliable insulation performance. EPS and XPS provide alternatives with varying water absorbency and cost considerations. Finally, expanded perlite stands out with the lowest thermal conductivity among mineral insulation materials.

2.5 Cavity Space

The connection between the veneer and the backup wall typically accounts for a specific space between the veneer and insulation in cavity walls. This air cavity space serves the purpose of drying moisture within the cavity and impeding moisture penetration into the building's interior through the capillary break effect (Ibañez-Puy et al., 2017; Ismaiel et al., 2022). Weep holes, positioned at the top and bottom of the veneer, facilitate the ventilation of air within the cavity through its connection to the external environment, which is crucial for effective moisture management (Figure 9). Proper moisture management is essential to prevent mold growth, which can damage the building and reduce its durability (Sanjuan et al., 2011; T. G. Theodosiou et al., 2015).

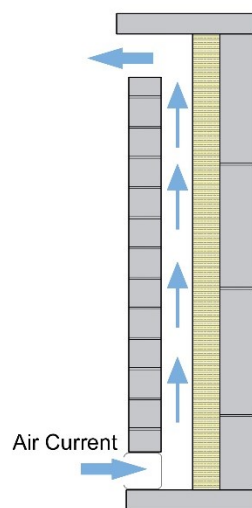


Figure 9. Weep holes in a ventilated cavity wall

It is important to note that the presence of air ventilation in the cavity reduces the insulating properties, thereby diminishing the overall R-value of the wall assembly (ISO-6946, 2017). Sanjuan et al. (2011) conducted simulations to compare the thermal performance of ventilated and unventilated cavity walls. Their findings revealed that ventilated air cavities could reduce the R-value of the wall assembly by over 50% in cold weather conditions. Mingotti et al. (2011) suggested that in cold climate zones, minimizing the dimensions of weep holes is advisable to reduce excessive heat loss through the building envelope. Consequently, despite the effective moisture control provided by cavity spaces, the decrease in the R-value resulting from ventilated air is an inherent concern.

The R-value of insulation has a significant effect on the R-value of the cavity space. A higher insulation R-value results in a substantially greater enhancement in the R-value of the cavity space. Shao (2021) demonstrated that incorporating insulation with an R-value of $0.88 \text{ m}^2 \cdot \text{K}/\text{W}$ improved the thermal resistance of the cavity space by 26%. As a result, insulation with higher R-values significantly enhances the cavity space R-value.

2.6 Blocks for Cold Climate Zones

The changes in the configurations of simple blocks can have a large impact on their R-value. Exterior walls in moderate climates can be constructed with the improved blocks without additional thermal insulation. However, in cold climate zones, the attainment of the requisite R-values for exterior walls via simple blocks alone becomes unfeasible. In such cases, the incorporation of continuous thermal insulation becomes imperative, as it predominantly determines the R-value of the wall assemblies (Schumacher et al., 2013). Blocks with integral insulation can offer exceptional R-values, rendering them highly suitable for cold climate zones. An example of such an insulated block is the LiaTop50 (Liapor, 2022), which benefits from the removal of webs and the inclusion of an insulation layer to mitigate thermal bridging (Figure 10). This design features two load-bearing shells connected to the middle insulation layer via indentations. This block with integral insulation effectively minimizes the thermal bridges, thereby substantially improving the thermal performance.



Figure 10. Liatop50 insulated block (Liapor, 2022)

In a study by Al-Jabri et al. (2005), a comparative analysis was performed among three block types: a hollow concrete block with EPS bead aggregates in its mixture (referred to as Polyblock1), a block with integral insulation composed of two concrete face-shells interconnected by EPS insulation featuring indentations (referred to as Polyblock2), and a conventional two-core block. These blocks are presented in Figure 11. The findings revealed that Polyblock2 exhibited a 61% reduction in thermal conductivity compared to the conventional block, nearly matching the thermal conductivity of Polyblock1. Moreover, Polyblock2 showcased a threefold enhancement in structural performance when compared to Polyblock1. According to the findings of this study, the intertwining of load-bearing components with thermal insulation parts within a single piece facilitates heat transfer and compromises the R-value. Furthermore, while the utilization of lightweight materials can increase the R-value, it mostly comes at the expense of structural performance. Consequently, separation of structural and insulation components by utilizing an integral insulation considerably enhances the R-value of the block.

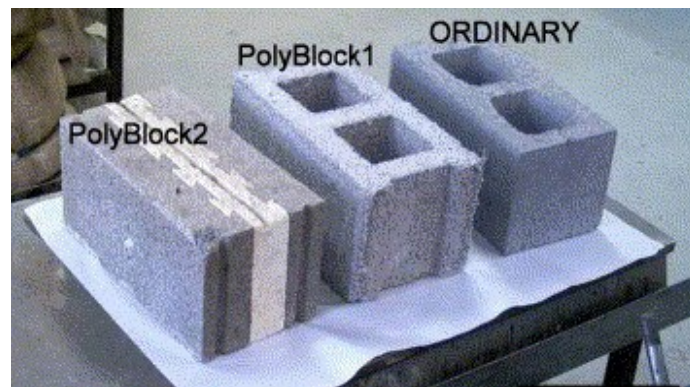


Figure 11: Investigated blocks by Al-Jabri et al. (2005)

In cold climate zones, the consideration of masonry cavity walls or masonry double walls has emerged to enhance energy efficiency and minimize moisture intrusion into the building's interior (Zhang et al., 2016). The design of a cavity within the wall aims to facilitate moisture drying within the cavity and establish a capillary break to prevent moisture from reaching the inner layer of the wall (Ismail et al., 2022). An example of an insulated cavity block is OneStep (2022), which offers an R-value ranging from 3.5 to 4.5 $\text{m}^2\cdot\text{K}/\text{W}$ (Figure 12). The inclusion of a weep cavity acts as a moisture barrier, further improving the block's thermal performance. Consequently, masonry cavity walls prove practical in cold climate zones due to the vented air gap's positive influence on the thermal performance of the blocks.

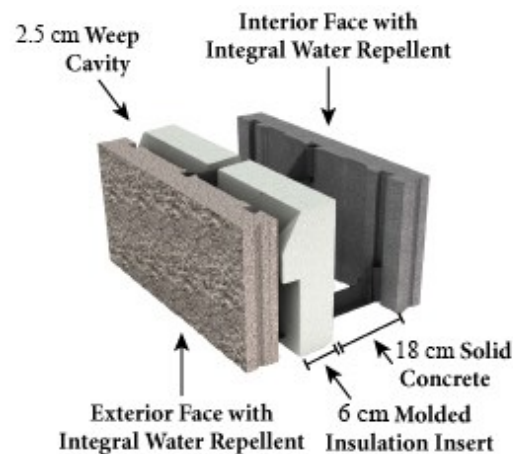


Figure 12. One Step cavity block

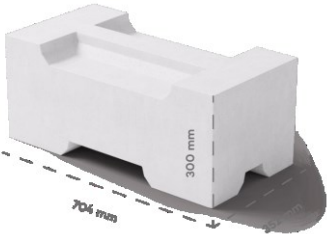



In summary, blocks with integral insulation and cavity walls are effective techniques for achieving thermal efficiency in cold climate zones. Blocks with integral insulation provide high R-values by providing continuous insulations throughout the masonry wall assembly. Additionally, cavity walls incorporate an air layer between two walls to facilitate moisture drying and increase the R-value. These approaches demonstrate their effectiveness in addressing the specific challenges of cold climate zones while enhancing the overall thermal performance of masonry blocks.

2.7 Existing Dry-Stacked Blocks

In order to comprehensively evaluate the current state of dry-stacked masonry blocks, this section conducts a comprehensive survey of existing dry-stacked blocks. The assessment encompasses blocks available in the commercial market and those developed through research initiatives. This

survey is further detailed through the presentation of findings in separate tables. Specifically, Table 5 provides an overview of eight unique simple dry-stacked blocks, while Table 6 offers insights into the characteristics of 12 composite dry-stacked blocks.

Table 5. Existing simple dry-stacked blocks

Block	Shape	Material	R-value, (m ² .K/W)
System3E (2021)		Perlite with mineral binders	5.05
TPB (2022)		Cement and recycled EPS	2.8-5.6
E-Zblock (2021)		Aerated concrete	1.95-4
Litebuilt (2022)		Aerated concrete	0.28-1.54

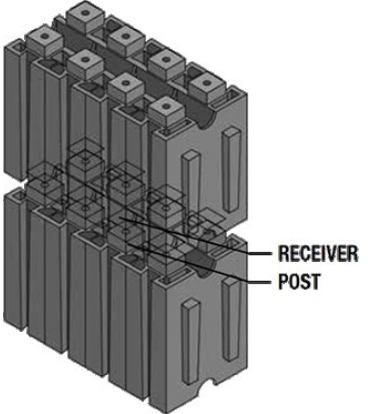


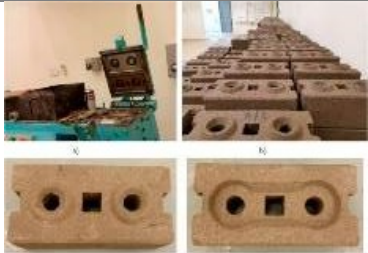
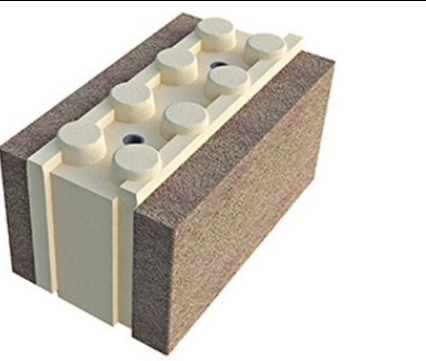



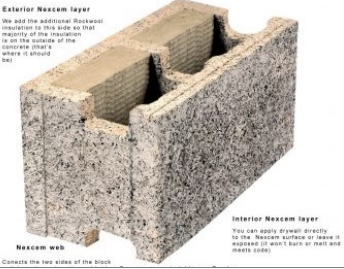

<p>Lok-N-Blok (2021)</p>		<p>Polypropylene polymer with 30% of recycled content</p>	<p>1.05</p>
<p>Eco-friendly hybrid block (Shakir et al., 2020)</p>		<p>Cement and POCP</p>	<p>0.44-0.92</p>
<p>CEB stabilized with fly ash (Leitão et al., 2017)</p>		<p>Earth and fly ash</p>	<p>0.34</p>
<p>Rubberized concrete interlocking block (Al-Fakih et al., 2022)</p>		<p>Concrete and crumb rubber particles</p>	<p>0.171</p>

Table 6. Existing composite dry-stacked blocks

Block	Shape	Material	R-value, (m ² .K/W)
<p>EPIC-Block (2022)</p>		<p>Concrete and closed cell insulating foam core</p>	<p>7</p>

Gablok (2021)		OSB of Wood and EPS with graphite additive	6.66
Isotex (2021)		Wood-cement and Neopor insulation	2.94-6.66
Isospan (2022)		wood-concrete	0.57-6.51
Nexcem (2022)	 <p data-bbox="483 1157 576 1220">Exterior Nexcem layer We add the additional dimensional insulation to this side so that majority of the insulation is on the outside of the concrete block where it should be!</p> <p data-bbox="711 1367 824 1409">Interior Nexcem layer You can easily do wall details to the Nexcem surface of leave it exposed to water, sun or heat and freeze cycles!</p> <p data-bbox="483 1398 548 1409">Nexcem web Connects the two sides of the block.</p>	cement-bonded wood fiber and expanded cork insulation	1.41-6.34
ComfortBlock (2022)		G-mix concrete and EPS	5.3

Faswall (2022)		85% mineralized wood fiber and 15% Portland and slag cement and Polyisocyanurate expanded foam as insulation	2.1-4.48
HempcreteBlock (2022)		Hemp and concrete	3.7
Steko (2022)		Wood, interior Cellulose fibre	2.94
Polycare (2021)		Polymer concrete and EPS	2.7


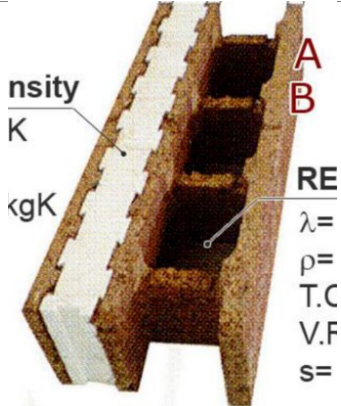
<p>Almanaratain sandwich block (Almanaratain, 2022)</p>		<p>Lightweight concrete and EPS insulation</p>	<p>1.56</p>
<p>Wood-cement block (Nardi et al., 2016)</p>		<p>Wood-cement and EPS</p>	<p>4.16</p>

Table 5 and Table 6 reveal that only four research studies have been dedicated to the investigation of the thermal performance of dry-stacked blocks (Al-Fakih et al., 2022; Leitão et al., 2017; Nardi et al., 2016; Shakir et al., 2020). In addition, an assessment of the R-values derived from these studies indicates that these blocks are mostly not applicable to cold climate zones. This comprehensive evaluation of the existing landscape of dry-stacked masonry blocks underscores the imperative need for further research and development endeavors aimed at aligning these blocks with the specific requirements of cold climate zones.

Existing dry-stacked blocks, produced from a diverse range of dimensions, densities and insulation thicknesses, exhibit a spectrum of thermal characteristics as presented in Table 7. The examination of dimensions within the context of existing dry-stacked blocks highlights the span of lengths between 25 and 125 cm, heights ranging from 10 to 32 cm, and thicknesses varying from 12 to 44 cm for existing dry-stacked blocks.

Table 7. Characteristics of existing dry-stacked blocks

Block	Dimension, L×H×t (cm)	Insulation thickness (cm)	Density, ρ (kg/m ³)	R-value, (m ² .K/W)
System3E (2021)	70.4×30×35.2	No insulation	430	5.05
TPB (2022)	122×30.5×15-25	No insulation	244-258	2.8-5.6
E-Zblock (2021)	122×30.5×25	No insulation	240.3	1.95-4
Litebuilt (2022)	40×20×20	No insulation	600-1100	0.28-1.54
Lok-N-Blok (2021)	31×23×15.5	No insulation	253	1.05
Eco-friendly hybrid block (Shakir et al., 2020)	25×10×12	No insulation	853-1561	0.44-0.92
CEB stabilized with fly ash (Leitão et al., 2017)	28×10×14	No insulation	1800	0.34
Rubberized concrete interlocking block (Al-Fakih et al., 2022)	25×10.5×12.5	No insulation	1890	0.171
EPIC-Block (2022)	-	-	-	7
Gablok (2021)	60×30×30	26.4	140	6.66
Isotex (2021)	50×25×20-44	0-20	510	2.94-6.66
Isospan (2022)	125×25×15-36.5	0-16.5	1334-1420	0.57-6.51
Nexcem (2022)	61or91×30.5×15-35	3.8-17.8	680-800	1.41-6.34
ComfortBlock (2022)	30.5×20.3×40.6	3×6.43	989	5.3
Faswall (2022)	61×20×30	7.5	545-641	2.1-4.48
HempcreteBlock (2022)	54.2×20.3×27.2	No insulation	434	3.7
Steko (2022)	64×24-32×16	No insulation	280	2.94
Polycare (2021)	40×31×20	16	500-550	2.7
Almanaratain sandwich block (Almanaratain, 2022)	40×20×20	3×2	1425	1.56
Wood-cement block (Nardi et al., 2016)	80×20×37.5	10	1183	4.16

Note:

-: The presence of this symbol beneath a specific feature indicates that the block lacks information about that feature.

In Table 8, the permissible climate zones attributed to the blocks which are derived from NECB (2020) are presented. Blocks with R-values lower than 3.45 m².K/W, such as Polycare (2021), Lok-N-Blok (2021), and CEB stabilized with fly ash (Leitão et al., 2017), are considered not applicable (N/A) in cold climate zones and require additional insulation to meet the standards. Table 8. Permissible climate zones for existing dry-stacked blocks

Block	R-value, (m ² .K/W)	Applicable climate zones					
		4	5	6	7A	7B	8
System3E (2021)	5.05	*	*	*	*		

TPB (2022)	2.8-5.6	*	*	*	*	*
E-Zblock (2021)	1.95-4	*	*			
Litebuilt (2022)	0.28-1.54					N/A
Lok-N-Blok (2021)	1.05					N/A
Eco-friendly hybrid block (Shakir et al., 2020)	0.44-0.92					N/A
CEB stabilized with fly ash (Leitão et al., 2017)	0.34					N/A
Rubberized concrete interlocking block (Al-Fakih et al., 2022)	0.171					N/A
EPIC-Block (2022)	7	*	*	*	*	*
Gablok (2021)	6.66	*	*	*	*	*
Isotex (2021)	2.94-6.66	*	*	*	*	*
Isospan (2022)	0.57-6.51	*	*	*	*	*
Nexcem (2022)	1.41-6.34	*	*	*	*	*
ComfortBlock (2022)	5.3	*	*	*	*	*
Faswall (2022)	2.1-4.48	*	*	*		
HempereteBlock (2022)	3.7	*	*			
Steko (2022)	2.94					N/A
Polycare (2021)	2.7					N/A
Almanaratain sandwich block (Almanaratain, 2022)	1.56					N/A
Wood-cement block (Nardi et al., 2016)	4.16	*	*			

Notes:

N/A: The presence of this symbol indicates that the block is not applicable for cold climate zones.

-. The presence of this symbol beneath a specific feature indicates that the block lacks information about that feature.

The existing dry-stacked blocks are stabilized by different methods including interlocking mechanism, grouting, rebars, adhesives and vertical dowels as presented in Table 9.

Table 9. Stabilization and compressive strength of existing dry-stacked blocks

Block	Stabilization method					Compressive strength, σ_c (MPa)
	Interlocking mechanism	Grouting	Rebars	Adhesive	Vertical dowels	
System3E (2021)	☐					1.5
TPB (2022)		☐	☐			-
E-Zblock (2021)		☐				0.1
Litebuilt (2022)			*			2-8.5
Lok-N-Blok (2021)	*		*			8.2
Eco-friendly hybrid block (Shakir et al., 2020)	*					5-14.5
CEB stabilized with fly ash (Leitão et al., 2017)	*					3
Rubberized concrete interlocking block (Al-Fakih et al., 2022)	*	*				10.99 for grouted and

					5.83 for ungrouted
EPIC-Block (2022)	*		*		0.384
Gablok (2021)	*				0.15
Isotex (2021)		*	*		35-49
Isospan (2022)		*	*		-
Nexcem (2022)		*	*		2
ComfortBlock (2022)		*	*	*	-
Faswall (2022)		*	*		-
HempcreteBlock (2022)			*	*	-
Steko (2022)				*	-
Polycare (2021)			*		-
Almanaratain sandwich block (Almanaratain, 2022)				*	7
Wood-cement block (Nardi et al., 2016)		*	*		-

Notes:

□: The presence of this symbol beneath a specific feature indicates that the block includes that feature.

-: The presence of this symbol beneath a specific feature indicates that the block lacks information about that feature.

Simple blocks, manufactured from diverse materials including perlite and AAC, present varied R-values and structural performances. Notably, only three of the eight simple blocks satisfy the requisite R-value for cold climate zones (E-Zblock, 2021; System3E, 2021; TPB, 2022). These three blocks are constructed using materials characterized by low thermal conductivities, substantially mitigating the thermal bridging effects and consequently contributing to high R-values. However, these simple blocks tend to be less structurally robust, making them more appropriate for one-story buildings. As a result, only a limited number of simple blocks meet the necessary R-value standards for cold zone applications, albeit with a trade-off involving diminished structural performance.

The examined composite blocks, totaling 12, are predominantly suitable for cold zone applications. Only a subset of three blocks among them is not compatible with such zones (Almanaratain, 2022; Polycare, 2021; Steko, 2022). It's worth noting that these three blocks have smaller thicknesses compared to the other investigated composite blocks. The Almanaratain sandwich block incorporates scattered cavities filled with EPS insulation, improving its thermal performance. However, thermal bridging still exists in the structural component, thereby compromising the overall thermal performance. Increasing the block's thickness by 5 cm yields only a 20%

improvement in its R-value, revealing the limitations of this strategy. On the other hand, Polycare predominantly comprised of EPS with a polymer concrete cover. By increasing the thickness by 5 cm, the R-value enhances by 63%, making the block suitable for cold climate zones. A similar scenario pertains to Steko, which could achieve the requisite R-value for cold climate zones through a relatively small increase in thickness. As a result, except for the Almanaratain sandwich block, all the composite blocks are thermally efficient for cold zone application.

Among the evaluated composite dry-stacked blocks, several exhibit remarkable thermal performances with high R-values. EPIC-Block (2022) with an integral insulation has the highest R-value among the blocks. Next, Isotex (2021) and Gablok (2021) deliver exceptional R-values of $6.66 \text{ m}^2 \cdot \text{K}/\text{W}$, rendering them suitable for cold climate zones. The unique material composition of Gablok (2021), utilizing wood and EPS, contributes to its elevated R-value, albeit at the cost of a low compressive strength of 0.5 MPa. Isotex (2021), comprised of woodcrete and Neopor, emerges as a versatile choice with both high thermal and structural performance. Hence, the assessed blocks showcase promising thermal capabilities for cold climate zones.

The rubberized concrete interlocking block of Al-Fakih et al. (2022), the eco-friendly hybrid block of Shakir et al. (2020), and Isotex (2021) exhibit the three highest compressive strengths. The rubberized concrete interlocking block derives its strength from the material composition and grouting, while the eco-friendly hybrid block achieves high structural performance through its material properties and interlocking mechanism. Woodcrete-based blocks like Isotex (2021) function as ICFs, and despite their initial lack of structural strength, they can attain impressive compressive strengths of up to 49 MPa through the reinforcement and grouting processes.

Among the examined blocks, Isotex (2021) emerges as the most promising dry-stacked block in both the market and research studies due to its high thermal and structural performance. Additionally, it is lightweight and provides sufficient space for plumbing and reinforcement, making it a versatile option for construction applications.

2.8 Conclusion

A comprehensive literature review on the thermal performance of dry-stacked masonry blocks was presented in this chapter. Throughout this review, a thorough investigation into material composition, block shape, ties, insulation, cavity spaces, and their impact on thermal performance

was carried out. Furthermore, this chapter addressed the critical considerations for cold climate zone applications while also evaluating the properties of existing dry-stacked masonry blocks.

Notably, it was observed that perlite with mineral binders demonstrated the lowest thermal conductivity among all the materials used in dry-stacked blocks, resulting in higher R-value albeit with a trade-off involving diminished structural performance. Additionally, the employment of novel materials such as cement and POCP mixture, rubberized concrete, and concrete including recycled masonry aggregates and EPS showed promise in enhancing both thermal performance and compressive strength. Nevertheless, it should be acknowledged that the discussed materials are relatively new and still being investigated, limiting their widespread use and resulting in higher costs.

The review also underscored the significance of incorporating insulation into the block structure. Filling block cavities with foam proved to be more impactful in enhancing thermal performance than the removal of exterior side webs. This underlined the pivotal role of insulation within the block configuration.

In cold climate zones, the integral insulation and cavity walls played crucial roles in achieving thermal efficiency. Hence, the utilization of composite blocks with integral insulation offered significant advantages for buildings located in cold climate zones. In such cases, the thermal performance of masonry assemblies with integral insulation was primarily governed by the insulation component.

In this study, concrete is chosen for the structural components due to its significantly high compressive strength in comparison to alternative materials. Concrete is not only cost-effective but also widely available. Furthermore, two key features, integral insulation and cavity space, are incorporated into the development of two new dry-stacked blocks.

In the subsequent chapters, a comprehensive investigation is conducted to explore the utilization of composite and simple blocks in cold climate zones.

3 Design Development of New Dry-Stacked Blocks

Two masonry blocks A and B, are meticulously designed, drawing upon insights garnered from the extensive literature review and technology survey. The design process is underpinned by a comprehensive consideration of vital specifications, with a particular focus on meeting the demands of cold climate zones and the requisites of dry-stacked block construction.

In regions characterized by cold climates, the implementation of integral insulation and cavity walls assumes a pivotal role in achieving thermal efficiency. As elucidated in the preceding section, the utilization of composite blocks featuring integral insulation confers substantial advantages upon assemblies situated in cold climate zones.

The design requirements for these blocks encompass a range of critical aspects, including the provision of sufficient space for reinforcement and plumbing, the incorporation of self-alignment components, and the deployment of a stability method. These factors are fundamental to ensuring the structural integrity and thermal performance of the blocks in the context of their application in cold climate zones.

The self-alignment feature can be achieved through the incorporation of a design component or mechanism that facilitates the automatic and precise alignment of blocks during the assembly process. Self-alignment feature eliminates the need for temporary supports and enhances the overall structural stability during construction. This feature streamlines the construction process by eliminating the necessity for manual block alignment. In this study, the self-alignment feature is enabled through the utilization of interlocking components integrated within the blocks. For vertical alignment, in addition to interlocking members, the wall is grouted every 5 courses. This process ensures required time for attaining sufficient stability for the grout, thereby providing adequate support during construction process.

The stability of dry-stacked block walls can be achieved through a range of methods. These include utilizing friction between surfaces (System3E, 2021), employing grouting (Faswall, 2022; Isotex, 2021; Versaloc, 2021), applying surface bonding (Fonseca & Murray, 2012), implementing pre/post-tensioning of blocks (Al-Manaseer & Neis, 1987; Biggs, 2002; Dawe & Aridru, 1992; Dyskin et al., 2012; Lohr Sr, 1992; Sokairste et al., 2017) and incorporating interlocking components such as protrusions and grooves (Anand & Ramamurthy, 2005; Liu et al., 2016).

These options can be employed in combination, offering designers a multitude of possibilities for configuring dry-stacked block arrangements. In this study, wall stability is ensured through the application of grouting. This choice stems from the inherent benefits of grouting in masonry construction. By filling the gaps within masonry units, grout serves as a unifying agent, transforming a series of individual units into a single, solid structure.

In the pursuit of developing these innovative blocks, concrete was chosen as the primary material for the structural components. This preference is based on concrete's wide availability, low-cost, and high structural performance. Furthermore, two key features, integral insulation and cavity space, are incorporated into the development of two new dry-stacked blocks.

This chapter presents a comprehensive account of the development processes of blocks A and B, providing insights into the iterative design and simulation procedures that lead to the final configurations. In addition, it provides a detailed explanation of the specifications of these blocks in two distinct sections.

3.1 Block A

This section elaborates on the design process involved in the development of Block A and its specifications. Block A is a dry-stacked composite block with integral insulation. The creation of this block includes a series of iterative steps, including modifications, simulation, and investigation, to arrive at the final configuration. Figure 13 presents the initial design options for Block A, which are modeled with same overall thickness to establish a common basis for comparison. Incorporating ties and webs that disrupt the insulation in the first and second options introduces significant thermal bridges, thereby negatively impacting the R-values of the blocks. The R-values of each design options are simulated and listed in Figure 13. The details of the numerical modeling approach are explained in the subsequent chapters.

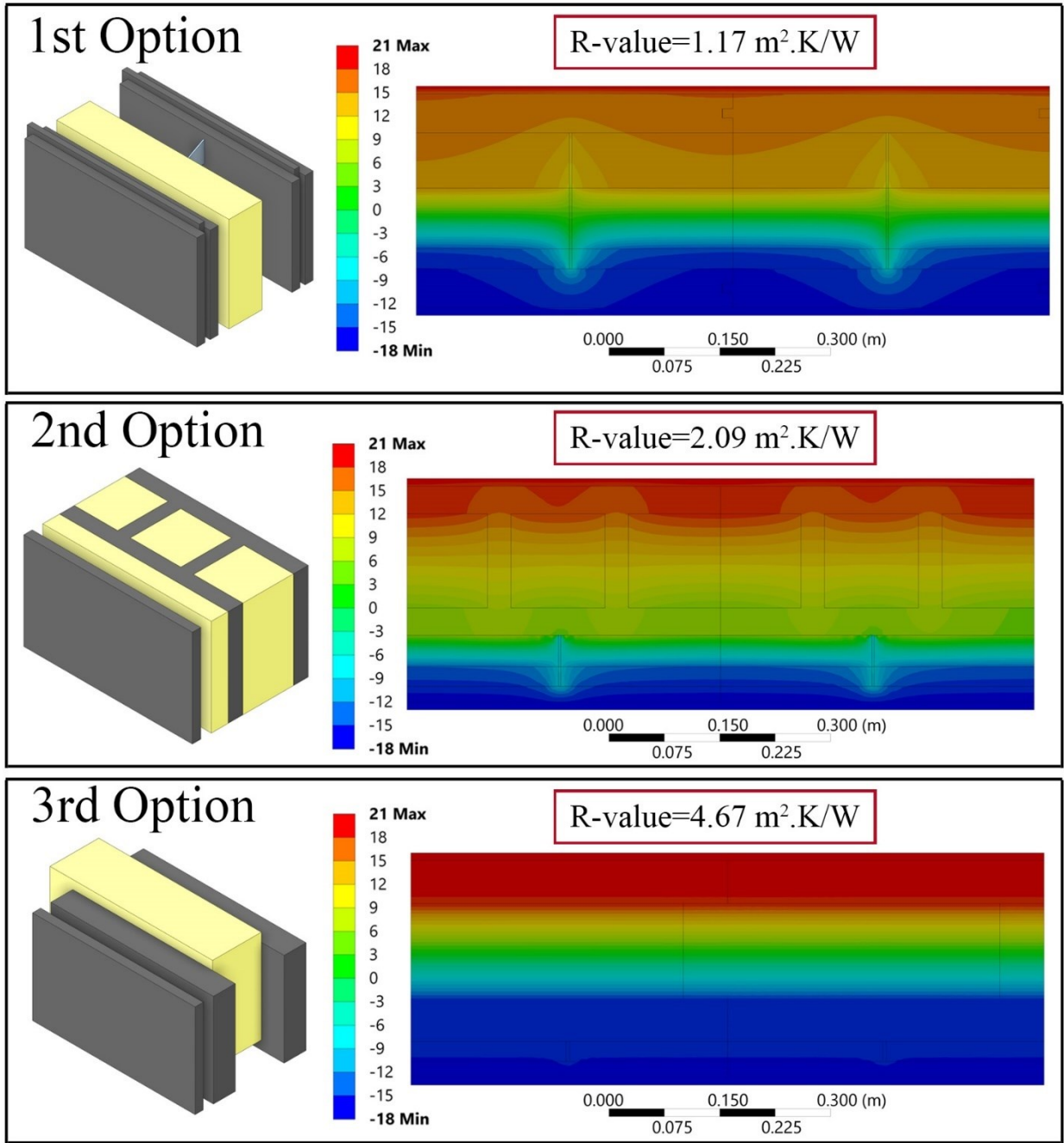


Figure 13. Initial design options for Block A

The third option undergoes successive rounds of modifications, simulations, and evaluations aimed at optimizing its performance. During the development of Block A, as illustrated in Figure 14.1, four tongues are incorporated on its top surface, matched with four corresponding grooves on its bottom surface. These tongues and grooves serve a dual purpose by facilitating connections

between the blocks and ensuring self-alignment during assembly, streamlining the construction process.

The simple placement of insulation alongside structural elements in masonry composite blocks can lead to unreliable connections, thus diminishing the block's service life (Su et al., 2019). To address this concern, indentations are introduced, as depicted in Figure 14.2, to strengthen the connections between two concrete layers to the central insulation layer. Spaces for reinforcement and plumbing are introduced, as illustrated in Figure 14.3. The application of grout within the block enhances stability. Finally, integration of the veneer with the exterior concrete layer is implemented to improve the thermal performance of the block while eliminating the need for ties (Figure 14.4).

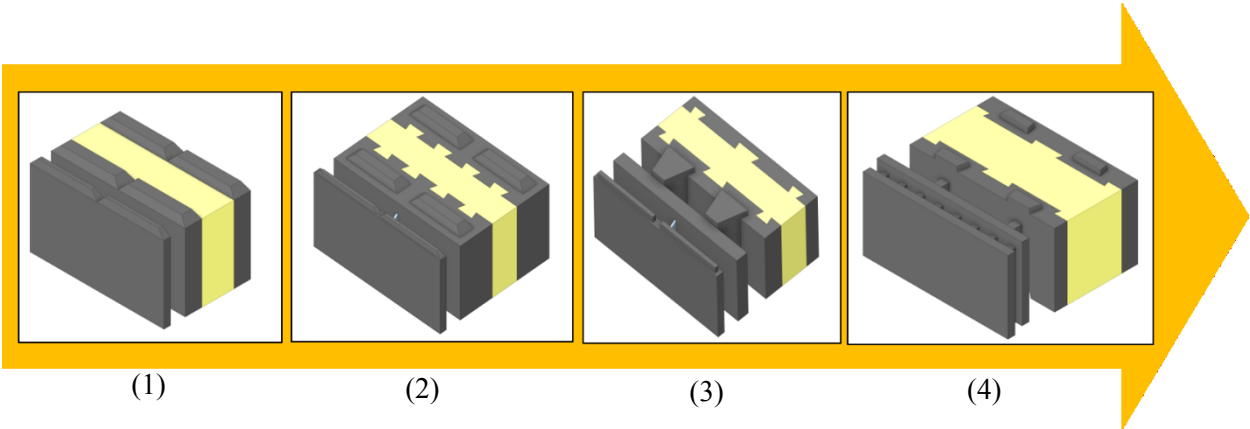


Figure 14. Design process of Block A

The perforated layer creates a rainscreen to prevent rainwater infiltration into the interior layers of the wall (Figure 15.1). The walls on the back and front of the cavity space have different heights, with the back wall being taller to minimize moisture penetration (Figure 15.2).

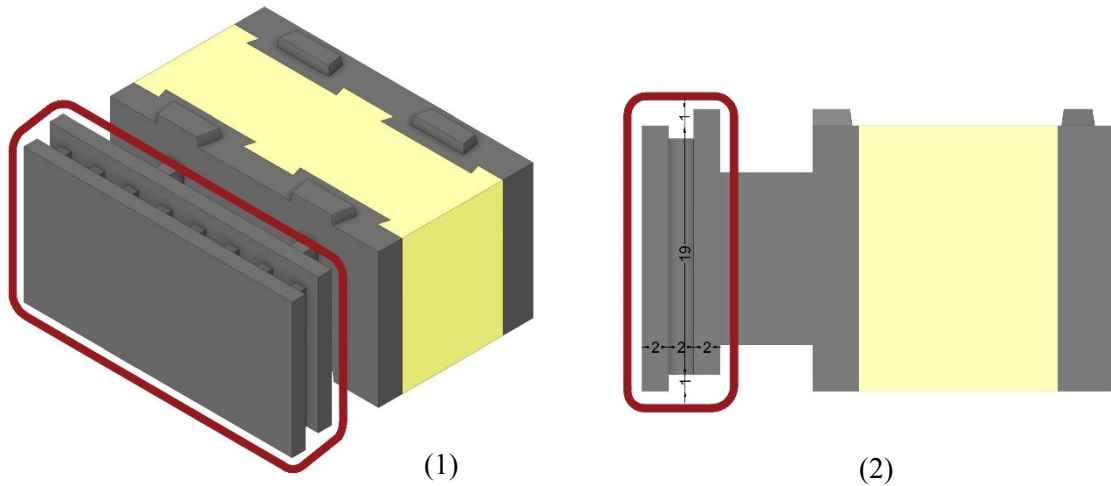


Figure 15. Perforated layer: 1) location in the block, 2) Back and front walls of the cavity space

To facilitate adaptation to current construction practices, dimensions of the final design of Block A are chosen to match that of a standard CMU in terms of height and length. Block A measures 36 cm in thickness, 20 cm in height, and 40 cm in length. Notably, the increased thickness of Block A compared to a standard CMU is attributed to the integration of an insulation layer within the block's composition. This block comprises two concrete layers that sandwich the central EPS insulation layer. The insulation thickness for Block A measures 12 cm excluding the indentations. Figure 16 represents the various components in a main block, corner and half blocks, and the wall constructed from blocks type A (referred to as wall A).

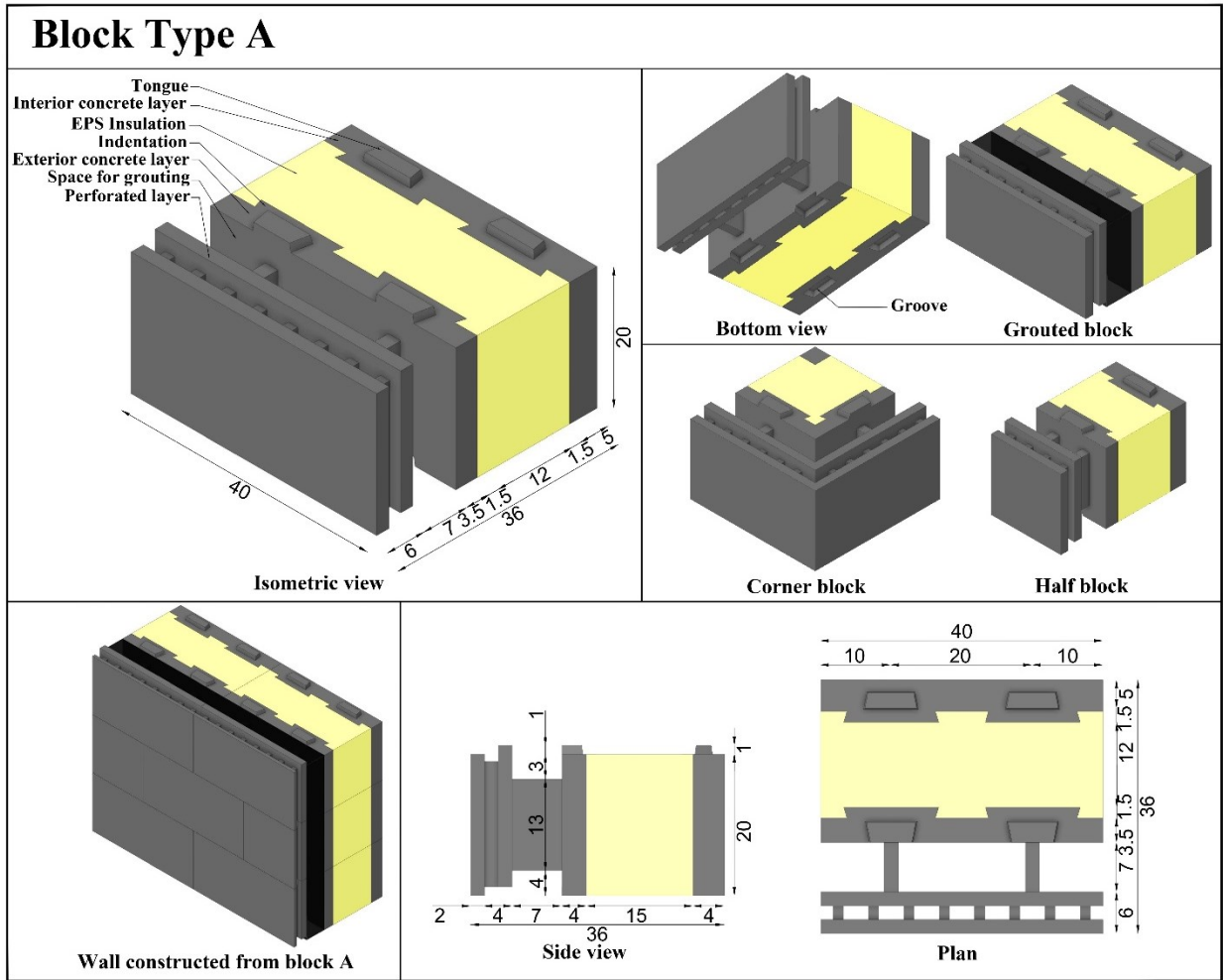


Figure 16. Configuration of Block A, corner and half blocks of type A, and wall A

Wall A benefits from running bond pattern and grouting, enhancing its structural performance. The running bond pattern involves offsetting each course of blocks to prevent vertical joints from aligning, resulting in a staggered arrangement. This pattern effectively redistributes the load over a wider surface area, thereby enhancing the wall's stability. The application of grout within the wall forms a robust network, resulting in enhanced stability. To further bolster the structural performance of wall A, reinforcement bars can be incorporated.

On the exterior face of wall A, a plaster layer can be applied, while on the interior face, a paint layer performs as the interior finish and vapor and air barrier (Figure 17). The vapor barrier helps prevent moisture penetration, ensuring the durability and longevity of the wall.

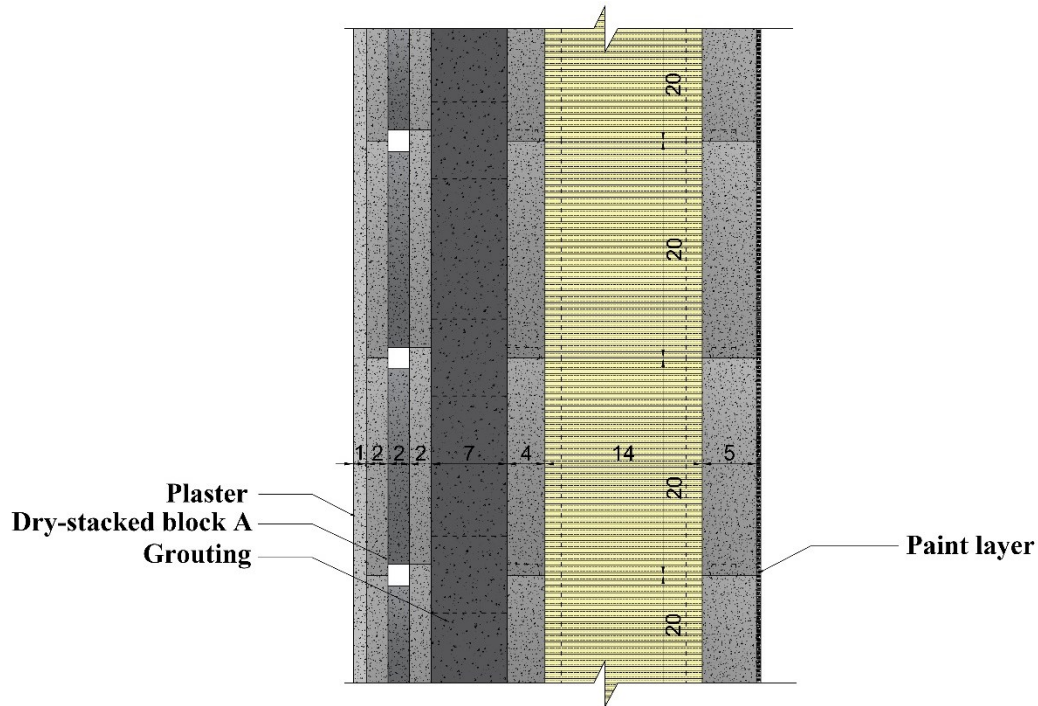


Figure 17. Wall A section

3.2 Block B

Block B is categorized as a simple block. During the developmental stages of block B, as depicted in Figure 18, a sequence of iterative design, simulation, and investigative steps are undertaken. These actions are instrumental in discerning the optimal thermal efficiency configuration for the block. The influence of the block's shape on thermal performance is minimal, remaining under 2% for each iteration. Therefore, the selected design prioritizes efficiency by utilizing the smallest amount of concrete material, employing the fewest variations in block types, and adopting the most straightforward construction process. This approach is preferred because it minimizes material usage, reduces complexity in block production, and streamlines the construction process, ultimately leading to a more cost-effective and practical solution.

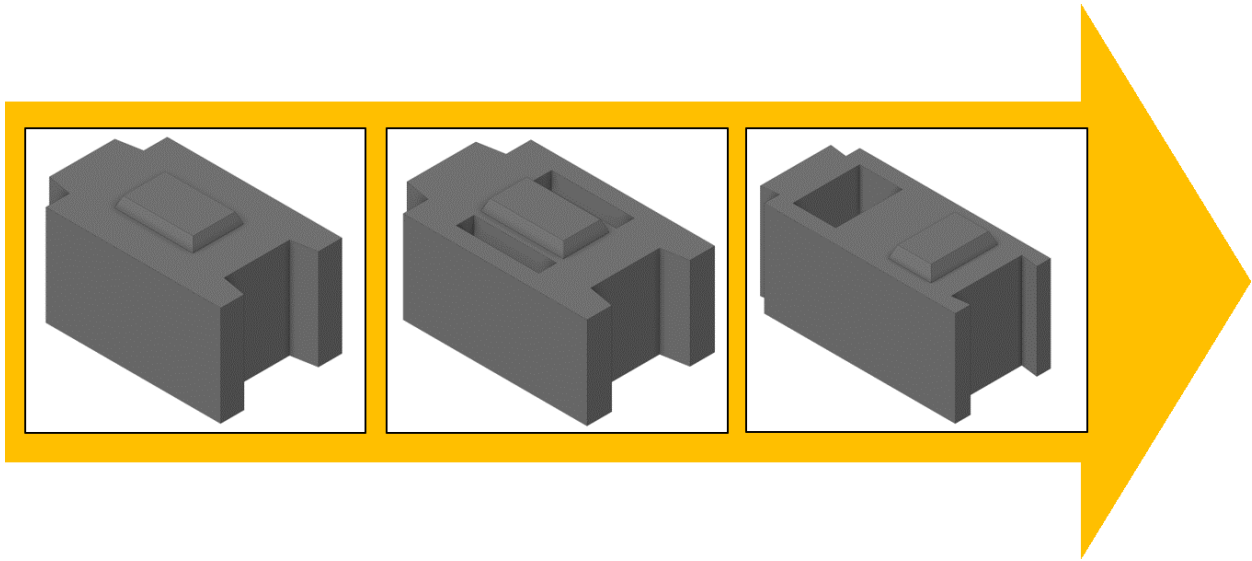


Figure 18. Design process of block B

The final design of Block B conforms to standard CMU dimensions, measuring 20 cm in thickness, 20 cm in height, and 40 cm in length. Two half blocks of type B are developed, with the choice between them dependent on whether the number of courses is even or odd. Additionally, a corner block is applicable in both even and odd course configurations. Figure 19 illustrates the main block, corner block, and half blocks.

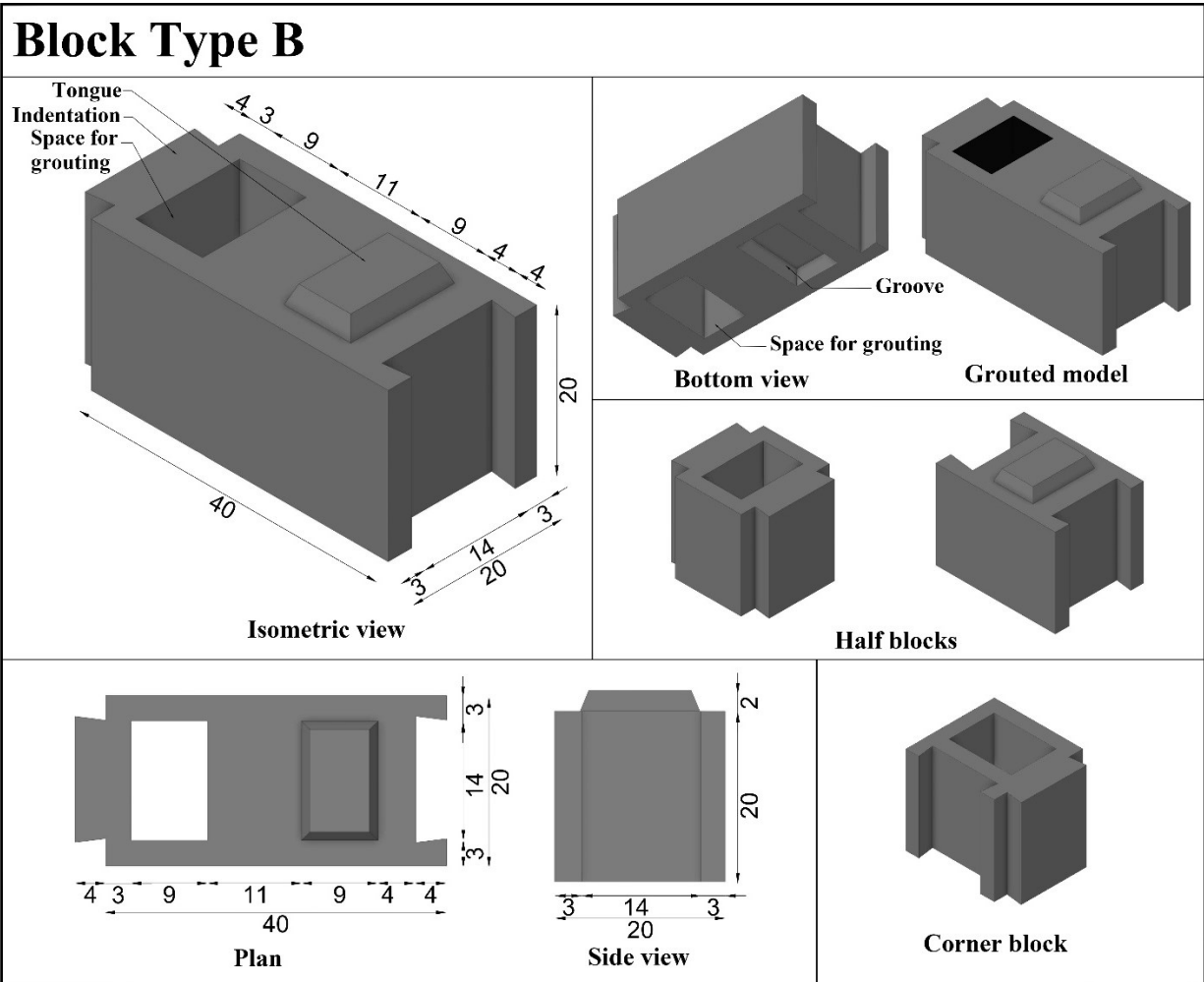


Figure 19. Configuration of Block B, corner and half blocks of type B, and wall B

The resulting wall constructed using Block B (referred to as wall B) is presented in Figure 20. Block B requires a continuous insulation layer to meet the R-value for cold climate zones. This insulation is accompanied by an air cavity and a veneer. To attach the veneer to wall B, hot-dip galvanized (HDG) steel ties are used. However, these ties penetrate the mineral wool insulation, creating thermal bridges in the insulation layer, which negatively impacts the overall thermal performance (Khoukhi, 2018; T. Theodosiou et al., 2019).

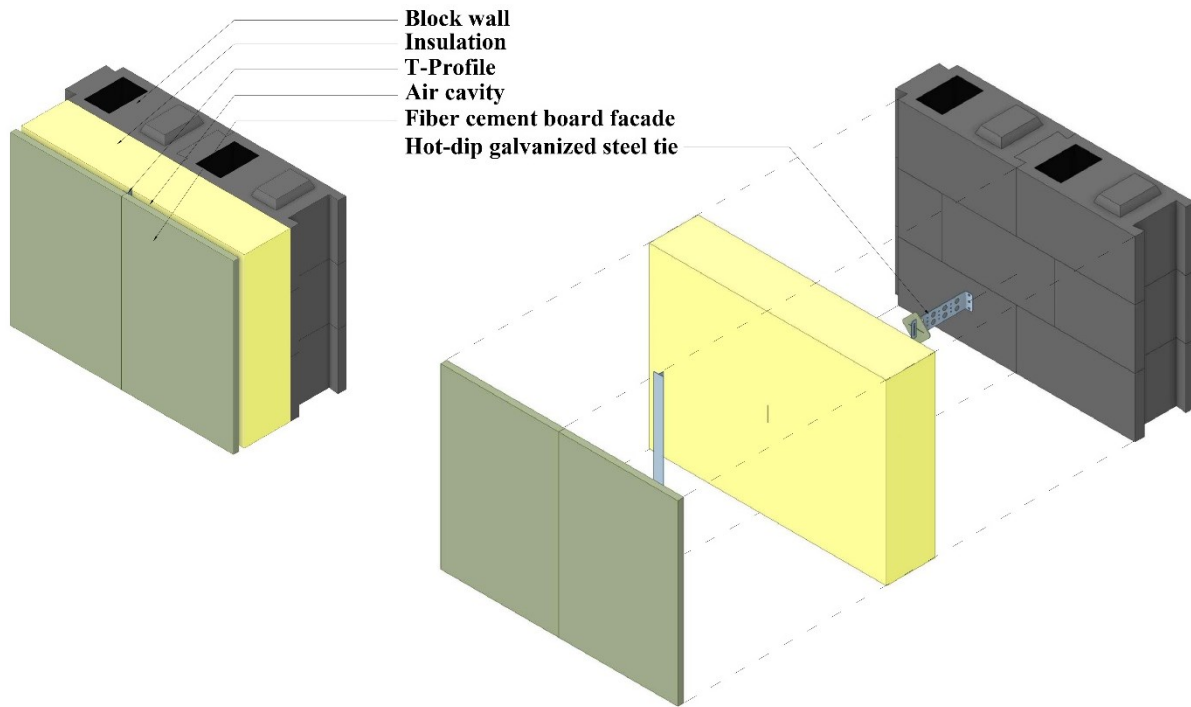


Figure 20. Wall B with insulation, tie and veneer

In order to streamline the construction process by minimizing the variety of block types, wall B is constructed with courses laid in alternating directions, with each subsequent course being the inverse of the previous one, as illustrated in Figure 21. This approach contributes to structural stability by developing a running bond pattern.

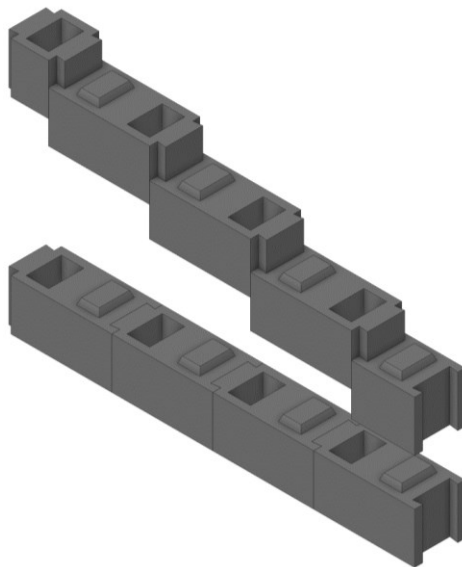


Figure 21. Construction process of Block B courses

Similar to Block A, Block B also benefits from running bond pattern and grouting process, which enhances its structural performance. Block B incorporates interlocking tongues and grooves, fulfilling dual roles of facilitating self-alignment and forming connections between adjacent blocks.

For Wall B, a paint layer serves as the interior finishing material. A layer of vapor barrier is applied to the warm side of the insulation at the outer surface of the backup wall as shown in Figure 22.

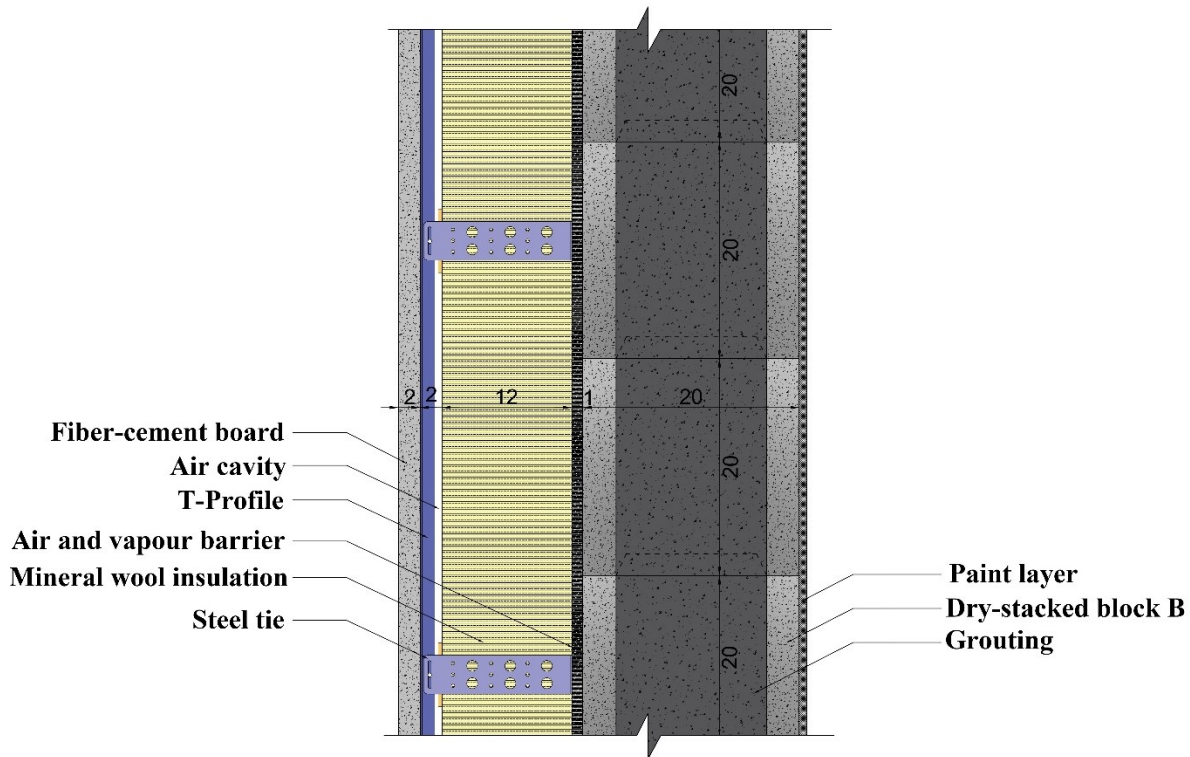


Figure 22. Wall B section

This chapter has elaborated on the design and development of the two new dry-stacked masonry Blocks A and B. Block A is a composite block with integral insulation. Wall A follows a running bond pattern, ensuring structural strength. The inclusion of grouting further reinforces wall A, providing both stability and air-tightness to the masonry wall.

On the other hand, Block B is a simple block assembled in a running bond pattern for wall B, with the courses constructed in an alternating direction every two courses. To address the thermal requirements in zone 7A, wall B includes an additional insulation layer. The ties that penetrate the insulation layer support the veneer of the wall B. Similar to wall A, wall B is also grouted to ensure

stability and enhance the overall performance of the structure. Both blocks are equipped with tongues and grooves, streamlining the alignment of the blocks during construction.

In the subsequent chapter, the methodology for the numerical modeling approach employed to simulate the thermal performance of the new blocks is comprehensively detailed. This numerical analysis sheds light on the thermal resistance of blocks A and B.

4 Numerical Modeling

This chapter describes the methodology employed for numerical modeling. The chapter begins by outlining the assumptions made and explanation of the equations implemented for the simulation. Furthermore, this section includes a thorough description of the models developed, along with the specifications regarding boundary conditions, contact resistances, mesh convergence, and validation. In the validation process, the reliability of the simulations is evaluated by replicating the geometries of seven market blocks, three assemblies of ASHRAE RP-1365 by MorrisonHershfield (2011), and three examples of ASHRAE (2021). ASHRAE examples were replicated to present the accuracy of two-dimensional assembly calculation methods in determining the R-value by comparing the calculated values with the hot-box experiments' results. The reported values obtained from block manufacturers' specifications and ASHRAE are compared with the results generated through numerical simulations to assess the level of accuracy of the simulation models. This comparison provides insights into the validity of the simulation approach.

The thermal performance of the blocks is simulated under steady-state conditions using ANSYS (2022). The FEM model employed is based on the following assumptions:

- Isotropic materials: The materials used in the models are considered isotropic, meaning their properties remain constant regardless of changes in temperature.
- Steady-state heat transfer: The simulation is conducted under steady-state heat transfer conditions, implying that the temperature of the environment remained constant throughout the analysis.

The thermal simulation in this study offers heat flux density values (W/m^2). To further analyze the thermal performance, these heat flux density values are converted into effective R-values ($\text{m}^2 \cdot \text{K}/\text{W}$). The effective R-value encompasses the combined resistance of all components within the assembly, accounting for factors such as surface film resistance and contact resistances between the components. Unlike solely considering material conductivity, the effective R-value captures the interactions between components and provides a more comprehensive representation of the actual R-value. Equation (1) is utilized to determine the effective R-value of the assembly, utilizing the results obtained from the numerical modeling process:

$$R = \frac{\Delta T}{q} \quad (1)$$

Where: R is the effective R-value of the studied assembly ($\text{m}^2 \cdot \text{K}/\text{W}$), ΔT represents the temperature variation between interior and exterior surfaces (K), and q is the average heat flux per unit area of the wall assembly obtained by numerical modeling (W/m^2).

4.1 Models Description

In this study, ANSYS SpaceClaim (2022) software is employed to create the geometries. Three distinct type of models are used for simulating the thermal performance of walls A, B, and the conventional masonry cavity wall (wall C), respectively. It's noteworthy that due to the consideration of average heat flux values and the symmetry in Block A geometry, it becomes unnecessary to model the entire wall A. Essentially, a section of wall A will yield the same results as the entire wall. Consequently, model A is configured with dimensions of $80 \times 40 \times 36$ cm, encompassing a primary block of type A and half of the surrounding blocks, as depicted in Figure 23.1.

To accurately investigate the thermal performance of wall B, a model measuring $164 \times 120 \times 36$ cm is developed (Figure 23.2). These specific dimensions are chosen to accommodate four ties, spaced at intervals of 82×60 cm, in accordance with the maximum spacing permitted by CSA-A370:14 (2018). Simultaneously, the selected dimensions allow us to efficiently manage the available hardware capability and time for the evaluation.

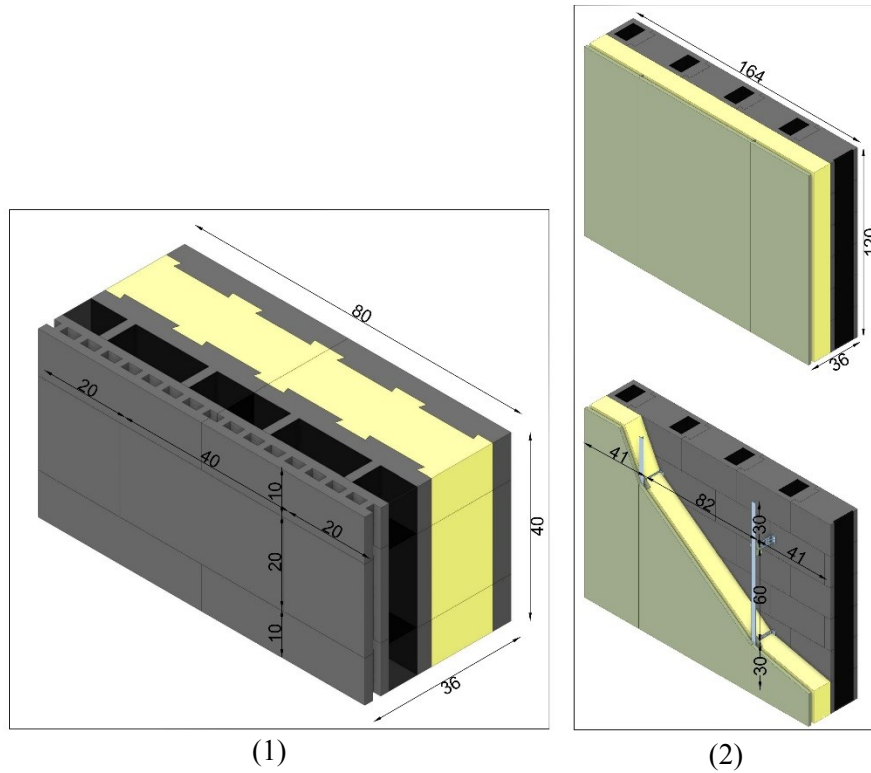


Figure 23. Dimensions of models: 1) A, and 2) B

The wall C features dimensions of $164 \times 120 \times 44.5$ cm with tie spacings set at 82×60 cm. Wall C components and model dimensions are presented in Figure 24.

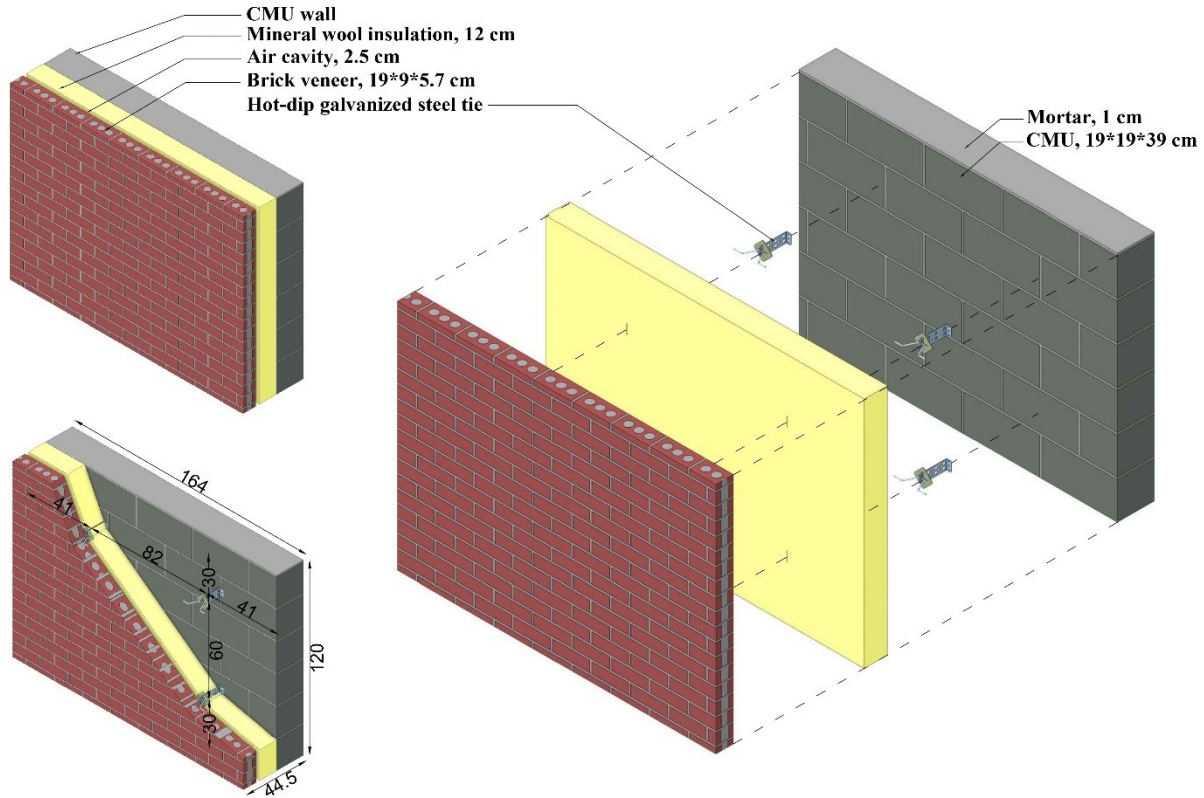


Figure 24. Model dimensions and components of wall C

4.2 Material Properties

The material properties of the walls A, B, and C are presented in Table 10. The properties utilized in the analysis are primarily adopted from ASHRAE (2021). However, for certain parameters requiring enhanced accuracy, alternative resources are included. For example, the R-value of the vented air gap is obtained from Shao (2021), providing a value of $0.135 \text{ m}^2\cdot\text{K}/\text{W}$. Concrete material thickness varies based on its assigned component. For instance, when allocated to Block A, it can exhibit different thicknesses in the exterior perforated layer and the interior face shell.

Table 10. Material properties of the components in walls A, B, and C

Wall	Material	Thermal conductivity, k (W/m·K)	Density, ρ (kg/m ³)	Thickness, t (cm)	R-value (m ² ·K/W)
A	Concrete	1.4	1900	Varies	Varies
	Interior film	0.083	N/A	1	0.12
	Exterior film	0.34	N/A	1	0.03
	Grout	1.6	1500	7	0.043
	Vented air gap	0.14	N/A	2	0.135

	Expanded polystyrene	0.029	38	12	4.137
B	Concrete	1.4	1900	Varies	Varies
	Interior film	0.083	N/A	1	0.12
	Exterior film	0.34	N/A	1	0.03
	Grout	1.6	1500	14	0.087
	Vented air gap	0.14	N/A	2	0.135
	HDG steel tie	62	7830	0.16	0
	Mineral wool	0.029	98	12	4.137
	Polyethylene support	0.4	952	0.2	0.005
	T-profile	62	7830	0.09	0
	Fiber cement board	0.2	1000	2	0.1
C	Concrete	1.4	1900	Varies	Varies
	Interior film	0.083	N/A	1	0.12
	Exterior film	0.34	N/A	1	0.03
	Grout	1.6	1500	12	0.075
	Vented air gap	0.185	N/A	2.5	0.135
	HDG steel tie	62	7830	0.16	0
	Mineral wool	0.029	98	12	4.137
	Polyethylene support	0.4	952	0.2	0.005
	Brick	0.78	1760	9	-
	Mortar	0.5	1200	1	0.02

Note: The thickness of expanded polystyrene for wall A excludes the indentations.

4.3 Boundary Conditions

The thermal performance analysis of the models in this study involves the consideration of specific boundary conditions, as depicted in Figure 25. These boundary conditions include:

- Outdoor temperature ($T_{outdoor}$) set at -18°C in accordance with NECB (2020).
- Indoor temperature (T_{indoor}) maintained at 21°C as specified by NECB (2020).
- Adiabatic conditions applied to the side surfaces, meaning no heat transfer occurs through these surfaces.

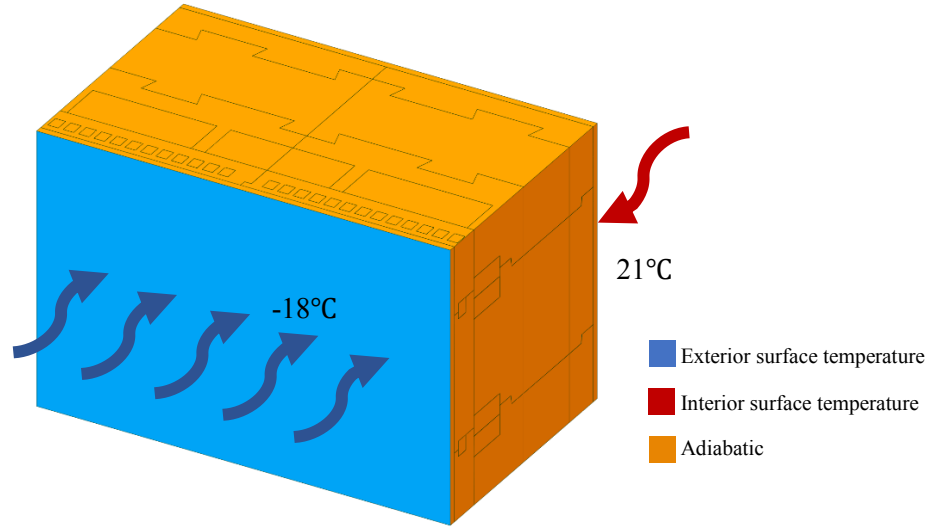


Figure 25. Boundary conditions of the ANSYS model

Changes in the temperatures that are defined as boundary conditions do not change the R-value as the material properties are assumed constant. For the purposes of calculations, the air film present on both the exterior and interior surfaces is treated as a solid layer with a thickness of 1 cm. For the exterior air film, the R-value is determined to be $0.03 \text{ m}^2 \cdot \text{K}/\text{W}$, while for the interior air film, it is $0.12 \text{ m}^2 \cdot \text{K}/\text{W}$ (ASHRAE, 2021; MorrisonHershfield & BCHydro, 2021). To obtain the thermal conductivity of the interior and exterior air film objects, the following equation can be utilized in the calculations:

$$k = \frac{t}{R} \quad (2)$$

Where: k is the thermal conductivity of the component ($\text{W}/\text{m} \cdot \text{K}$), t is the thickness of the component (m), and R is the R-value of the component ($\text{m}^2 \cdot \text{K}/\text{W}$).

The thermal conductivities of the interior and exterior air films are determined as follows:

- $0.34 \text{ W}/\text{m} \cdot \text{K}$ for the external film
- $0.083 \text{ W}/\text{m} \cdot \text{K}$ for the internal film

These values represent the thermal conductivities associated with the air films on the respective surfaces.

4.4 Contact Resistances

For this study, contact resistances are assigned based on the guidelines provided in ASHRAE RP-1365 by MorrisonHershfield (2011). The specific contact resistances utilized in the analysis can be found in Table 11. These contact resistances play a crucial role in capturing the thermal interactions between different components within the system, contributing to a more accurate evaluation of the thermal performance.

Table 11. Contact resistances

Location	Contact resistance ($\text{m}^2 \cdot \text{K}/\text{W}$)
Steel flanges at sheathing interfaces	0.03
Insulation interfaces	0.01
Steel to concrete interfaces	0.01
Steel to steel interfaces	0.002

4.5 Mesh Convergence

The meshing process is conducted using ANSYS's advanced sizing factors, enabling precise control over the mesh density. For the more intricate case of Block A, a relatively fine mesh is generated to capture the intricate details of the model, such as the perforated concrete layer. To reach a balance between accuracy and computational efficiency, a series of mesh convergence tests are performed. These tests examine the variation of the heat flux as the number of mesh nodes is adjusted. The objective is to identify a mesh size that would provide an optimal combination of accuracy and computational time. The analysis concludes that a mesh size of 1 cm, corresponding to approximately 3.5×10^5 nodes, offers a satisfactory level of accuracy while maintaining computational efficiency. This mesh size is deemed suitable for the models, ensuring reliable results within a reasonable computational timeframe. The results of the mesh convergence tests can be observed in Figure 26.

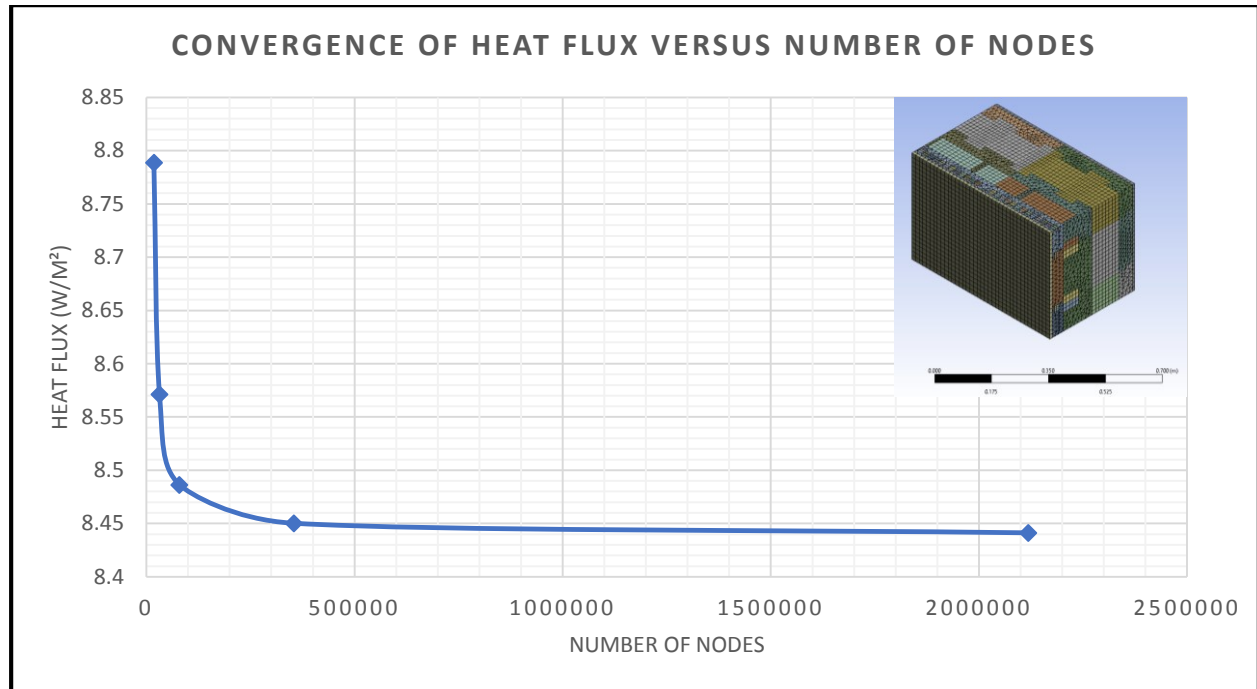


Figure 26. Results of mesh tests

4.6 Validation

To validate the numerical modeling employed in this study, the R-values of seven market dry-stacked blocks (Almanaratain, 2022; ComfortBlock, 2022; Faswall, 2022; Gablok, 2021; Isotex, 2021; OneStep, 2022; System3E, 2021), three assemblies of ASHRAE RP-1365 by MorrisonHershfield (2011), and three guarded hot-box examples of ASHRAE (2021) are simulated using ANSYS Workbench. The simulated R-values obtained from the models are then compared with the reported results from the original resources. The comparison between the reported and simulated values shows an average difference of 4.68%, as presented in Table 12.

Table 12. Percentage difference of simulated and reported values for validating the numerical modeling

Replicated model	Simulated R-value (m ² ·K/W)	Reported R-value (m ² ·K/W)	Percentage Difference
Faswall (2022)	3.6	3.69	2.44%
System3E (2021)	5.39	5.05	-6.73%
OneStep (2022)	3.2	3.52	9.09%
Almanaratain (2022)	1.58	1.56	-1.28%
Isotex (2021)	3.55	3.7	4.05%

ComfortBlock (2022)	5.24	5.3	1.13%
Gablok (2021)	6.66	6.6	-0.9%
Detail 8 of ASHRAE RP-1365	1.78	1.92	-7.86%
Detail 13 of ASHRAE RP-1365	3.56	3.77	5.57%
Detail 19 of ASHRAE RP-1365	1.34	1.22	9.83%
First example of ASHRAE (2021)	0.55	0.551	0.18%
Second example of ASHRAE (2021)	0.81	0.854	5.15%
Third example of ASHRAE (2021)	2.53	2.71	6.64%
Average difference			4.68%

Note: In calculating the percentage difference, the reported R-value serves as the denominator.

This chapter has focused on the numerical modeling approach used to assess the thermal performance of designed blocks. The methodology section has included underlying assumptions, material properties, detailed models' description, boundary conditions, contact resistances, the mesh convergence process, and validation. The validation process has presented a comparison between the simulated values and the reported ones. The achieved comparison demonstrates that the average difference is 3.7%. In the next chapter, the results and discussion from the numerical simulation are presented.

5 Results and Discussion

This chapter provides the results and discussion of the simulations conducted using FEM modeling. The analysis focuses on three key aspects:

- Comparison of designed blocks: The thermal resistance of the two designed blocks is compared to assess their respective effectiveness.
- Comparison with Wall C: Blocks A and B are compared with Wall C having an equivalent insulation thickness.
- Comparison with existing dry-stacked blocks: Block A is compared with existing dry-stacked blocks available in the market to evaluate its R-value.

These results and discussions provide valuable insights into the thermal performance of simple and composite block walls and their performance relative to conventional masonry walls. Furthermore, they offer a comparative perspective on the thermal performance of Block A when compared to other dry-stacked blocks currently available in the market.

5.1 Analysis of Thermal Performance of Walls A and B

This section provides a detailed analysis of the thermal performance of the designed blocks A and B in wall assemblies, and highlights the key differences between them. Figure 27 depicts the temperature distribution within the wall A. The observed temperature gradient reveals a gradual decrease from the internal surface towards the external surface. Notably, the insulation layer exhibits the most pronounced decline in temperature. This phenomenon is due to the inverse relationship between the temperature gradient and the thermal conductivity of the material. The EPS layer, with a thermal conductivity of $0.029 \text{ W/m}\cdot\text{K}$, exhibits significantly lower thermal conductivity in comparison with concrete ($1.4 \text{ W/m}\cdot\text{K}$), grout ($1.6 \text{ W/m}\cdot\text{K}$), and air cavity (equivalent of $0.14 \text{ W/m}\cdot\text{K}$). Consequently, the insulation layer plays a substantial role in effectively limiting the heat flow across the wall assembly. Moreover, no discernible disparity in the temperature distribution is observed between the middle of the block and its vicinity near the block joint, thereby indicating the absence of thermal bridges resulting from block interfaces.

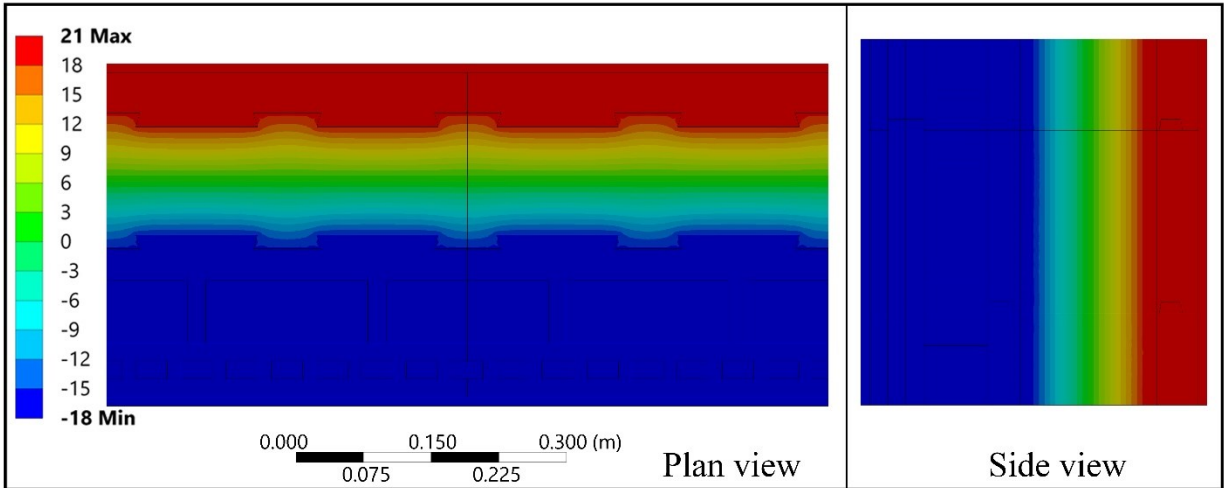


Figure 27. Temperature distribution in wall A

Figure 28 depicts the heat flux density distribution within the wall A. The analysis reveals that the majority of areas in the wall, including the internal concrete component, insulation layer, and external concrete part, exhibit low heat flux density. This observation indicates the effectiveness of the insulation layer, which efficiently restricts heat transfer through the wall assembly. Nevertheless, notable instances of high heat flux density are evident at the interfaces between the insulation and concrete components, as well as between the air cavity layers inside the perforate concrete layer.

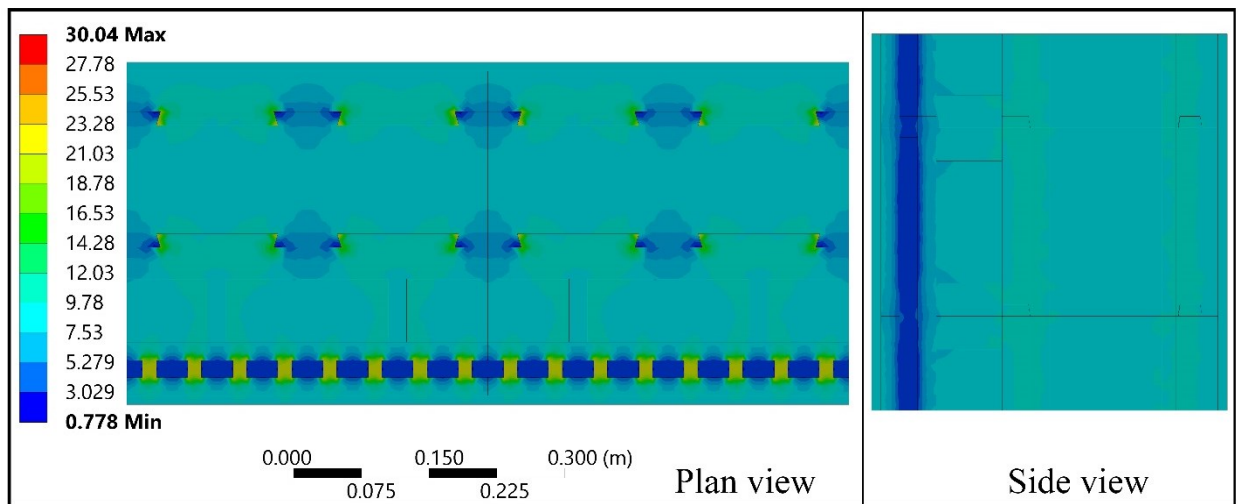


Figure 28. Heat flux density distribution of Block A

Wall B exhibits distinctive thermal performance due to the incorporation of steel ties within its configuration (Figure 29). The presence of these ties introduces thermal bridging effects by

interrupting the continuity of insulation and creating direct thermal pathways between the interior and exterior surfaces of the wall. Figure 29 illustrates the impact of these ties on the temperature distribution within the wall. The thermal bridging effect caused by the ties is clearly evident in the temperature distribution lines. Unlike the nearly parallel temperature contour lines observed in wall A, the presence of ties in wall B results in curved lines of temperature distribution that are stretched towards the interior warm surfaces and exterior cold surfaces in the ties area. This deviation from a straight line indicates that heat is being transferred through the ties, leading to localized areas of increased temperature. The thermal bridging effect induced by the steel ties in wall B compromises the overall thermal performance of the wall.

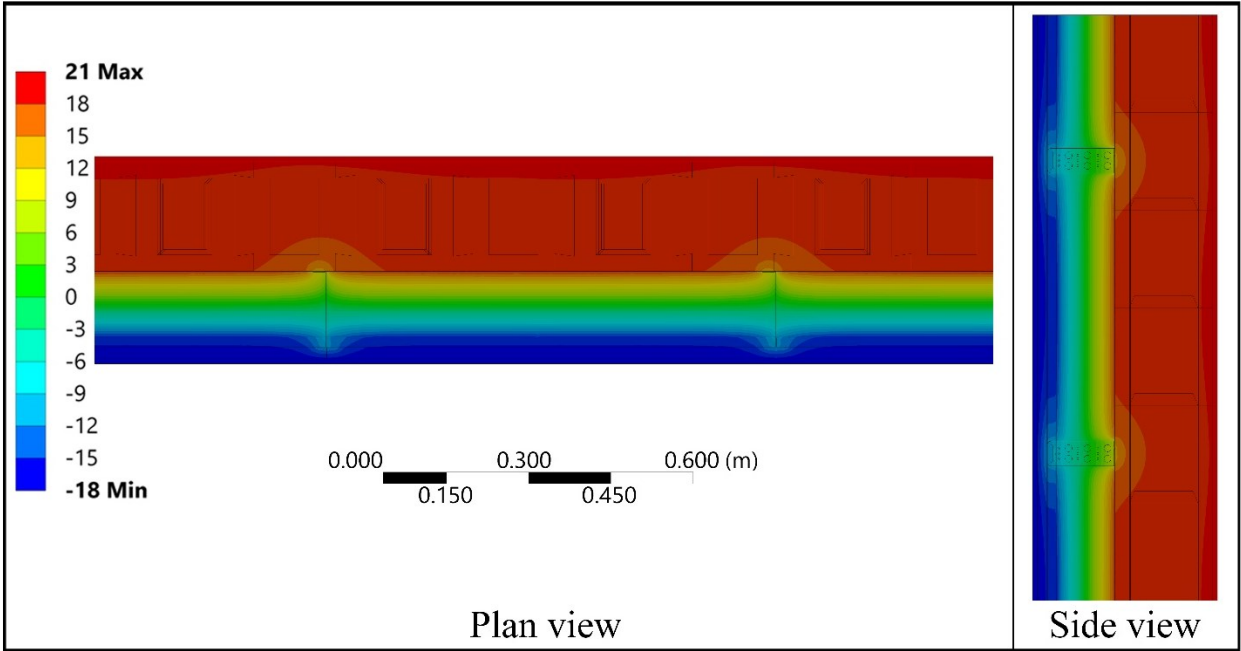


Figure 29. Temperature distribution of wall assembly B

The presence of thermal bridges is primarily observed in the ties. In these regions, heat transfer through the ties passes the insulation, reducing the effectiveness of the insulation. The concentrated high heat flux in the tie areas is a clear indication of the thermal bridging phenomenon and emphasizes the need for effective mitigation strategies to minimize energy losses associated with these thermal bridges.

The substantial thermal bridges identified in wall B serve as a reminder of the challenges posed by the presence of ties in masonry walls. The findings emphasize the need for careful design

considerations and material selection to mitigate thermal bridging effects and enhance the overall thermal performance of masonry structures.

Block A demonstrates a promising potential for achieving an R-value of 4.7 m²·K/W by incorporating a 12 cm thick insulation layer. However, the presence of thermal bridging effects in wall B significantly impacts its thermal performance. Consequently, wall B attains an R-value of 4.19 m²·K/W when employing insulation in the same thickness and thermal conductivity. This R-value falls below the desired level for walls in zone 7A. To address this issue, it becomes necessary to enhance the insulation thickness. A final insulation thickness of 14 cm is deemed necessary to achieve an R-value of 4.75 m²·K/W, which aligns with the required thermal performance standards. Minimum insulation thicknesses of walls A and B required for cold climate zones are presented in Table 13.

Table 13. Minimum insulation thicknesses of walls A and B for climate zones in Canada

Climate zone	4	5	6	7A	7B	8
Required R-value (m²·K/W)	3.45	3.77	4.17	4.65	5.26	6.1
Minimum Insulation Thickness for Wall A (cm)	8.5	9.5	10.5	12	14	16
Minimum Insulation Thickness for Wall B (cm)	9.5	10.5	12	14	16	19

5.2 Comparative Analysis of Walls A, B, and C

The configuration of wall C and its material properties have been shown in Chapter 4. Figure 30 depicts the temperature distribution within the wall C.

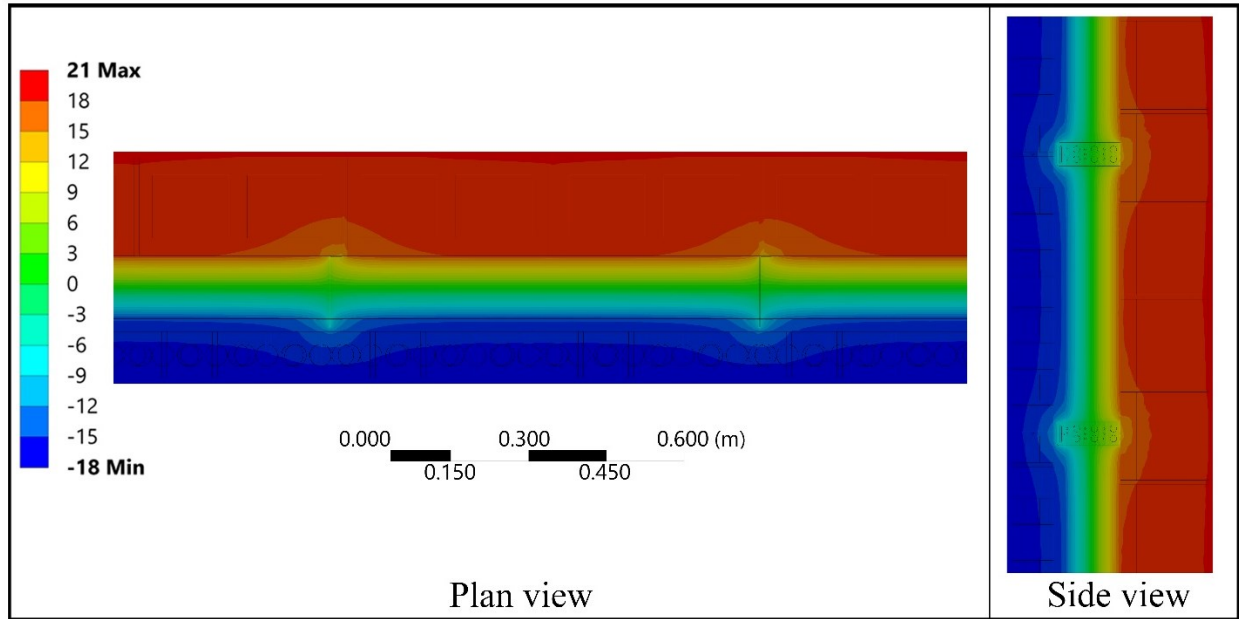


Figure 30. Temperature distribution of wall C

The temperature distribution and heat flux distribution in wall C closely resemble those in wall B, primarily due to the similarity in tie spacing and thickness. However, the R-value of wall C experiences a more significant reduction due to the presence of both mortar and tie in the wall assembly.

With the same thickness of insulation, wall C achieves an R-value of $3.77 \text{ m}^2 \cdot \text{K}/\text{W}$. This represents a 9% reduction in R-value compared to wall B, which is due to different ties' shape and grouted masonry cores. The R-value of wall C is 19% less than that of wall A due to the existence of thermal bridging through the insulation. Table 14 summarizes the comparison among three wall assemblies.

Table 14. Comparison among three investigated wall assemblies

Wall	Block Type	Material of the Block	Dimensions of the Block, L×H×t (cm)	Insulation thickness (cm)	Total thickness of wall assembly (cm)	Wall layers	R-value, ($\text{m}^2 \cdot \text{K}/\text{W}$)
A	A	Concrete and EPS insulation	40×20×36	12	36	Gypsum board, Block A, plaster	4.7
B	B	Concrete	40×20×20	12	36	Gypsum board, Block B, mineral wool,	4.19

						insulation, air cavity (2cm), fiber-cement board veneer	
C	CMU	Concrete	39×19×19	12	44.5	Gypsum board, CMU, mineral wool, insulation, air cavity (2.5 cm), brick veneer	3.77

Note: The thickness of insulation for wall A excludes the indentations.

While wall A demonstrates a competitive advantage in terms of its R-value when compared to wall C, its structural integrity is compromised due to the separation of two structural concrete components by the insulation layer. Moreover, the production of Block A presents notable challenges, with difficulties arising from the placement of the insulation layer within the mold and the implementation of raised surfaces for the interlocking components.

Block B, on the other hand, requires a 2 cm thicker insulation layer to meet the demands of zone 7A. However, its structural performance surpasses that of Block A. Although Block B also faces production challenges related to interlocking components, these are comparatively less daunting due to the fewer interlocking elements and the absence of an insulation layer within the block, as compared to Block A. Block B presents greater weight compared to both Block A and a CMU, giving rise to challenges concerning transportation and labor handling. Wall B's structural performance is compromised when compared to wall C due to the absence of grout or mortar in the region with interlocking components, which accounts for more than half of the wall's total area.

In summary, Block A proves to be the most suitable choice when rapid construction, limited labor, and lightweight characteristics are the key considerations, and structural performance is of secondary importance. This is due to the inclusion of insulation and cavity space within the block, streamlining and expediting the construction process. Conversely, Block B becomes the preferred option when block production challenges are present, on-site block production is feasible, and structural performance is not the top priority.

5.3 Comparative Analysis of Block A Against Existing Dry-Stacked Blocks

A comparative analysis is conducted to assess the competitiveness of composite Block A against existing composite blocks available in the market. Table 15 presents the results of this comparison, entailing the assessment of Block A in conjunction with five of the most thermally efficient composite blocks currently available (Almanaratain, 2022; ComfortBlock, 2022; Faswall, 2022; Gablok, 2021; Isotex, 2021). To standardize the comparison, it is necessary to ensure that all blocks share the same overall thickness. Notably, Block A possesses an exterior perforated concrete layer, a feature absent in all existing dry-stacked blocks. Consequently, to achieve uniformity, the perforated layer in Block A is eliminated, resulting in a total thickness of 32 cm for this block. Subsequently, all five blocks are adjusted to align with the thickness of Block A for the sake of consistency in the evaluation.

Table 15. Comparison of Block A against existing market blocks

Block	R-value, (m ² ·K/W)	Percentage Difference	Stabilization Method	Space for plumbing and reinforcement	Self-alignment
Block A	4.63	0%	Grouting	☐	☐
Faswall (2022)	3.56	-23.1%	Grouting	☐	☐
Isotex (2021)	3.44	-25.7%	Grouting	☐	-
Gablok (2021)	7.1	53.3%	Interlocking members	-	☐
ComfortBlock (2022)	4.16	-10.2%	Masonry adhesive and grouting	-	☐
Almanaratain (2022)	2.43	-47.9%	Adhesive	-	-

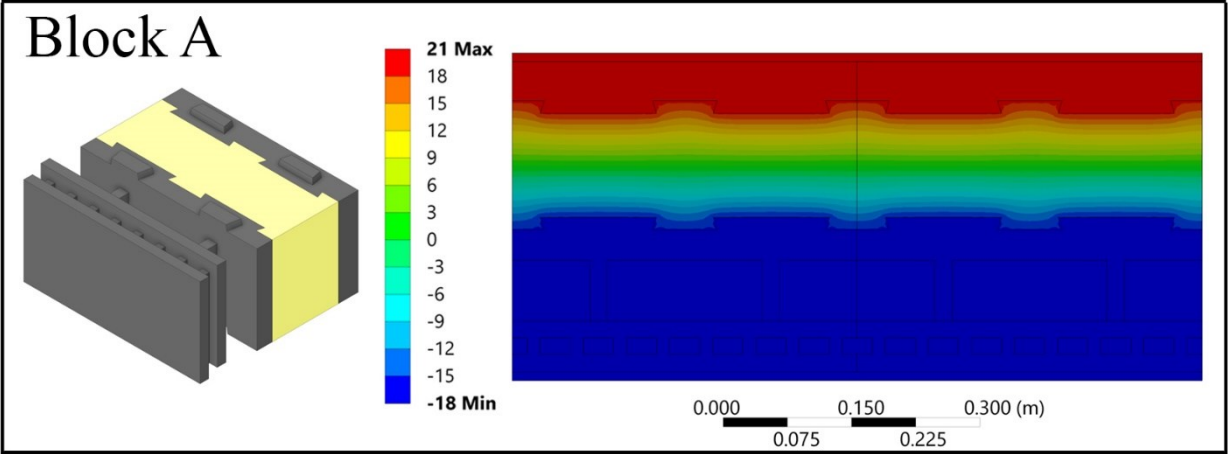
Notes:

- ☐: The presence of this symbol beneath a specific feature indicates that the block includes that feature.
- : The presence of this symbol beneath a specific feature indicates that the block excludes that feature.

The comparison reveals that Block A generally exhibits a higher R-value than most of the dry-stacked blocks on the market. Only Gablok surpasses Block A in terms of R-value. This disparity can be attributed to the materials employed in the construction of Gablok, which include wood and EPS, known for their excellent thermal efficiency. However, it is important to note that the structural performance of Gablok is inversely affected by the presence of 80% EPS in its material composition. A mere 20% of Gablok’s volume consists of OSB with a compressive strength of 0.5 MPa, serving the structural role. In contrast, Block A is constituted of 63% concrete with significantly higher compressive strength compared to OSB. Moreover, the structural performance

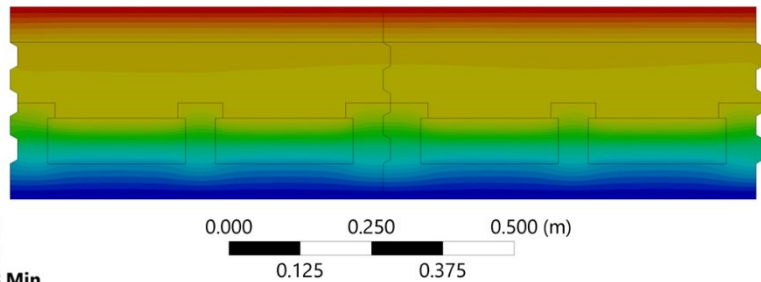
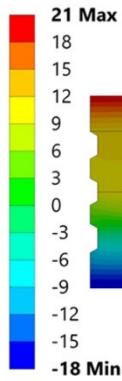
of Block A can be further improved through the incorporation of reinforcement bars within its cavities.

Figure 31 presents the shape and temperature distribution within each block, simulated in ANSYS. In Gablok, almost straight and uniform temperature distribution indicates minimal thermal bridging across the block thickness. Conversely, in Almanaratain, the temperature distribution lines are stretched in the concrete area, signifying the presence of thermal bridging.



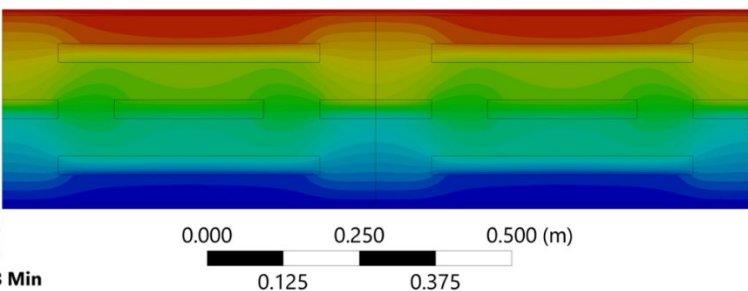
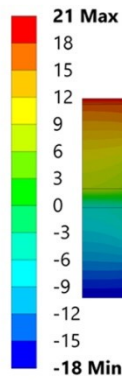
(1)

Faswal



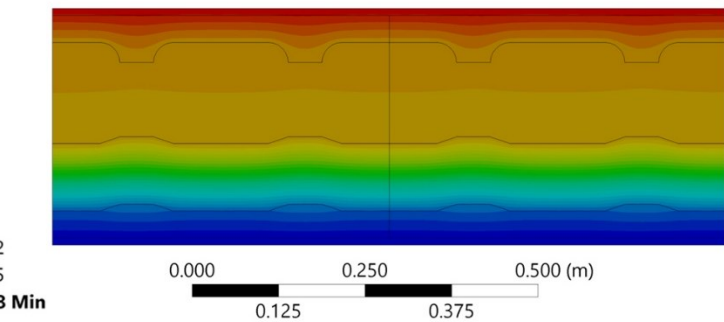
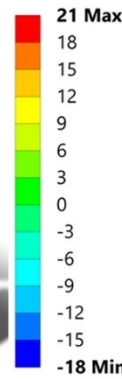
(2)

Almanaratain

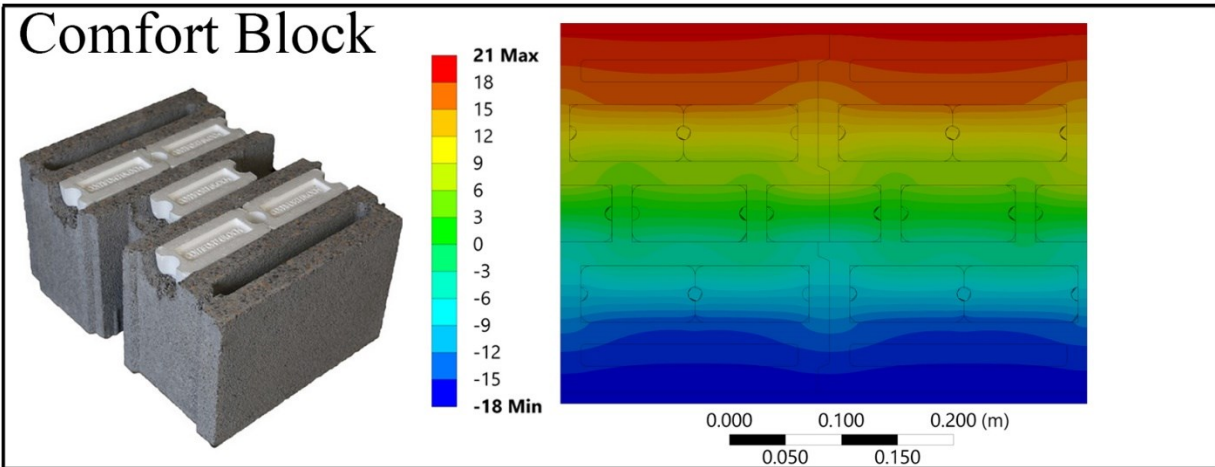


(3)

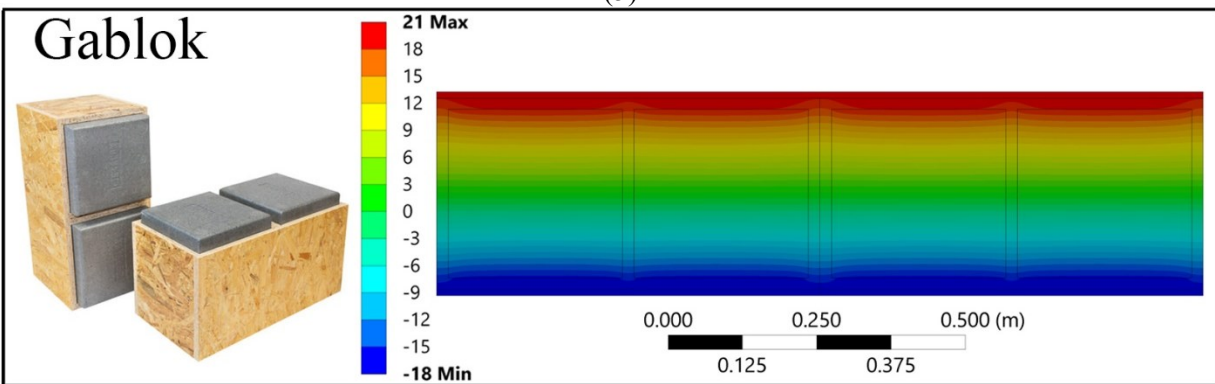
Isotex



(4)



(5)



(6)

Figure 31. Temperature distribution and shapes of 1) Block A, 2) Faswall, 3) Almanaratain, 4) Isotex, 5) Comfort Block, and 6) Gablok

Block A has a self-alignment feature that eliminates the need for manual alignment of blocks and enhances the stability of the structure during the construction process. Faswall, Gablok, and Comfort Block similarly incorporate self-alignment through interlocking components.

The cavity space within block A plays a pivotal role in preventing moisture infiltration, particularly in cold climate zones. This feature is absent in all existing blocks, necessitating additional time and cost for retrofitting such spaces.

The findings emphasize the competitive performance of Block A in terms of thermal performance when compared to existing composite blocks. Its relatively high thermal performance positions it favorably among the market blocks, with only one block outperforming it in this aspect. However, it is crucial to consider the trade-off between thermal resistance and structural behavior when evaluating the overall suitability of a composite block for construction. Block A has the potential

for enhancing its structural strength through the integration of reinforcement bars within its grouting section, thus rendering it a competitive option concerning compressive strength.

This chapter has presented the results and discussions pertaining to the thermal analysis of the blocks A and B, and comparing Block A with five market blocks. It has been observed that the presence of ties significantly compromises the thermal resistance of wall B. Despite the presence of some thermal bridging areas in Block A, it achieves an R-value that is 12% higher than Block B. In addition, when comparing Block A with existing blocks in the market, it outperforms most of them.

6 Conclusion and Future Research Recommendations

This study extensively reviewed the thermal resistance of dry-stacked masonry blocks for masonry walls' systems, analyzing the impact of materials and shapes on their thermal performance. Among the materials used, perlite demonstrated the lowest thermal conductivity, resulting in a higher R-value for blocks of equal thickness. The combination of cement and POCP showed positive effects on both thermal performance and compressive strength, yet these materials are still relatively novel and costly.

Changes in block shape influenced thermal resistance. Reducing the cross-sectional area of webs proved crucial in mitigating thermal bridging and enhancing thermal performance. Integrating insulation into the block configuration proved more effective in enhancing thermal efficiency than shape alterations alone. In cold climate zones, integral insulation played a vital role in achieving higher thermal resistance. Additionally, cavity walls facilitated moisture drying and improved thermal performance.

To practically apply these findings, two blocks with identical thicknesses were developed. Block A, a composite block with integral insulation, outperformed Block B, a simple block with additional insulation. The insulation layer experienced the most significant temperature drop due to the inverse relationship between the temperature gradient and the thermal conductivity of the material, thus enhancing the R-value of the wall significantly. The composite block system emerged as a promising solution, demonstrating the potential to achieve an overall R-value of $4.7 \text{ m}^2 \cdot \text{K}/\text{W}$. However, the presence of thermal bridging effects in the simple block wall significantly reduced its thermal performance, yielding a 11% lower R-value.

In comparison to a conventional masonry wall with the same thickness of insulation, wall A represented a 24% higher R-value, and wall B demonstrated an 11% higher R-value, showcasing their improved thermal performance. In addition, comparatively assessing composite Block A against available market options showcased its superior thermal performance. As a result, Block A excelled in rapid construction with limited labor, emphasizing lightweight characteristics, while giving less priority to structural performance. In contrast, Block B was preferable in situations involving block production challenges, on-site production feasibility, and less emphasis on structural performance.

There are still research gaps in topics that affect the thermal performance of dry-stacked masonry blocks. These gaps include the study of moisture and the thermal mass effect, which require further research. Furthermore, future studies should investigate the structural performance of dry-stacked blocks with integral insulation to provide a comprehensive understanding of their thermal and structural characteristics.

References

- Abdellatef, Y., Khan, M. A., Khan, A., Alam, M. I., & Kavgic, M. (2020). Mechanical, Thermal, and Moisture Buffering Properties of Novel Insulating Hemp-Lime Composite Building Materials. *Materials*, 13(21), 5000. <https://doi.org/10.3390/ma13215000>
- Abdou, O. A., & Murali, K. S. (1994). The Effect of Air Cells and Mortar Joints on the Thermal Resistance of Concrete Masonry Walls. *Energy and Buildings*, 21(2), 111-119. [https://doi.org/10.1016/0378-7788\(94\)90004-3](https://doi.org/10.1016/0378-7788(94)90004-3)
- Al-Fakih, A., Mohammed, B. S., Al-Osta, M. A., & Assaggaf, R. (2022). Evaluation of the Mechanical Performance and Sustainability of Rubberized Concrete Interlocking Masonry Prism. *Journal of Materials Research and Technology*, 18, 4385-4402. <https://doi.org/10.1016/j.jmrt.2022.04.115>
- Al-Fakih, A., Mohammed, B. S., Nuruddin, F., & Nikbakht, E. (2018). *Development of Interlocking Masonry Bricks and Its' Structural Behaviour: A Review Paper*. Paper presented at the IOP Conference Series: Earth and Environmental Science.
- Al-Hazmy, M. M. (2006). Analysis of Coupled Natural Convection–Conduction Effects on the Heat Transport through Hollow Building Blocks. *Energy and Buildings*, 38(5), 515-521. <https://doi.org/10.1016/j.enbuild.2005.08.010>
- Al-Jabri, K. S., Hago, A., Al-Nuaimi, A., & Al-Saidy, A. (2005). Concrete Blocks for Thermal Insulation in Hot Climate. *Cement and Concrete Research*, 35(8), 1472-1479. <https://doi.org/10.1016/j.cemconres.20p04.08.018>
- Al-Manaseer, A., & Neis, W. (1987). Load Tests on Post-Tensioned Masonry Wall Panels. *Structural Journal*, 84(6), 467-472. <https://doi.org/10.14359/2768>
- Al-Sanea, S. A., & Zedan, M. (2012). Effect of Thermal Bridges on Transmission Loads and Thermal Resistance of Building Walls under Dynamic Conditions. *Applied energy*, 98, 584-593. <https://doi.org/10.1016/j.apenergy.2012.04.038>
- Alhazmy, M. M. (2010). Numerical Investigation on Using Inclined Partitions to Reduce Natural Convection inside the Cavities of Hollow Bricks. *International Journal of Thermal Sciences*, 49(11), 2201-2210. <https://doi.org/10.1016/j.ijthermalsci.2010.06.009>
- Ali, M., Gultom, R. J., & Chouw, N. (2012). Capacity of Innovative Interlocking Blocks under Monotonic Loading. *Construction and Building Materials*, 37, 812-821. <https://doi.org/10.1016/j.conbuildmat.2012.08.002>

- Almanaratain. (2022). Almanaratain Sandwich Block. Retrieved February 10, 2022, from <https://almanaratain.com/product/insulated-blocks>.
- Anand, K. B., & Ramamurthy, K. (2000). Development and Performance Evaluation of Interlocking-Block Masonry. *Journal of Architectural Engineering*, 6(2), 45-51. [https://doi.org/10.1061/\(ASCE\)1076-0431\(2000\)6:2\(45\)](https://doi.org/10.1061/(ASCE)1076-0431(2000)6:2(45))
- Anand, K. B., & Ramamurthy, K. (2005). Development and Evaluation of Hollow Concrete Interlocking Block Masonry System. *TMS Journal*.
- ANSYS. (2022). from <https://www.ansys.com/products/connect>.
- Antar, M. A., & Baig, H. (2009). Conjugate Conduction-Natural Convection Heat Transfer in a Hollow Building Block. *Applied Thermal Engineering*, 29(17-18), 3716-3720. <https://doi.org/10.1016/j.applthermaleng.2009.04.033>
- ArmoSystem. (2021). Mexican Dry-Stacked Interlocking Block. Retrieved October 20, 2021, from <https://www.armo-system.com>.
- Asava, R., & Rusu, Z. (2017). *Simulating the Thermal Impact of Masonry Ties*. Paper presented at the Advances in Hygrothermal Performance of Building Envelopes: Materials, Systems and Simulations.
- Ascione, F., Bianco, N., Maria Mauro, G., & Napolitano, D. F. (2019). Building Envelope Design: Multi-Objective Optimization to Minimize Energy Consumption, Global Cost and Thermal Discomfort. Application to Different Italian Climatic Zones. *Energy*, 174, 359-374. <https://doi.org/10.1016/j.energy.2019.02.182>
- ASHRAE. (2021). *Ashrae Handbook: Fundamentals*: American Society of Heating, Refrigeration and Air-Conditioning Engineers.
- ASTM-C90. (2022). Standard Specification for Loadbearing Concrete Masonry Units. *Annual book of ASTM standards, United States*.
- Aswad, A., YILMAZ, M. C., & İsmail, S. H. (2022). A Systematic Review Study on Different Kinds of Interlocking Concrete Blocks Designs and Properties. *Turkish Journal of Engineering*, 6(4), 327-337. <https://doi.org/10.31127/tuje.931076>
- Bahar, R., Benazzoug, M., & Kenai, S. (2004). Performance of Compacted Cement-Stabilised Soil. *Cement and concrete composites*, 26(7), 811-820. <https://doi.org/10.1016/j.cemconcomp.2004.01.003>

- Barozzi, M., Lienhard, J., Zanelli, A., & Monticelli, C. (2016). The Sustainability of Adaptive Envelopes: Developments of Kinetic Architecture. *Procedia Engineering*, 155, 275-284. <https://doi.org/10.1016/j.proeng.2016.08.029>
- Bathe, K.-J. (2006). *Finite Element Procedures*: Klaus-Jurgen Bathe.
- Beall, C. (2000). New Masonry Products and Materials. *Progress in Structural Engineering and Materials*, 2(3), 296-303. [https://doi.org/10.1002/1528-2716\(200007/09\)2:3<296::AID-PSE38>3.0.CO;2-6](https://doi.org/10.1002/1528-2716(200007/09)2:3<296::AID-PSE38>3.0.CO;2-6)
- Biggs, D. T. (2002). *Development of a Mortarless Post-Tensioned Masonry Wall System*. Paper presented at the Proc., 6th Int. Masonry Conf., British Masonry Society, London.
- Bilgen, E. (2002). Natural Convection in Enclosures with Partial Partitions. *Renewable Energy*, 26(2), 257-270. [https://doi.org/10.1016/S0960-1481\(00\)00206-8](https://doi.org/10.1016/S0960-1481(00)00206-8)
- Bosro, M. Z. M., Samad, A. A. A., Mohamad, N., Goh, W. I., Tambichik, M. A., & Iman, M. A. (2018). A Review on Past and Present Development on the Interlocking Loadbearing Hollow Block (Ilhb) System. *IOP Conference Series: Earth and Environmental Science*, 140, 012135. <https://doi.org/10.1088/1755-1315/140/1/012135>
- Bouchair, A. (2008). Steady State Theoretical Model of Fired Clay Hollow Bricks for Enhanced External Wall Thermal Insulation. *Building and Environment*, 43(10), 1603-1618. <https://doi.org/10.1016/j.buildenv.2007.10.005>
- Bradfield, M., & Szoke, S. (1992). *Insulating Masonry Walls*. Paper presented at the Proceedings of the ASHRAE/DOE/BTECC Conference.
- Brenner, S. C., Scott, L. R., & Scott, L. R. (2008). *The Mathematical Theory of Finite Element Methods* (Vol. 3): Springer.
- Callejas, I. J. A., Durante, L. C., & Oliveira, A. S. d. (2017). Thermal Resistance and Conductivity of Recycled Construction and Demolition Waste (Rcdw) Concrete Blocks. *REM-International Engineering Journal*, 70, 167-173. <https://doi.org/10.1590/0370-44672015700048>
- Caniato, M., Bettarello, F., Ferluga, A., Marsich, L., Schmid, C., & Fausti, P. (2017). Thermal and Acoustic Performance Expectations on Timber Buildings. *Building Acoustics*, 24(4), 219-237. <https://doi.org/10.1177/1351010X17740477>
- Cécire, L. F. (2002). Azar Dry-Stack Block™. *CCMC Evaluation Reports and Listings*. National Research Council of Canada. Canadian Construction Materials Centre.

- Chaipanich, A., & Chindaprasirt, P. (2015). The Properties and Durability of Autoclaved Aerated Concrete Masonry Blocks. In *Eco-Efficient Masonry Bricks and Blocks* (pp. 215-230): Elsevier.
- ComfortBlock. (2022). Comfort Block, a New Generation of Building Systems. Retrieved February 25, 2022, from <https://www.comfortblock.com>.
- CSA-A370:14. (2018). Canadian Standards Association A370:14, Connectors for Masonry. Mississauga, ON, Canada.
- Da Silva, A., & Gosselin, L. (2005). On the Thermal Performance of an Internally Finned Three-Dimensional Cubic Enclosure in Natural Convection. *International Journal of Thermal Sciences*, 44(6), 540-546. <https://doi.org/10.1016/j.ijthermalsci.2004.11.011>
- Dawe, J., & Aridru, G. (1992). *Posttensioned Concrete Masonry Walls Subjected to Uniform Lateral Loadings*. Paper presented at the Proceedings of the 6th Canadian Masonry Symposium.
- del Coz Díaz, J., Nieto, P. G., Sierra, J. S., & Biempica, C. B. (2008). Nonlinear Thermal Optimization of External Light Concrete Multi-Holed Brick Walls by the Finite Element Method. *International Journal of Heat and Mass Transfer*, 51(7-8), 1530-1541. <https://doi.org/10.1016/j.ijheatmasstransfer.2007.07.029>
- Drysdale, B. G., & Hamid, A. A. (2005). *Masonry Structures Behaviour and Design* (4th ed.): Canadian Masonry Design Center.
- Drysdale, R. G., & Guo, P. (1995). *Strength Characteristics of Interlocking Dry-Stacked Concrete Block Masonry*. Paper presented at the 7th Canadian Masonry Symposium, Ontario, Canada.
- Dyskin, A. V., Pasternak, E., & Estrin, Y. (2012). Mortarless Structures Based on Topological Interlocking. *Frontiers of Structural and Civil Engineering*, 6(2), 188-197. <https://doi.org/10.1007/s11709-012-0156-8>
- E-Zblock. (2021). E-Z Insulating Concrete Foam Block. Retrieved September 21, 2021, from <https://www.e-zblock.com>.
- EPIC-Block. (2022). Eco-Panels Insulated Concrete Block. Retrieved March 18, 2022, from <https://www.theepicblock.com>.
- Erdem, C., Cuce, P. M., & BESİR, A. B. (2020). Improving Thermal Resistance of Lightweight Concrete Hollow Bricks: A Numerical Optimisation Research for a Typical Masonry Unit. *Journal of Energy Systems*, 4(3), 121-144. <https://doi.org/10.30521/jes.775961>
- Fangueiro, R. (2011). *Fibrous and Composite Materials for Civil Engineering Applications*: Elsevier.

- Faswall. (2022). Faswall Wood-Concrete Icf Product. Retrieved March 15, 2022, from <https://www.faswall.com>.
- Finch, G., Wilson, M., & Higgins, J. (2013). Thermal Bridging of Masonry Veneer Claddings & Energy Code Compliance. *ASTM International: Philadelphia, PA, USA*.
- Fonseca, F., & Murray, E. (2012). *Axial Capacity of Dry-Stacked Endura Masonry Walls*. Paper presented at the 15th International Brick and Block Masonry Conference.
- Gablok. (2021). Wood Insulated Block. Retrieved September 12, 2021, from <https://www.gablok.be/en>.
- Gu, H., & Hunt, J. F. (2007). Two-Dimensional Finite Element Heat Transfer Model of Softwood. Part Iii. Effect of Moisture Content on Thermal Conductivity. *Wood and fiber science*, 159-166.
- Haenerblock. (2021). The Mortarless Interlocking System. Retrieved August 10, 2021, from <http://www.haenerblock.com>.
- Han, Y., Fan, C., Geng, Z., Ma, B., Cong, D., Chen, K., & Yu, B. (2020). Energy Efficient Building Envelope Using Novel Rbf Neural Network Integrated Affinity Propagation. *Energy*, 209, 118414. <https://doi.org/10.1016/j.energy.2020.118414>
- HempcreteBlock. (2022). Developing Structural Hempcrete Block in Calgary. Retrieved August 19, 2022, from <https://www.justbiofiber.com>.
- Hendry, A. (2001). Masonry Walls: Materials and Construction. *Construction and Building Materials*, 15(8), 323-330. [https://doi.org/10.1016/S0950-0618\(01\)00019-8](https://doi.org/10.1016/S0950-0618(01)00019-8)
- Hendry, A. W. (1998). *Structural Masonry*: Macmillan Education UK.
- Hines, T., & Mehta, M. (1991). Effect of Mortar Joint on the Permeance of Masonry Walls. *Brick and Block Masonry*, 2, 1227-1234.
- Houben, H., & Guillaud, H. (1994). *Earth Construction: A Comprehensive Guide*.
- Hurtado, P. L., Rouilly, A., Vandenbossche, V., & Raynaud, C. (2016). A Review on the Properties of Cellulose Fibre Insulation. *Building and environment*, 96, 170-177.
- Huygen, N., & Sanders, J. (2022). *Impact of Wall Ties on the Steady-State Thermal Performance of Wall Systems*. Paper presented at the 2022 Masonry Symposium: Advancing Masonry Technology.

- Hydraform. (2021). Interlocking Soil Cement Block. Retrieved November 10, 2021, from <https://www.hydraform.com>.
- Ibañez-Puy, M., Vidaurre-Arbizu, M., Sacristán-Fernández, J. A., & Martín-Gómez, C. (2017). Opaque Ventilated Façades: Thermal and Energy Performance Review. *Renewable and sustainable energy reviews*, 79, 180-191.
- IEA. (2022). Buildings: A Source of Enormous Untapped Efficiency Potential. from Available at <https://www.iea.org/topics/buildings>.
- Ismail, M., Chen, Y., Cruz-Noguez, C., & Hagel, M. (2022). Thermal Resistance of Masonry Walls: A Literature Review on Influence Factors, Evaluation, and Improvement. *Journal of Building Physics*, 45(4), 528-567. <https://doi.org/10.1177/17442591211009549>
- ISO-6946. (2017). Building Components and Building Elements: Thermal Resistance and Thermal Transmittance: Calculation Method. In: International Organization for Standardization
- Isospan. (2022). Isospan Hollow Woodchip-Concrete Blocks. Retrieved from <https://www.isospan.eu>
- Isotex. (2021). Wood Cement Blocks and Floor Slabs. Retrieved December 15, 2021, from <https://www.en.blocchiisotex.com>.
- Khoukhi, M. (2018). The Combined Effect of Heat and Moisture Transfer Dependent Thermal Conductivity of Polystyrene Insulation Material: Impact on Building Energy Performance. *Energy and Buildings*, 169, 228-235. <https://doi.org/10.1016/j.enbuild.2018.03.055>
- Kuhn, J., Ebert, H.-P., Arduini-Schuster, M., Büttner, D., & Fricke, J. (1992). Thermal Transport in Polystyrene and Polyurethane Foam Insulations. *International journal of heat and mass transfer*, 35(7), 1795-1801.
- Kwon, Y., & Yarbrough, D. (2004). A Comparison of Korean Cellulose Insulation with Cellulose Insulation Manufactured in the United States of America. *Journal of Thermal Envelope and Building Science*, 27(3), 185-197.
- Kyriakidis, A., Michael, A., & Illampas, R. (2016). Parametric Numerical Assessment of the Energy Efficiency and the Environmental Impact of an Innovative Masonry Construction Component. *Journal of Sustainable Architecture and Civil Engineering*, 16(3), 6-19. <https://doi.org/10.5755/j01.sace.16.3.16174>
- Lakatos, Á., & Kalmár, F. (2013). Analysis of Water Sorption and Thermal Conductivity of Expanded Polystyrene Insulation Materials. *Building Services Engineering Research and Technology*, 34(4), 407-416.

- Leitão, D., Barbosa, J., Soares, E., Miranda, T., Cristelo, N., & Briga-Sá, A. (2017). Thermal Performance Assessment of Masonry Made of Iceb's Stabilised with Alkali-Activated Fly Ash. *Energy and Buildings*, 139, 44-52. <https://doi.org/10.1016/j.enbuild.2016.12.068>
- Li, L., Wu, Z., Li, Z., He, Y., & Tao, W. (2008). Numerical Thermal Optimization of the Configuration of Multi-Holed Clay Bricks Used for Constructing Building Walls by the Finite Volume Method. *International Journal of Heat and Mass Transfer*, 51(13-14), 3669-3682. <https://doi.org/10.1016/j.ijheatmasstransfer.2007.06.008>
- Liapor. (2022). Liatop50. Retrieved April 28, 2022, from <https://www.liapor.com/at/anwendungen/hochbau/steine/liatop-50.html>.
- Litebuilt. (2022). Litebuilt Aerated Concrete Block. Retrieved April 12, 2022, from <http://www.litebuilt.com>.
- Liu, H., Liu, P., Lin, K., & Zhao, S. (2016). Cyclic Behavior of Mortarless Brick Joints with Different Interlocking Shapes. *Materials*, 9(3), 166. <https://doi.org/10.3390/ma9030166>
- Lohr Sr, J. R. (1992). *Evaluation Offormwall'-a Post-Tensioned, Dry-Stacked Masonry System*. Retrieved from
- Lok-N-Blok. (2021). Fiber Reinforced Plastic Modular Wall System. Retrieved October 15, 2021, from <http://www.lok-n-blok.com>.
- Love, A. (2011). *Material Impacts on Operational Energy Usage*. Massachusetts Institute of Technology,
- Marshall, A. (1972). The Thermal Properties of Concrete. *Building Science*, 7(3), 167-174. [https://doi.org/10.1016/0007-3628\(72\)90022-9](https://doi.org/10.1016/0007-3628(72)90022-9)
- Martínez, M., Huygen, N., Sanders, J., & Atamturktur, S. (2018). Thermo-Fluid Dynamic Analysis of Concrete Masonry Units Via Experimental Testing and Numerical Modeling. *Journal of Building Engineering*, 19, 80-90. <https://doi.org/10.1016/j.jobe.2018.04.029>
- McCall, C. W. (1985). Thermal Properties of Sandwich Panels. *Concrete International*, 7(1), 35-41.
- Mezrhab, A., Bouali, H., Amaoui, H., & Bouzidi, M. (2006). Computation of Combined Natural-Convection and Radiation Heat-Transfer in a Cavity Having a Square Body at Its Center. *Applied energy*, 83(9), 1004-1023. <https://doi.org/10.1016/j.apenergy.2005.09.006>

- Mingotti, N., Chenvidyakarn, T., & Woods, A. W. (2011). The Fluid Mechanics of the Natural Ventilation of a Narrow-Cavity Double-Skin Facade. *Building and environment*, 46(4), 807-823. [10.1016/j.buildenv.2010.09.015](https://doi.org/10.1016/j.buildenv.2010.09.015)
- Mohammed, B. S., & Aswin, M. (2016). *Properties and Structural Behavior of Sawdust Interlocking Bricks*. Paper presented at the Proceedings of the 3rd International Conference on Civil, Offshore and Environmental Engineering, Kuala Lumpur-Malaysia.
- Mohammed, B. S., Liew, M. S., Alaloul, W. S., Al-Fakih, A., Ibrahim, W., & Adamu, M. (2018). Development of Rubberized Geopolymer Interlocking Bricks. *Case studies in construction materials*, 8, 401-408. <https://doi.org/10.1016/j.cscm.2018.03.007>
- MorrisonHershfield. (2011). Thermal Performance of Building Envelope Details for Mid-and High-Rise Buildings. *ASHRAE 1365-RP*.
- MorrisonHershfield, & BCHydro. (2021). Building Envelope Thermal Bridging Guide, Version 1.6. In: Vancouver: BC Hydro Power Smart.
- Nambiar, E. K. K., Ramamurthy, K., & Anand, K. B. (2004). *Accelerated Masonry Construction with Innovative Interlocking Blocks*. Paper presented at the 13th International Brick and Block Masonry Conference, Amsterdam, Netherland.
- Nardi, I., De Rubeis, T., Buzzi, E., Sfarra, S., Ambrosini, D., & Paoletti, D. (2016). Modeling and Optimization of the Thermal Performance of a Wood-Cement Block in a Low-Energy House Construction. *Energies*, 9(9), 677. <https://doi.org/10.3390/en9090677>
- Nayak, R., Tarkes, D. P., & Satapathy, A. (2010). A Computational and Experimental Investigation on Thermal Conductivity of Particle Reinforced Epoxy Composites. *Computational Materials Science*, 48(3), 576-581. <https://doi.org/10.1016/j.commatsci.2010.02.025>
- NCMA. (2013). R-Values and U Factors of Single-Wythe Concrete Masonry Walls. *TEK 06-02C, National Concrete Masonry Association*. Retrieved from <https://ncma.org/resource/rvalues-ufactors-of-single-wythe-concrete-masonry-walls/>
- NECB. (2015). National Energy Code of Canada for Buildings: 2015. Canadian Commission on Building and Fire Codes. In: National Research Council of Canada.
- NECB. (2017). National Energy Code of Canada for Buildings: 2017. Canadian Commission on Building and Fire Codes. In: National Research Council of Canada.
- NECB. (2020). National Energy Code of Canada for Buildings: 2020. Canadian Commission on Building and Fire Codes. In: National Research Council of Canada.

- Nexcem. (2022). Nexcem Block. Retrieved January 11, 2022, from <https://nexcembuild.com/insulated-concrete-forms>.
- Omar, W., & Mohamed, R. N. (2002). The Performance of Pretensioned Prestressed Concrete Beams Made with Lightweight Concrete. *Malaysian Journal of Civil Engineering*, 14(1).
- OneStep. (2022). Onestep Building System. Retrieved September 25, 2022, from <https://www.onestepbuildingsystem.com>.
- Ozel, M. (2011). Thermal Performance and Optimum Insulation Thickness of Building Walls with Different Structure Materials. *Applied Thermal Engineering*, 31(17-18), 3854-3863. <https://doi.org/10.1016/j.applthermaleng.2011.07.033>
- Pacheco-Torgal, F., & Jalali, S. (2012). Earth Construction: Lessons from the Past for Future Eco-Efficient Construction. *Construction and Building Materials*, 29, 512-519. <https://doi.org/10.1016/j.conbuildmat.2011.10.054>
- Pavlu, T., Fortova, K., Divis, J., & Hajek, P. (2019). The Utilization of Recycled Masonry Aggregate and Recycled Eps for Concrete Blocks for Mortarless Masonry. *Materials*, 12(12), 1923. <https://doi.org/10.3390/ma12121923>
- Pěňčík, J., & Matějka, L. (2011). *Fea Analysis and Monitoring of Long-Term Behavior of an Insulation Block from Recycled Polymer Hdpe*. Paper presented at the Advanced Materials Research.
- Perković, N., Rajčić, V., & Pranjić, M. (2021). Behavioral Assessment and Evaluation of Innovative Hollow Glue-Laminated Timber Elements. *Materials*, 14(22), 6911. <https://doi.org/10.3390/ma14226911>
- Pierquet, P., Bowyer, J. L., & Huelman, P. (1998). Thermal Performance and Embodied Energy of Cold Climate Wall Systems. *Forest Products Journal*, 48(6), 53.
- Pierzchlewicz, J. (1996). Modern Concrete Wall-Units with Improved Thermal Resistance for Housing in Hot Climate. *Sultan Qaboos University Journal for Science [SQUJS]*, 1, 69-80. <https://doi.org/10.24200/squjs.vol1iss1pp69-80>
- Polycare. (2021). Polymer Concrete Block. Retrieved August 10, 2021, from <https://www.polycare.de/en>.
- Ramamurthy, K., & Nambiar, E. K. K. (2004). Accelerated Masonry Construction Review and Future Prospects. *Progress in Structural Engineering and Materials*, 6(1), 1-9. <https://doi.org/10.1002/pse.162>

- Ramli, A., Abdullah, C. S., & Mohd Nawawi, M. N. (2014). *A Study of Potential Load Bearing Masonry (Lbm) System in Malaysia Construction Industry*.
- Ratanathavorn, W., Charoenjai, S., Janbuala, S., Chalermssinsuwan, B., & Poochinda, K. (2015). *Effects of Design Parameters for Clay Brick Kiln Using Computational Fluid Dynamics and Experimental Design*. Paper presented at the Advanced Materials Research.
- Reddy, B. V., & Kumar, P. P. (2010). Embodied Energy in Cement Stabilised Rammed Earth Walls. *Energy and Buildings*, 42(3), 380-385. <https://doi.org/10.1016/j.enbuild.2009.10.005>
- Saari, S., Bakar, B. H. A., & Surip, N. A. (2021). Factors of Non-Uniform Properties of Interlocking Compressed Earth Brick Units. *Developments in the Built Environment*, 5, 100042. <https://doi.org/10.1016/j.dibe.2021.100042>
- Safiee, N. A., Jaafar, M. S., Alwathaf, A. H., Noorzaeei, J., & Abdulkadir, M. R. (2011). Structural Behavior of Mortarless Interlocking Load Bearing Hollow Block Wall Panel under out-of-Plane Loading. *Advances in Structural Engineering*, 14(6), 1185-1196. <https://doi.org/10.1260/1369-4332.14.6.1185>
- Sanjuan, C., Suárez, M. J., González, M., Pistono, J., & Blanco, E. (2011). Energy Performance of an Open-Joint Ventilated Façade Compared with a Conventional Sealed Cavity Façade. *Solar Energy*, 85(9), 1851-1863.
- Sassine, E., Cherif, Y., Dgheim, J., & Antczak, E. (2020). Investigation of the Mechanical and Thermal Performances of Concrete Hollow Blocks. *Sn Applied Sciences*, 2(12), 1-17. <https://doi.org/10.1007/s42452-020-03881-x>
- Sathiparan, N., Anburuvel, A., Muralitharan, M., & Isura Kothalawala, D. A. (2022). Sustainable Use of Coco Pith in Cement-Sand Mortar for Masonry Block Production: Mechanical Characteristics, Durability and Environmental Benefit. *Journal of Cleaner Production*, 360, 132243. <https://doi.org/10.1016/j.jclepro.2022.132243>
- Schiavoni, S., Bianchi, F., & Asdrubali, F. (2016). Insulation Materials for the Building Sector: A Review and Comparative Analysis. *Renewable and sustainable energy reviews*, 62, 988-1011.
- Schierhorn, C. (1994). Is the Us Ready for Cellular Concrete Block? *Masonry Construction*, 7(12), 554,556-559.
- Schumacher, C., Straube, J., Ober, D., & Grin, A. (2013). Development of a New Hot Box Apparatus to Measure Building Enclosure Thermal Performance. *Proceedings of Buildings XII*, 1-19.

- Shakir, A. A., Ibrahim, M. W., Othman, N., Mohammed, A. A., & Burhanudin, M. (2020). Production of Eco-Friendly Hybrid Blocks. *Construction and Building Materials*, 257, 119536. <https://doi.org/10.1016/j.conbuildmat.2020.119536>
- Shao, Y. (2021). *Evaluating the Thermal Impacts of Different Masonry Wall Tie Designs Using Fem.* (Master of Science). University of Alberta, Edmonton, Canada.
- Shea, A., Lawrence, M., & Walker, P. (2012). Hygrothermal Performance of an Experimental Hemp–Lime Building. *Construction and Building Materials*, 36, 270-275. <https://doi.org/10.1016/j.conbuildmat.2012.04.123>
- Silva, R. A., Soares, E., Oliveira, D. V., Miranda, T., Cristelo, N. M., & Leitão, D. (2015). Mechanical Characterisation of Dry-Stack Masonry Made of Cebs Stabilised with Alkaline Activation. *Construction and Building Materials*, 75, 349-358. <https://doi.org/10.1016/j.conbuildmat.2014.11.038>
- Sindanne, S. A., Ntamack, G. E., Sanga, R. P. L., Moubeke, C. A., Sallaboui, E. S. K., Bouabid, H., . . . D'ouazzane, S. C. (2014). Thermophysical Characterization of Earth Blocks Stabilized by Cement, Sawdust and Lime. *Journal of Building Materials and Structures*, 1(2), 58-64. <https://doi.org/10.34118/jbms.v1i2.12>
- Singh, M., & Garg, M. (1991). Perlite-Based Building Materials—a Review of Current Applications. *Construction and Building Materials*, 5(2), 75-81.
- Sokairge, H., Rashad, A., & Elshafie, H. (2017). Behavior of Post-Tensioned Dry-Stack Interlocking Masonry Walls under out of Plane Loading. *Construction and Building Materials*, 133, 348-357. <https://doi.org/10.1016/j.conbuildmat.2016.12.071>
- Sore, S. O., Messan, A., Prud'Homme, E., Escadeillas, G., & Tsobnang, F. (2018). Stabilization of Compressed Earth Blocks (Cebs) by Geopolymer Binder Based on Local Materials from Burkina Faso. *Construction and Building Materials*, 165, 333-345.
- SpaceClaim. (2022). 3d Modeling Software of Ansys. from <https://www.ansys.com/products/3d-design/ansys-spaceclaim>.
- Steko. (2022). Steko Wood Block. Retrieved November 27, 2022, from <https://www.steko.ch>.
- Sturm, T., Ramos, L. F., & Lourenço, P. B. (2015). Characterization of Dry-Stack Interlocking Compressed Earth Blocks. *Materials and Structures*, 48(9), 3059-3074. <https://doi.org/10.1617/s11527-014-0379-3>

- Su, H., Wu, D., Shen, M., Chen, W., & Wang, S. (2019). Development and Performance Test Including Mechanical and Thermal of New Tenon Composite Block Masonry Walls. *Advances in Materials Science and Engineering*, 2019, 1-11. <https://doi.org/10.1155/2019/5253946>
- Subasic, C. A. (2022). *A Survey of Innovations in Masonry Units Addressing Sustainability*. Paper presented at the Advancing Masonry Technology, ASTM International, West Conshohocken, PA.
- Sutcu, M., del Coz Díaz, J. J., Rabanal, F. P. Á., Gencel, O., & Akkurt, S. (2014). Thermal Performance Optimization of Hollow Clay Bricks Made up of Paper Waste. *Energy and Buildings*, 75, 96-108. <https://doi.org/10.1016/j.enbuild.2014.02.006>
- Svetozarevic, B., Begle, M., Jayathissa, P., Caranovic, S., Shepherd, R. F., Nagy, Z., . . . Schlueter, A. (2019). Dynamic Photovoltaic Building Envelopes for Adaptive Energy and Comfort Management. *Nature Energy*, 4(8), 671-682. <https://doi.org/10.1038/s41560-019-0424-0>
- System3E. (2021). Ecological, Energy Saving and Economical Masonry System. Retrieved August 10, 2021, from <https://www.system3e.com/en>.
- Thanoon, W. A., Jaafar, M. S., Kadir, M. R. A., Ali, A. A. A., Trikha, D. N., & Najm, A. M. S. (2004). Development of an Innovative Interlocking Load Bearing Hollow Block System in Malaysia. *Construction and Building Materials*, 18(6), 445-454. <https://doi.org/10.1016/j.conbuildmat.2004.03.013>
- Theodosiou, T., Tsikaloudaki, K., Tsoka, S., & Chastas, P. (2019). Thermal Bridging Problems on Advanced Cladding Systems and Smart Building Facades. *Journal of Cleaner Production*, 214, 62-69. <https://doi.org/10.1016/j.jclepro.2018.12.286>
- Theodosiou, T. G., Tsikaloudaki, A. G., Kontoleon, K. J., & Bikas, D. K. (2015). Thermal Bridging Analysis on Cladding Systems for Building Facades. *Energy and Buildings*, 109, 377-384. [10.1016/j.enbuild.2015.10.037](https://doi.org/10.1016/j.enbuild.2015.10.037)
- Topçu, İ. B., & Işıkdag, B. (2007). Manufacture of High Heat Conductivity Resistant Clay Bricks Containing Perlite. *Building and environment*, 42(10), 3540-3546.
- TPB. (2022). The Perfect Block. Retrieved February 20, 2022, from <https://www.theperfectblock.com>.
- Urban, B., Engelmann, P., Kossecka, E., & Kosny, J. (2011). *Arranging Insulation for Better Thermal Resistance in Concrete and Masonry Wall Systems*. Paper presented at the 9th Nordic symposium on building physics, Finland.

- Uzoegbo, H. (2001). Lateral Loading Tests on Dry-Stack Interlocking Block Walls. In *Structural Engineering, Mechanics and Computation* (pp. 427-436): Elsevier.
- Uzoegbo, H. (2020). Dry-Stack and Compressed Stabilized Earth-Block Construction. In *Nonconventional and Vernacular Construction Materials* (pp. 305-350): Elsevier.
- Uzoegbo, H., Senthivel, R., & Ngowi, J. (2007). Loading Capacity of Dry-Stack Masonry Walls. *The masonry society journal*, 25(1), 41-52.
- Varol, Y., Oztop, H. F., & Pop, I. (2009). Natural Convection in a Diagonally Divided Square Cavity Filled with a Porous Medium. *International Journal of Thermal Sciences*, 48(7), 1405-1415.
- Versaloc. (2021). Dry-Stacked Walling System. Retrieved October 17, 2021, from <https://www.midlandbrick.com.au>.
- Wakili, K. G., & Tanner, C. (2003). U-Value of a Dried Wall Made of Perforated Porous Clay Bricks: Hot Box Measurement Versus Numerical Analysis. *Energy and Buildings*, 35(7), 675-680. [https://doi.org/10.1016/S0378-7788\(02\)00209-8](https://doi.org/10.1016/S0378-7788(02)00209-8)
- Walker, P. (1999). Bond Characteristics of Earth Block Masonry. *Journal of Materials in Civil Engineering*, 11(3), 249-256. [https://doi.org/10.1061/\(Asce\)0899-1561\(1999\)11:3\(249\)](https://doi.org/10.1061/(Asce)0899-1561(1999)11:3(249))
- Wolfe, R. W., & Gjinolli, A. (1996). Cement-Bonded Wood Composites as an Engineering Material. *The use of recycled wood and paper in building applications*, 84-91.
- Wu, J.-W., Sung, W.-F., & Chu, H.-S. (1999). Thermal Conductivity of Polyurethane Foams. *International journal of heat and mass transfer*, 42(12), 2211-2217.
- Yan, T., Sun, Z., Gao, J., Xu, X., Yu, J., & Gang, W. (2020). Simulation Study of a Pipe-Encapsulated Pcm Wall System with Self-Activated Heat Removal by Nocturnal Sky Radiation. *Renewable Energy*, 146, 1451-1464. <https://doi.org/10.1016/j.renene.2019.07.060>
- Zhang, T., Tan, Y., Yang, H., & Zhang, X. (2016). The Application of Air Layers in Building Envelopes: A Review. *Applied energy*, 165, 707-734. <https://doi.org/10.1016/j.apenergy.2015.12.108>
- Zukowski, M., & Haese, G. (2010). Experimental and Numerical Investigation of a Hollow Brick Filled with Perlite Insulation. *Energy and Buildings*, 42(9), 1402-1408.